

**ALMA MATER STUDIORUM – UNIVERSITÀ DI BOLOGNA**

**DOTTORATO DI RICERCA IN BIOINGEGNERIA**

**Ciclo XXIX**

Settore Concorsuale di afferenza: 09/G2

Settore Scientifico disciplinare: ING-INF/06

**Sensor technologies for on-line monitoring of  
biological parameters during hemodialysis**

Presentata da: **Enrico Ravagli**

Coordinatore Dottorato  
**Prof. Elisa Magosso**

Revisori  
**Prof. Elisa Magosso**  
**Giustina Casagrande, PhD**

Relatore  
**Stefano Severi, PhD**

Correlatore  
**Ing. Paolo Rovatti**

**Esame finale anno 2017**



**ALMA MATER STUDIORUM – UNIVERSITÀ DI BOLOGNA**

**DOTTORATO DI RICERCA IN BIOINGEGNERIA**

**Ciclo XXIX**

Settore Concorsuale di afferenza: 09/G2

Settore Scientifico disciplinare: ING-INF/06

**Sensor technologies for on-line monitoring of  
biological parameters during hemodialysis**

Presentata da: **Enrico Ravagli**

Coordinatore Dottorato  
**Prof. Elisa Magosso**

Revisori  
**Prof. Elisa Magosso**  
**Giustina Casagrande, PhD**

Relatore  
**Stefano Severi, PhD**

Correlatore  
**Ing. Paolo Rovatti**

**Esame finale anno 2017**



*To my mom and dad*



*The creation of something new is not accomplished by the intellect,  
but by the play instinct acting from inner necessity.  
The creative mind plays with the object it loves.*

C.G.Jung



# Aim and Outline

Hemodialysis is the most common renal replacement therapy in developed countries. It is a blood purification therapy that aims at removing toxins and excess liquid accumulated in the patient's body due to the complete or almost complete loss of renal function. It also has the additional purpose of rebalancing the correct plasmatic concentrations of electrolytes. Over the course of the years, hemodialysis underwent a number of technological advancements.

One of such advancements is the use of sensors to monitor the proper functioning of the machine, the safety of the treatment and the intra-session alterations of the hematic properties of the patient. Recently, sensing gained an additional role in hemodialysis: retrieving information for the purpose of therapy customization, by means of biofeedback algorithms. Unfortunately, economical costs and the nature of the treatment severely limit the available options for measurements, making non-invasive sensing quite an attractive choice. Non-invasive sensing techniques have the advantage of not requiring contact with the patient's blood, increasing safety and avoiding any sterilization issue or the use of disposable elements. Increased patient safety is the primary benefit of non-invasive sensing; however, another significant factor is that the use of additional disposable material for each treatment is avoided. This is not only important in economic terms, but also in terms of environmental impact of hemodialysis.

The primary aim of this doctoral thesis was the development of non-invasive sensing techniques for the measurement of physiological parameters during the hemodialysis session. The experience and data collected while pursuing this primary aim allowed to carry out an additional activity related to mathematical modeling of the dialysis process.

The thesis is composed of four chapters. Chapter 1 serves as an introduction to the field of hemodialysis, giving the reader an overview of the different aspects of this medical therapy. Chapters 2 and 3 are related to the topic of non-invasive sensing, main aim of the thesis, whereas in Chapter 4 the topic is the mathematical modeling of the hemodialysis process. The content of these chapters is based on scientific papers in preparation or already published, and the original article structure was kept. This way, each chapter is self-contained and can be read independently from the others.

In Chapter 2, a new method for the contactless estimation of plasmatic conductivity is described. The presented method uses high-frequency impedance measurement and model fitting to estimate electrical conductivity of the liquid contained inside the bloodline. The characterization of the electrical properties of the bloodline's biopolymer was also a fundamental step for the development of the new method. Good results were obtained with measurements on saline solution and a blood-mimicking fluid.

In Chapter 3, a system for continuous estimation of relative blood volume loss and plasmatic sodium concentration is described. The system integrates information from multiple sensors, among which is a new fiber-optic sensor, to estimate these two variables with satisfying accuracy.

In Chapter 4, a model of sodium diffusion across the hemodialysis filter is reported. The innovative aspect of the model is that it interconnects mathematical descriptions of both the patient and the dialyzer, at different abstraction levels, in order to give a more realistic representation of sodium exchange during the treatment.

The thesis closes with some final remarks on the presented work and an outlook for the possible future developments.

The work described in this thesis is the result of a collaboration with a private company operating in the field of hemodialysis, Gambro Dasco S.p.A. (now a part of Baxter Healthcare Corporation), which funded the PhD studentship of the author and supported the fulfillment of the experimental part of the work.



# Summary

<b>Aim and Outline .....</b>	<b>v</b>
<b>Summary .....</b>	<b>ix</b>
<b>1. Chapter 1 – Background .....</b>	<b>1</b>
1.1. End-stage renal disease and dialysis .....	3
1.2. The hemodialysis process .....	4
1.3. The role of sensors in modern hemodialysis .....	8
1.4. Mathematical and numerical modeling of different aspects of dialysis .....	14
1.5. Biofeedback therapies .....	16
1.6. Current and future trends in hemodialysis .....	18
1.7. Current limitations to sensing and modeling in dialysis .....	21
1.8. References .....	23
<b>2. Chapter 2 - Non-invasive conductivity measurement in hemodialysis .....</b>	<b>29</b>
2.1. Introduction .....	31
2.2. Methods .....	34
2.2.1. Cell prototype .....	34
2.2.2. Electrical properties of the biocompatible polymer .....	35
2.2.3. Preparation of solution samples .....	37
2.2.4. Impedance Spectroscopy .....	38
2.2.5. Lumped-Parameters Modeling .....	39
2.2.6. Frequency range reduction analysis .....	41
2.3. Results .....	41
2.4. Discussion .....	48
2.5. Conclusions .....	51
2.6. References .....	53
<b>3. Chapter 3 - Estimation of relative blood volume and plasmatic sodium concentration during hemodialysis .....</b>	<b>55</b>
3.1. Introduction .....	57
3.2. Methods .....	59
3.2.1. Optical measurement system .....	59

3.2.2. Experimental sessions .....	62
3.2.3. Data pre-processing .....	64
3.2.4. State space modeling and estimation .....	67
3.3. Results .....	75
3.4. Discussion .....	78
3.5. Conclusions .....	81
3.6. References .....	83
<b>4. Chapter 4 - Modeling of sodium diffusion across the hollow fiber of the hemodialyzer .....</b>	<b>85</b>
4.1. Introduction .....	87
4.2. Methods .....	88
4.2.1. Hollow fiber FEM model .....	88
4.2.2. ODE-FEM model coupling .....	92
4.2.3. Experimental data .....	93
4.2.4. Data processing .....	95
4.3. Results .....	97
4.4. Discussion .....	103
4.4.1. Limitations .....	104
4.5. Conclusions .....	105
4.6. References .....	107
<b>Concluding Remarks .....</b>	<b>109</b>
<b>Acknowledgements .....</b>	<b>113</b>





# Chapter 1

## Background

In this chapter, a brief overview of the hemodialysis therapy is given, addressing topics like the different dialysis techniques, the involved physical processes and technologies, and the innovation trends which will most likely shape the future of this medical procedure.

## **Abbreviations**

$\Delta$ RBV: Relative blood volume loss

1D: One-dimensional

2D: Two-dimensional

AKI: Acute kidney injury

AVF: Artero-venous fistula

AVG: Artero-venous graft

BVM: Blood volume monitor

BTM: Blood temperature monitor

CKD: Chronic kidney disease

ESRD: End-stage renal disease

HD: Hemodialysis

HF: Hemofiltration

Hgb: Hemoglobin

HDF: Hemodiafiltration

IDH: Intra-dialytic hypotension

PD: Peritoneal dialysis

RBV: Relative blood volume

RRT: Renal replacement therapy

TPC: Total protein concentration

TWL: Total weight loss

UF: Ultrafiltration

## **Keywords:**

Hemodialysis; Sensor; Mathematical model; Biofeedback.

## 1.1 End-stage renal disease and dialysis

End-stage renal disease (ESRD) is a term employed to describe all the pathological conditions in which the patient is left with kidney functionality below 10% [1]. It is usually associated with the late stage of a slowly-developing chronic kidney disease (CKD), but may also be the consequence of acute kidney injury (AKI) if full renal function is not recovered. It has been estimated that the population of ESRD patients expands roughly by 5-10% each year [2-4]. Treatment of ESRD condition is carried out by renal replacement therapy (RRT), which can assume three different forms: hemodialysis (HD), peritoneal dialysis (PD) and renal transplantation. In practice, due to the low rate of renal transplantation, dialysis is the most common type of RRT [2]. Dialysis treatment presents a very high economic impact [4,5]. Access to dialysis and RRT is, generally, more common in prosperous, high-income countries [6]. Recently, Liyanage et al. [7] quantified the worldwide burden of end-stage kidney disease and use of RRT, with the aim of estimating future trends in the field. According to their estimation, in 2010 a total of 2.618 million people received RRT, of which 2.050 million (78%) received dialysis (either HD or PD), and the remainder received a transplant. Also, according to their projection, the number of people receiving RRT will double by 2030.

Due to the lack of renal function, the ESRD patient tends to accumulate uremic toxins in blood and excess water in the whole body. Another consequence of kidney disease is the imbalance of electrolytes in blood (i.e. sodium, potassium, etc.). For this reason, both types of dialysis (HD/PD) have three main targets: the removal of uremic toxins, the removal of excess body water and the restoration of physiological concentrations of electrolytes. Dialysis only allows replacing the blood purification functions of the kidney, but not its endocrine functions, that must be substituted pharmacologically.

In hemodialysis, the body of the patient is connected to a hemodialysis machine through a vascular access [8]. Blood flows through an extracorporeal circulation system and inside a dialyzer (dialysis filter), where toxins and excess liquid are

transferred to a special fluid called dialysate, which also exchanges electrolytes with blood. Dialysate flows in the opposite direction of blood. After purification in the dialyzer, blood is returned to the patient's circulatory system.

Peritoneal dialysis [9] takes advantage of the peritoneum as a natural semipermeable membrane. In peritoneal dialysis, a dialysate bag is connected to the abdominal cavity, which is in this way filled by dialysate. Then, diffusion and osmosis drive waste and excess liquid from the other body compartments across the peritoneum, into dialysate. Dialysate is then drained from the abdominal cavity, concluding the cycle.

In developed countries, HD is the treatment employed for the large majority of patients, whereas the use of PD is much lower [10,11]. The mortality of ESRD patients treated with the two procedures has been investigated in many observational studies, as reported by Yang [10]. Nonetheless, the use of PD in its most recent forms is still advocated by some [11,12]. Due to its nature as a simpler treatment, PD offers many benefits for use in developing countries: lower cost, home-based therapy, single access, less requirement of highly trained personnel and major infrastructure, higher number of patients under a single nephrologist [13]. On the other hand, hemodialysis, due to its nature, allows many more treatment customization options, better treatment monitoring, and is in general a better recipient for technical innovation. This doctoral thesis focuses on the use of non-invasive sensors during HD sessions for CKD patients, for this reason further reference to PD will be omitted.

## **1.2 The hemodialysis process**

As described in the previous paragraph, hemodialysis replaces blood purification in uremic patients [14]. Conventional clinical hemodialysis [15] is usually carried out three times a week, in sessions with an average duration of four hours, under medical supervision.

At the beginning of each session, the patient is connected to the hemodialysis machine through a vascular access and a hydraulic circuit (Fig. 1.1). Such circuit,

the bloodline, is a biocompatible disposable part specifically developed for the extracorporeal circulation of blood. Due to the frequency of the sessions and the short time between consequent treatments, the presence of a safe and ready access to the circulatory system of the patient is particularly important and for this reason, a dedicated vascular access is created surgically, in the forms of an artero-venous fistula (AVF) or graft (AVG). AVF is the most common type of vascular access, characterized by the lowest occurrence of complications. It is usually created by joining an artery and a vein, usually in the forearm, and allowing for the consequent remodeling process: the result is a junction point able to withstand the pressures and flows of modern hemodialysis. Blood flowing from the vascular access inside the extracorporeal circuit is pumped by the machine inside the hemodialyzer, a disposable filter which is the core of the hemodialysis process, as already outlined in the previous paragraphs. Modern hemodialyzer, thanks to their hollow fiber structure, have a huge exchange surface area (in the order of 1-2 m<sup>2</sup>): each filter is composed by a large number ( $\approx 10000-14000$ ) of membranous fibers bundled together and potted at the extremities. Together, the internal lumens of all fibers constitute the blood-side compartment of the dialyzer. The joint space outside the fibers is filled with dialysate solution and constitutes the dialysate-side compartment. The dialyzer includes four connecting ports, to allow inlet and outlet flow for each compartment. Blood and dialysate flow inside the dialyzer in opposite directions (counter-flow), to maximize diffusion across the membrane. In modern single-pass machines, dialysate solution is prepared in real-time by the hemodialysis machine by mixing ultrapure water prepared from the water purification system of the hospital with the content of one or more bag/s of concentrates. Its composition is determined by the mixing factor between water and solutes coming from the bag of concentrates. The machine monitors and controls the mixing process, to guarantee a composition within a range of physiological compatibility with blood plasma.

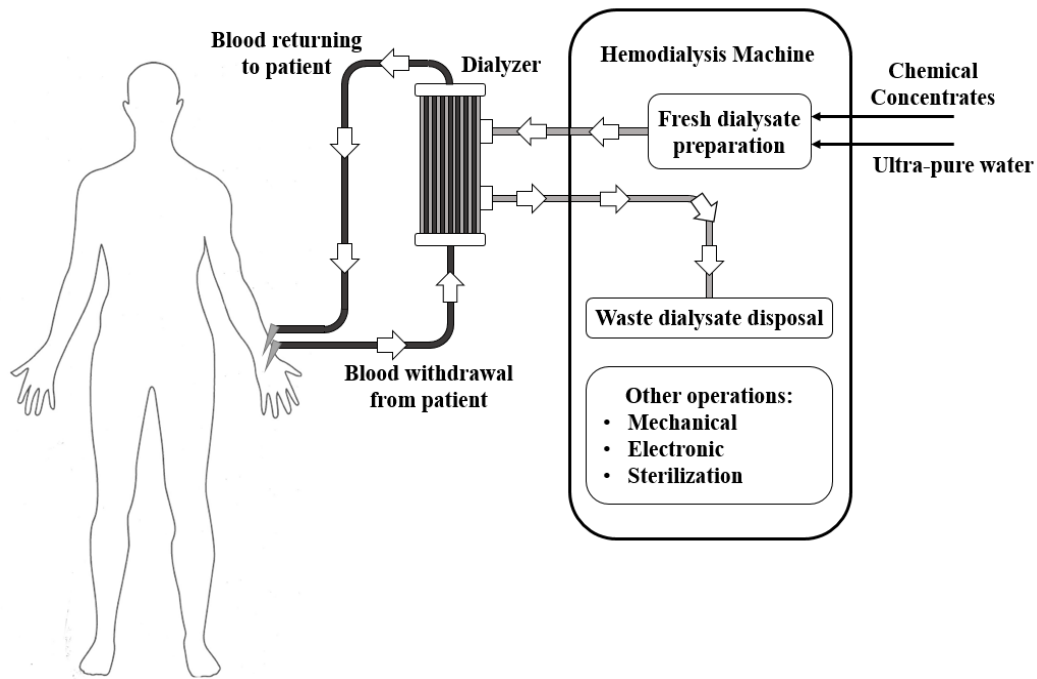


**Fig. 1.1 – Diagram of the hemodialysis process**  
Simple diagram of the interaction between the patient and the hemodialysis machine.

Inside the dialyzer, blood purification is achieved by means of two solute transport mechanisms, diffusion and convection [16,17]. Convection is a secondary effect of ultrafiltration (UF), a process used to remove excess liquid. Equations 1.1 and 1.2 report the mathematical descriptions for diffusion and convection.

$$J_D = -D \cdot A \cdot \frac{\Delta C}{\Delta x} \quad (1.1)$$

$$J_C = Q_{UF} \cdot C_B \cdot S \quad (1.2)$$

In equation 1.1, also known as Fick's law,  $D$  is the diffusion coefficient of the solute,  $A$  is the exchange surface area,  $\Delta C$  is the difference in the concentration of the solute across the membrane and  $\Delta x$  is the short distance between the opposite sides of the membrane. Diffusion is driven by the concentration gradient at the membrane, given by the ratio of  $\Delta C$  to  $\Delta X$ . Although the movements of single molecules of solute are random, on average the solute moves from areas of high

concentration to areas of low-concentration, in an effort compensation of the concentration gradient. This type of solute transport works better for small solutes, characterized by smaller weight and consequently a higher diffusion coefficient. In the case of uremic toxins, which are present only on the blood side of the membrane, the concentration gradient is always positive and movement is always one-way from blood to dialysate. In the case of solutes present in both blood and dialysate (i.e. electrolytes, glucose, etc.), the direction of solute movement is dictated by the difference between concentrations. The fact that fresh dialysate is often prepared with the same concentration, whereas the patient's body has finite volume and mass of solute, means that during the session plasmatic concentration of physiological solutes moves toward the concentration set in dialysate.

UF and convection are carried out by applying a positive hydrostatic pressure gradient across the dialyzer membrane: this mechanism generates a flow of liquid from the blood side of the membrane to the dialysate side of the membrane. The total amount of liquid to be removed during each session is set by medical prescription and programmed into the machine at session start, to correctly manage the ultrafiltration rate during treatment time. Convection is a physical process which implies transport of solutes across a membrane by movement of liquid: when the solvent flows to the opposite side of the membrane, molecules of solutes are dragged alongside it. Due to its nature, this type of solute transport is independent from the concentration gradient. In Equation 1.2,  $Q_{UF}$  is the UF rate across the membrane,  $C_B$  is the average solute concentration in blood, and  $S$  is the Sieving factor. The Sieving Factor accounts for the fact that convection of large molecules is reduced or even stopped by the dimensions of the membrane's pores.

Some variants to the standard therapy exist. Hemofiltration (HF) is normally used to treat AKI. In HF, only convection, and not diffusion, is carried out inside the hemodialyzer: the dialysate is not present. Physiological replacement fluid is instead added to the blood to replace fluid volume and rebalance electrolytes. In hemodiafiltration (HDF), HD and HF are combined: dialysate is present inside the dialyzer to allow diffusion, UF and convection are carried out at a high rate, and

substitution fluid is added to blood pre- or post-dialyzer. This solution combines the good removal of small molecules typical of diffusion and that of large molecules associated with convection.

After purification in the dialyzer, blood is returned to the patient's circulatory system through the vascular access.

### **1.3 The role of sensors in modern hemodialysis**

The use of sensors is a very important feature for hemodialysis machines for many purposes: patient safety, monitoring and control of machine operation, collection of clinically-relevant data, and biofeedback. Unfortunately, the nature of the hemodialysis treatment places large restrictions on the types of sensors that can be employed: given the frequency of the treatments (i.e.  $\approx 150$ -160 treatments per year per patient), to sustain an ever-increasing patient population national healthcare systems can only afford very cheap treatments. For this reason, no unnecessary single-session cost in addition to that of the basic disposable kit is usually considered by producers. Currently, the only sensors available on-machine are completely non-invasive at blood-side or able to withstand high-temperature sterilization at dialysate-side.

Many methods have been proposed along the years to extract additional information from blood or dialysate, but they usually present unacceptable disadvantages. Generally speaking, to increase significantly the information available during the session chemical analysis would be required, but any type of sensing that involves chemical analysis is either too complex to manage, too costly or has sterilization problems. For example, chemically-treated sensing probes may be employed for dialysate-side enhanced electrical or optical sensing, but such sensors are usually not resistant to high-temperature sterilization and present a cost too high to be used as disposable material. On blood-side, chemical analysis would require the management of an automated system for frequent blood sampling, which would be very complex and require regular maintenance.

Although chemical analysis is impractical during hemodialysis, the use of sensors based on general physical principles, together with some theoretical knowledge about the system and the processes involved, led to the development of current sensor solutions. Common sensors on current hemodialysis machines are based on ultrasonic, optical and electrical principles.

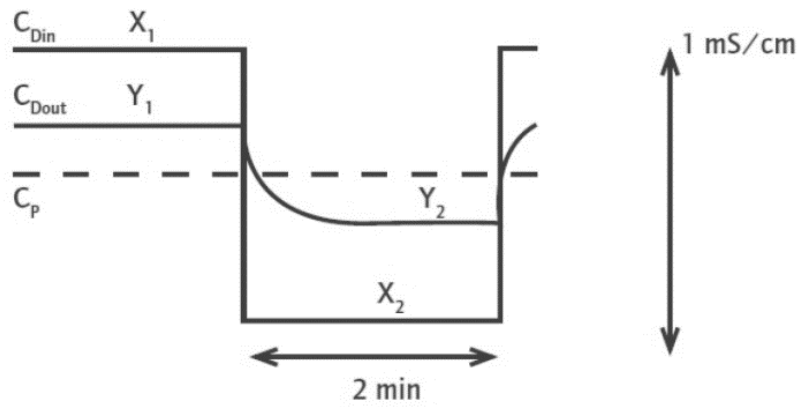
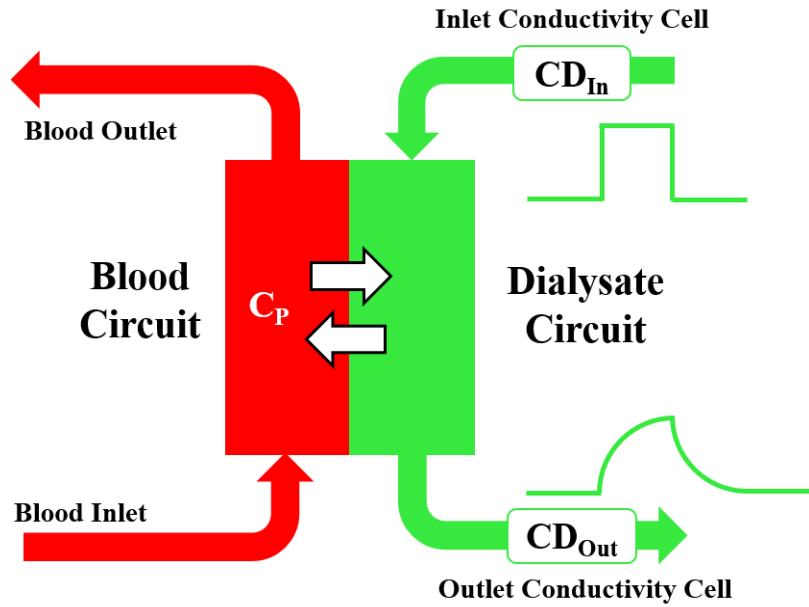
For example, ultrasonic sensors are employed to detect the presence of air bubbles inside the bloodline and activate a clamp mechanism before the bubble can reach the vascular access. Flow meters are employed to monitor the flow of dialysate, and the difference between measured flow rates at inlet and outlet is equivalent to the UF rate. Pressure sensors are employed to monitor the pressures of the arterial and venous traits of the bloodline. For example, in the Artis machine (Baxter, Medolla, Italy), pressures are transmitted from the artero-venous expansion chambers to the pressure sensors by deformable membranes.

Electrical conductivity sensors are placed on the dialysate-side hydraulic circuit both at inlet and outlet positions. The importance of monitoring the electrical conductivity of dialysate is determined by the high correlation between dialysate conductivity and its total content of electrolytes.

As already described in paragraph 1.2, dialysate is prepared in real-time by mixing ultrapure water and a bag of concentrates, composed mostly of electrolytes (sodium, chlorine, calcium, etc.) plus some glucose and other less-concentrated molecules. In diluted electrolytic solutions conductivity is determined by the sum of concentrations of the single ions, weighted by their ionic mobility [18]. Larger molecules contained in dialysate, like glucose, may affect conductivity depending on their electrical charge but larger sizes and lower concentration lead to a smaller influence.

Although conductivity cannot be used to determine the concentration of each separate ion, measured inlet conductivity can be employed to check if water and concentrates are mixed according to the proper mixing factor. Therefore, the first use of conductivity measurements in hemodialysis is in monitoring of dialysate preparation. A second use of dialysate conductivity measurements is clinical. Following the theory developed by Polaschegg [19], many systems have been

developed to estimate ionic clearance and plasmatic conductivity on the basis of a time-dependent measurement protocol (Fig. 1.2).



$$D = (Q_D + Q_P) \left( 1 - \frac{Y_1 - Y_2}{X_1 - X_2} \right) \quad C_P = \frac{X_1 Y_2 - X_2 Y_1}{(X_1 - X_2) - (Y_1 - Y_2)}$$

**Fig. 1.2 - Conductivity estimation by step-like protocol**

Upper panel: Inlet and outlet dialysate conductivity cells are used to estimate ionic dialysance and plasmatic conductivity. Lower panel: Step-based estimation protocol (Source: [22]).

Ionic clearance is important to quantify the efficacy of the dialysis treatment and is similar in value to urea clearance given that electrolytes and urea have similar molecular weights. The knowledge of plasmatic concentrations of electrolytes would be also clinically relevant, but as described in the first part of this paragraph, practical reasons prevents direct chemical analysis of blood. In particular, sodium is the most concentrated ion in dialysate and plasma, and is very important due to its influence on osmotic phenomena in the patient's body [20,21]. In this regard, plasmatic conductivity is the best sodium-related parameter which can be estimated non-invasively. The employed protocol works by recording inlet and outlet conductivity after applying a positive or negative conductivity step to inlet dialysate. Due to the fact that outlet conductivity is determined by inlet and plasmatic conductivity [22-24] because of the exchange of solutes at the filter, it is possible to estimate ionic clearance and plasmatic conductivity by observing the step-response outlet dynamics. The Diascan system [25] (Baxter, Medolla, Italy) is one example of commercial system currently in use developed on the basis of the Polaschegg theory.

Another physiological variable commonly monitored during hemodialysis by the use of sensors is the relative blood volume loss. During the session, the volume of blood  $V_B(t)$  contained in the patient's circulatory system is modified by the phenomena of ultrafiltration and vascular refilling according to equation (1.3), where  $V_{B,0}$  is the starting blood volume and  $J_{UF}$  and  $J_{Ref}$  are, respectively, the UF and refilling rates. Accordingly, relative blood volume (RBV) is defined as absolute blood volume  $V_B(t)$  at any given time, normalized to starting blood volume  $V_{B,0}(t)$ , as reported in equation (1.4). In turn, relative blood volume loss ( $\Delta RBV$ ) is defined as the relative variation in blood volume as reported in equation (1.5). It is usually expressed in percentage and during a typical session it can assume values down to -10%.  $\Delta RBV$  is also commonly described in models according to the ordinary differential equation reported in equation (1.6).

$$V_B(t) = V_{B,0} + \int_0^t (-J_{UF}(\tau) + J_{Ref}(\tau))d\tau \quad (1.3)$$

$$RBV(t) = \frac{V_B(t)}{V_{B,0}} = \frac{\int_0^t (-J_{UF}(\tau) + J_{Ref}(\tau))d\tau}{V_{B,0}} \quad (1.4)$$

$$\Delta RBV(t) = \frac{V_B(t) - V_{B,0}}{V_{B,0}} = \frac{\int_0^t (-J_{UF}(\tau) + J_{Ref}(\tau))d\tau}{V_{B,0}} \quad (1.5)$$

$$\Delta \dot{RBV}(t) = \frac{-J_{UF}(t) + J_{Ref}(t)}{V_{B,0}} \quad (1.6)$$

The possibility of direct  $\Delta RBV$  quantification is given by its relationship with some other physical property of blood. In particular, optical and ultrasonic sensors (Fig 1.3) are used for  $\Delta RBV$  estimation by monitoring other physiological parameters whose value change during the session mainly because of modifications of blood volume.

In the case of ultrasonic sensors, the relationship between  $\Delta RBV$  and total protein concentration (TPC) is exploited. During hemodialysis, TPC is mainly modified by the change in distribution volume of proteins, whereas the modification due to physiological activity is negligible. Therefore, measuring blood TPC variations by ultrasonic means allows to estimate  $\Delta RBV$  indirectly. An example of ultrasonic-based blood volume sensor employed on a commercial hemodialysis machine is the blood volume monitor (BVM, Fresenius Medical Care, Bad Homburg, Germany) [26-28].

In the case of optical sensors, simple systems composed by LEDs and photodiodes are employed to measure absorbance or reflectance depending on the geometrical placement of the sensor on the bloodline. Depending on the specific realization, the section of the bloodline where the optical measurement is carried out may be composed of a specific material with better optical properties. In this case, the optically transparent segment is usually called “cuvette”. In optical  $\Delta RBV$  sensors, the monitored variable is hemoglobin concentration ([Hgb]): as for TPC, the relative variation of [Hgb] during the dialysis session is more related to distribution volume changes than to production/degradation of the protein. Optical measurements are usually carried out at  $\approx 800-810$  nm, the point of the

absorbance spectrum of hemoglobin where absorbance is not determined by the oxygenation state of the molecule. An example of commercial optical RBV sensors is the Hemoscan system [29,30] (Baxter, Medolla, Italy).

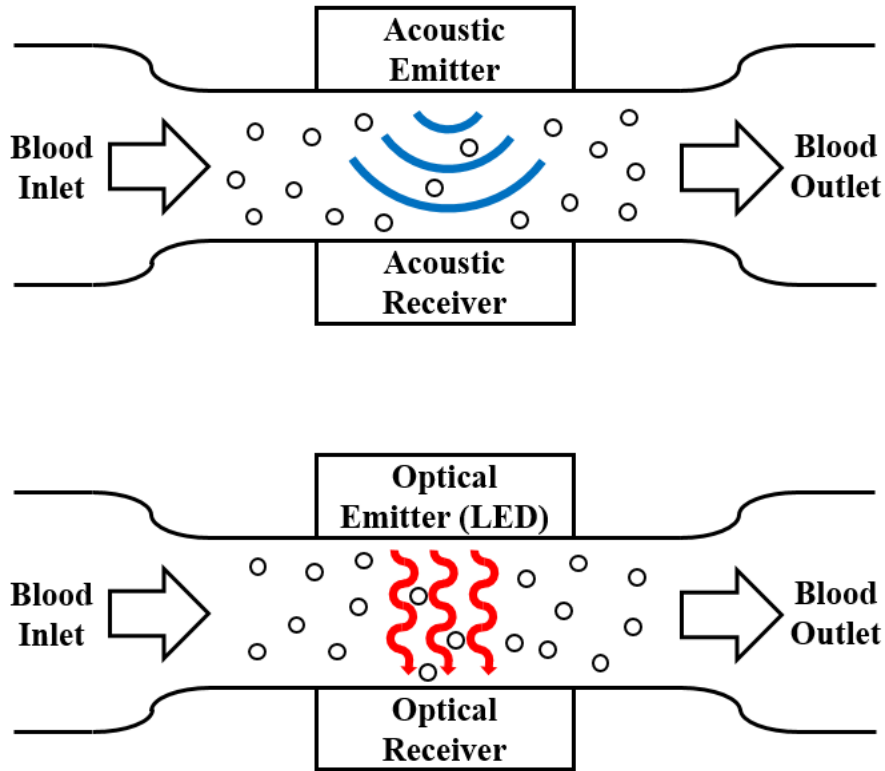


**Fig. 1.3 – Acoustic and optical methods for RBV estimation**

Upper panel: Estimation of RBV by ultrasonic measurement of total protein concentration.

Lower panel: Estimation of RBV by measurement of haemoglobin concentration.

In hemodialysis blood volume is measured as a relative quantity, rather than absolute, because currently no simple and non-invasive system for direct measurement of absolute blood volume exists. Some methods [31,32] have been proposed to estimate absolute blood volume at session start but no commercial solution has been developed yet.

Recently, a new type of optical sensor was developed to continuously measure ultraviolet absorbance in spent dialysate and track dialysis efficiency throughout the session [33,34]. A non-invasive sensor for blood temperature monitoring has

also been developed, the blood temperature monitor (BTM) system [35] (Fresenius, Bad Homburg, Germany). Another recent effort to collect clinical information about the dialysis patient non-invasively regards the extraction of the cardiac signal from data collected by the extracorporeal pressure sensors [36].

#### **1.4 Mathematical and numerical modeling of different aspects of dialysis**

Along the years mathematical modeling has been employed to study many different aspects of dialysis, both for descriptive and design purposes.

One of the most studied aspects of hemodialysis is the hemodialyzer: many models of the solute exchange and fluidodynamics phenomena happening inside the hemodialyzer have been proposed in the literature. The first mathematical models of the hemodialyzer activity were one-dimensional (1D) models of a single hollow fiber. 1D models of the “average” hollow fiber have the advantage of low computational requirements and mathematical simplification, and were first employed to study the effects of changes in the properties of the dialyzer (i.e. fiber length, permeability, etc.). In 2006, Waniewski et al. published a detailed review article [37] on mathematical modeling in hemodialysis which includes a section on the one-dimensional theory of the hemodialyzer and relative studies. Further modeling efforts led to the development of bidimensional (2D) models, where solute concentration and/or fluidodynamics are modeled both along the longitudinal and radial axes of the single fibers [38-42]. 2D modeling of the single hollow fiber is currently the most common approach, although 3D models are emerging in literature [43-45]. Mathematical modeling of the hemodialyzer is a topic with many repercussions on design activities, because it allows numerical investigation of possible changes to dialyzer properties.

A topic closer to physiological and clinical investigation is that of kinetic modeling [46]. In kinetic modeling, the hemodialysis process is described at high abstraction level and the interaction with patient physiology is taken into account. The body of the patient is considered as a volume for the distribution of a specific

solute, and the evolution of the solute's concentration during the hemodialysis session is described by mass balance equations. Kinetic models are employed to support clinical observations, to describe the kinetics of urea or other solutes, and to predict fluid and mass transfer between patient body compartments during hemodialysis [46-59]. Depending on the specific model, one or more compartments (“pools”) can be employed to describe the distribution volume. For example, in two-pools models (Fig. 1.4), the intracellular and extra-cellular components of volume are considered as different compartments. Three-pools models with intracellular, interstitial and plasma compartments were proposed by Ursino et al. [53] and, recently, by Casagrande et al. [59].

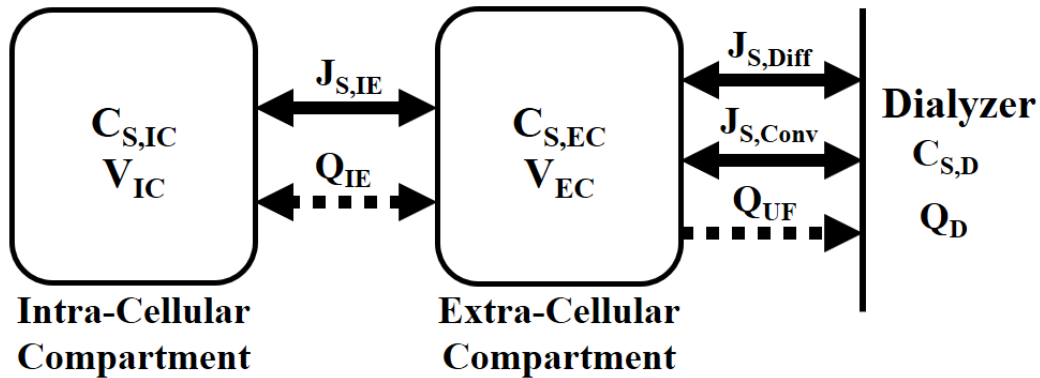


**Fig. 1.4 - Example of bicompartamental kinetic model for hemodialysis**

In bicompartamental models, two separate pools are used for intracellular and extracellular volumes ( $V_{IC}$ ,  $V_{EC}$ ) and concentrations of solutes ( $C_{S,IC}$ ,  $C_{S,EC}$ ). Mass flow represent the movement of molecules between the two compartments ( $J_{S,IE}$ ) or across the dialyzer membrane ( $J_{S,Diff}$  for diffusion,  $J_{S,Conv}$  for convection). Movement of liquid is represented by volume flow rates like  $Q_{IE}$  for intra/extracellular and  $Q_{UF}$  for ultrafiltration. Dialysate is not represented explicitly as a compartment, however significant parameters may be modelled (solute concentration  $C_{S,D}$  and flow rate  $Q_D$ ).

A third topic investigated many times by computational modeling is that of hemodynamics of the vascular access, especially in the most common case of the artero-venous fistula. The details of blood flow in the region of the vascular access have been investigated both for descriptive purposes [60] and for clinical and predictive purposes [61,62]. Also, the cardiovascular mechanics evolution induced by the fistula presence have been investigated by Casagrande et al. by development of a mathematical model of the circulatory system [63].

## 1.5 Biofeedback therapies

Traditionally, hemodialysis treatments are carried out by setting the values of specific parameters at session start. Such values are then modified only in case of intra-session complications, such as intra-dialytic hypotension (IDH). Examples of operational parameters are the blood and dialysate flow rates, the ultrafiltration rate, dialysate conductivity (or sodium concentration), and dialysate temperature. Some of them, like UF rate and dialysate sodium concentration, are chosen by medical prescription: for example, UF rate is computed automatically on the basis of treatment time and end-session total weight loss (TWL). Others are chosen on the basis of physiological considerations or clinical experience. However, the hemodialysis treatment aims at replacing lost renal function in a population of patients with their own physiological variability, implying that the standard set of parameters associated to “average” renal function may not be the optimal solution for each patient and each session. The aim of biofeedback therapies [64-67] is the transition toward a customized, more physiological treatment. Traditional hemodialysis can be categorized as open-loop, with direct perturbation of biological variables, regardless of patient’s response. In biofeedback treatments, biological variables are continuously monitored and collected data is employed to modulate further perturbations, implementing a closed-loop methodology. In this way, end-session targets are reached along a guided trajectory that is meant to avoid complications like IDH. Different biofeedback systems have been proposed and implemented on dialysis machines: examples are the Hemocontrol system [68] (Baxter, Medolla, Italy), the HFR-Aequilibrium [69] (Bellco, Medolla, Italy) and the feedback systems based on the BVM and BTM sensors Fresenius, Bad Homburg, Germany) described in paragraph 1.3.

The Hemocontrol system is a multi-input-multi-output biofeedback system that regulates blood volume contraction during the HD session by adjusting UF rate and inlet dialysate conductivity dynamically [70]. The system monitors RBV variation throughout the session using the on-board optical absorbance sensor, and integrates the optical information with data on measured dialysate conductivity

and end-session targets for TWL and sodium concentration (or its conductivity equivalent). By mean of its control algorithm, the system tries to achieve the different end-session targets while avoiding imbalance between volume loss and physiological refilling. The influence of Hemocontrol on the occurrence of intra-dialytic complications has been investigated in many studies [71-76], with seemingly positive results regarding the reduction of IDH events.

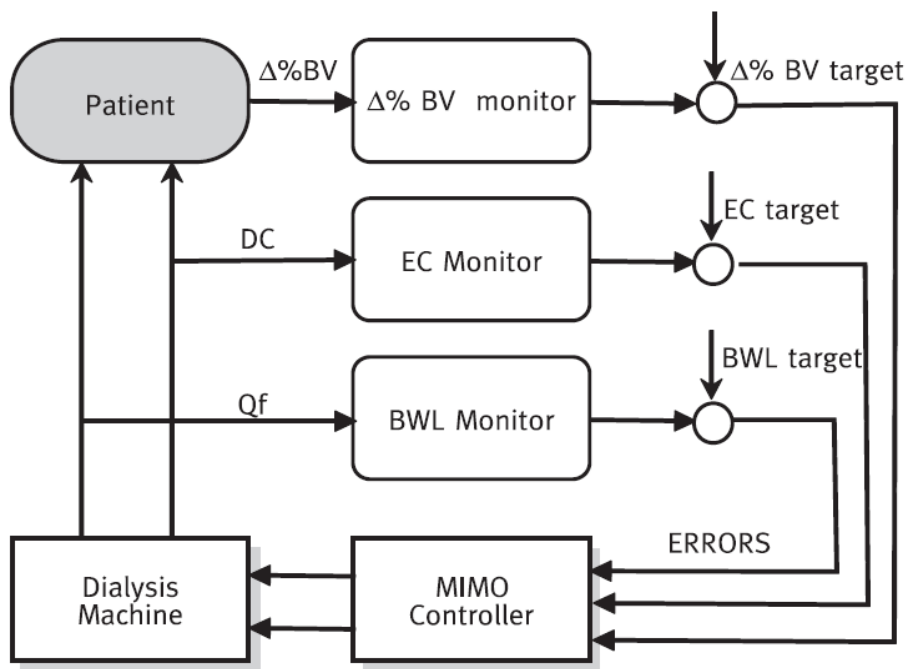


**Fig. 1.5 - Example of hemodialysis biofeedback system architecture**  
 Example of a multi-input multi-output (MIMO) controller employing blood volume loss ( $\Delta\% \text{ BV}$ ), dialysate equivalent conductivity (EC) and body weight loss (BWL) as controlled and monitored variables. (Source: [67])

The HFR-Aequilibrium system works conceptually in a similar way to Hemocontrol, meaning that UF rate and dialysate conductivity are the control variables, adjusted by the mathematical controller to avoid the osmotic differences between compartments that may lead to hypotension episodes. In this case, the monitored biological variable is the conductivity of plasmatic water measured by the Natrium biosensor. This system, however, is designed specifically for use during hemofiltration with endogenous reinfusion (HFR). Some studies have also been carried out to evaluate the effectiveness of this biofeedback system [77,78].

In the BVM-based system, the ultrasonic BVM biosensor described in paragraph 1.3 is employed as the basis for an RBV feedback system: differently from Hemocontrol and HFR-Aequilibrium, the BVM biofeedback only acts on UF rate as a control variable [30]. The BTM-based system is an example of temperature biofeedback, in which the temperature of dialysate is adjusted on the basis of the non-invasive measurement of blood temperature on the arterial and venous sides of the extracorporeal circuit. The system can be programmed either to deliver isothermal dialysis or to deliver a prescribed change in body temperature [79].

Given the architecture of closed-loop systems, sensor availability strongly conditions the innovation in the field of feedback therapies: the future development of additional non-invasive sensors for continuous monitoring is a main driver for new biofeedback systems able to integrate information from many different sources in order to reach a higher therapy customization power.

## **1.6 Current and future trends in hemodialysis**

As described in the previous paragraphs, over the last decades hemodialysis evolved from a complex experimental procedure to a standard and widely diffused therapy. Such evolution was possible thanks to many different kinds of innovations: the development of new biomaterials, the technical achievements in electronic and mechanical engineering, and the development of new therapeutic systems like biofeedback. Although it could be said that hemodialysis has reached now a consolidated form in regard to treatment modalities and machine architecture, some new trends are emerging and many open challenges remain, concerning both the achievement of optimal treatment and the access to the therapy.

One of the most common targets for innovation in dialysis is the hemodialyzer. It has been a few decades since the dialyzer reached its current design based on capillary hollow fibers, thanks to the advancements in manufacturing processes [80]. Since then, dialyzer innovation has focused more on the alteration of

different aspects of the current design: for example, the use of larger pore sizes to increase solute clearances (in particular for middle molecules) and changes in polymer composition [81]. The use of new biomaterials is also targeted at improved biocompatibility. Other possible ways to improve the blood purification process include taking advantage of additional phenomena like adsorption or membrane functionalization [81]. Generally speaking, the properties of the hemodialyzer have constantly improved in the past, and it is expected that this slow but steady process will continue in the future.

Regarding treatment modalities, efforts have been made to move on from the traditional schema of thrice-weekly diurnal dialysis to alternatives with lesser burdens, for two reasons. The first reason is related to quality of life: long and frequent diurnal sessions have a huge social cost on the patient's life. The second reason is medical: normal renal function works continuously at low flux, whereas hemodialysis works intermittently at high fluxes and is therefore not physiological. The results of these efforts are nocturnal hemodialysis and home hemodialysis.

In nocturnal dialysis, the patient is subjected to a normal in-center hemodialysis treatment, but the treatment is carried out during the night, allowing the patient to sleep. Treatment can be thrice-weekly [82] as in conventional dialysis or even more frequent [83]. The advantage of this kind of treatment is that by having a longer session ( $\approx 8$ h at night vs. 4h during day), the achievement of the prescribed TWL can be spread over a larger time period, thus leading to a lower UF rate. There is also the obvious social advantage of freeing up the patient's daytime and synchronizing with the normal sleep cycle. Nocturnal, in-center hemodialysis is associated with improved patient survival and favorable clinical features [82-84]. Home dialysis is carried out in the patient's home environment, and is usually carried out with shorter but more frequent sessions in respect to conventional therapy.

As for the case of nocturnal hemodialysis, home hemodialysis is associated with reported improvements in patient survival and clinical parameters [85,86]. Home hemodialysis programs have been started in many countries, but its diffusion is

still held back by the technical infrastructural requirements [86,87]. These two alternative modalities of treatment can also be combined: some studies reported the benefits of at-home nocturnal hemodialysis [88]. Unfortunately, in addition to the infrastructural requirements of home dialysis, the problem of remote monitoring of the sleeping patient has to be taken into account.

Another topic which is receiving much attention lately is that of “green” dialysis [89,90]. In hemodialysis, dialysate is prepared in real time during treatment by mixing ultrapure water from the hospital’s purification system with a super-concentrated electrolyte bag. For example, an average 4-hours treatment with a dialysate flow rate of 500 ml/min results in 120L of water consumed for a single session. This makes hemodialysis one of the most water-consuming among current medical procedures, which is a concern for multiple reasons. The first is environmental, due to the increasing worldwide water scarcity. The second is the fact that the requirement of a large water supply makes this therapy inaccessible to most developing countries. Many different points of intervention have been identified along the hemodialysis water cycle [91].

A more drastic approach to the reduction of dialysis water consumption is that of the regeneration of spent dialysate by the use of dialysate sorbents [92-94]. This topic is also related to that of portable and wearable dialysis systems, which are an additional step toward a more physiological and comfortable replacement of renal function. Recently, Davenport [95] published a review article on the topic of wearable and implantable dialysis devices. Although many technological advancements have been made that make these types of devices closer to realization, many problems related to anticoagulation, the maintenance of a constant vascular access and sorbent life still have to be solved before this new step in dialysis therapy becomes reality.

## 1.7 Current limitations to sensing and modeling in dialysis

As stated in the Aim and Outline section, the topics of this doctoral thesis are:

1. Development of new non-invasive sensing techniques for hemodialysis
2. Mathematical modeling of the hemodialysis process.

To be more specific, two new estimation systems are presented and a new approach to mathematical modeling of the dialysis session is proposed. In order to provide a clearer picture to the reader, this paragraph will list some of the current limitations to sensing technologies and mathematical models which the work reported in the ensuing chapters aims at overcoming.

- In paragraph 1.3 the Polaschegg step-like protocol for the determination of plasmatic conductivity is mentioned. As explained, plasmatic conductivity is a valid surrogate for plasmatic sodium concentration. Such protocol, also shown in Fig. 1.2, has a time duration in the order of minutes. The step shown in figure is 2 minutes long, however commercial systems may take longer time for a measurement. Also, the measurement cannot be repeated too frequently, since it involves a perturbation of plasmatic electrolytes. For example, the already mentioned Diascan system takes a 10-minutes measurement each 30 minutes. The obvious drawback of this protocol is that it does not allow for continuous real-time monitoring but offers only a few data points during the session. In Chapter 2, a new plasmatic conductivity estimation system is proposed. The new system allows for much faster measurements, thus making continuous real-time monitoring possible, without any loss of accuracy.
- Another sensing method, also reported in paragraph 1.3, is optical  $\Delta$ RBV estimation. Such method has been in use on hemodialysis machines for many years: examples are the already mentioned Hemoscan sensor (Baxter, Medolla, Italy) or the Hemox sensor (Bellco, Mirandola, Italy). However, recent publications [96-97] report the influence of osmolarity modifications on this type of estimation procedure. Briefly, changes in the osmolarity of blood have the effect of altering the volume of red blood cells, thus modifying the

light scattering properties of whole blood and leading to artifacts in  $\Delta$ RBV estimation. In Chapter 3, a measurement system is presented for artifact-free optical  $\Delta$ RBV estimation. The new system relies on enhanced optical sensing and integration with other on-machine sensors to remove the effect of scattering artifacts from  $\Delta$ RBV estimation. An additional feature of the proposed system is an estimation of plasmatic sodium concentration, which also makes it an alternative to the system proposed in Chapter 2 to overcome the current limitations of conductivity measurements.

- In paragraph 1.4, different types of mathematical and numerical models for hemodialysis are mentioned. Models with different levels of abstraction serve different purposes, and thus have different trade-offs in terms of complexity vs. descriptive power. For example, kinetic models are heavily abstracted and the description of the behaviour of the whole dialyzer is reduced to two coefficients for diffusion and convection. On the other hand, numerical hollow fiber models offer a more detailed description of the exchange of solutes and fluid along all the fiber, and thus offer potential for design activities. However, fiber models are not usually employed to simulate a complete dialysis session with evolving patient properties. In Chapter 4, a new approach to modeling of the hemodialysis process is proposed, in which a kinetic model of the blood pool is coupled to a numerical model of the hollow fiber. The proposed method aims at overcoming the limitations reported above while preserving the strengths of the two methodologies, namely a simple patient representation and a detailed dialyzer representation.

## 1.8 References

- [1] <https://www.nlm.nih.gov/medlineplus/ency/article/000500.htm>, last accessed March 2017
- [2] F. P. Schena, "Epidemiology of end-stage renal disease: International comparisons of renal replacement therapy," *Kidney Int*, vol. 57, pp. S39-S45.
- [3] M. J. Lysaght and J. A. O'Loughlin, "Demographic scope and economic magnitude of contemporary organ replacement therapies," *ASAIO J*, vol. 46, pp. 515-21, Sep-Oct 2000
- [4] M. J. Lysaght, "Maintenance dialysis population dynamics: current trends and long-term implications," *J Am Soc Nephrol*, vol. 13 Suppl 1, pp. S37-40, Jan 2002.
- [5] A. F. De Vecchi, M. Dratwa, and M. E. Wiedemann, "Healthcare systems and end-stage renal disease (ESRD) therapies--an international review: costs and reimbursement/funding of ESRD therapies," *Nephrol. Dial. Transplant.*, vol. 14 Suppl 6, pp. 31-41, 1999.
- [6] V. Jha, G. Garcia-Garcia, K. Iseki, Z. Li, S. Naicker, B. Plattner, et al., "Chronic kidney disease: global dimension and perspectives," *Lancet*, vol. 382, pp. 260-72, Jul 20 2013.
- [7] T. Liyanage, T. Ninomiya, V. Jha, B. Neal, H. M. Patrice, I. Okpechi, et al., "Worldwide access to treatment for end-stage kidney disease: a systematic review," *Lancet*, vol. 385, pp. 1975-82, May 16 2015.
- [8] <https://en.wikipedia.org/wiki/Hemodialysis>, last accessed March 2017
- [9] [https://en.wikipedia.org/wiki/Peritoneal\\_dialysis](https://en.wikipedia.org/wiki/Peritoneal_dialysis), last accessed March 2017
- [10] F. Yang, L. W. Khin, T. Lau, H. R. Chua, A. Vathsala, E. Lee, et al., "Hemodialysis versus Peritoneal Dialysis: A Comparison of Survival Outcomes in South-East Asian Patients with End-Stage Renal Disease," *PloS One*, vol. 10, p. e0140195, 2015.
- [11] J. Pajek, "Overcoming the Underutilisation of Peritoneal Dialysis," *BioMed Res Int*, vol. 2015, p. 431092, 2015.
- [12] J. M. Bargman, "Advances in peritoneal dialysis: a review," *Semin Dial*, vol. 25, pp. 545-9, Sep-Oct 2012.
- [13] G. Abraham, S. Varughese, M. Mathew, and M. Vijayan, "A review of acute and chronic peritoneal dialysis in developing countries," *Clin Kidney J*, vol. 8, pp. 310-7, Jun 2015.
- [14] <https://www.kidney.org/atoz/content/hemodialysis>, last accessed March 2017
- [15] A. R. Nissenson and R. N. Fine, *Clinical Dialysis*, Fourth Edition. McGraw-Hill, 2005.
- [16] J.A. Sargent and F.A. Gotch, "Principles and biophysics of dialysis," in *Replacement of Renal Function by Dialysis*, W. Drukker, F.M. Parsons, J.F. Maher (Eds.), Springer, 1983
- [17] C. Ronco, P. M. Ghezzi, A. Brendolan, C. Crepaldi, and G. La Greca, "The haemodialysis system: basic mechanisms of water and solute transport in extracorporeal renal replacement therapies," *Nephrol. Dial. Transplant.*, vol. 13 Suppl 6, pp. 3-9, 1998.
- [18] R. H. Stokes and R. A. Robinson, *Electrolyte Solutions*, Second Revised Edition, Dovers Publications, 2002.
- [19] H. D. Polaschegg, "Automatic, noninvasive intradialytic clearance measurement," *Int J Artif Organs*, vol. 16, pp. 185-91, Apr 1993.
- [20] F. G. Heineken, M. C. Evans, M. L. Keen, and F. A. Gotch, "Intercompartmental Fluid Shifts in Hemodialysis Patients," *Biotechnol Prog*, vol. 3, pp. 69-73, 1987.
- [21] M. J. Flanigan, "Role of sodium in hemodialysis," *Kidney Int, Supp*, vol. 76, pp. S72-8, Aug 2000.
- [22] Moret, K.E., The role of technological advances in sodium prescription and adequacy assessment during hemodialysis, Doctoral Thesis, Maastricht University, 2011
- [23] T. Petitclerc, "Recent developments in conductivity monitoring of haemodialysis session," *Nephrol. Dial. Transplant.*, vol. 14, pp. 2607-2613, November 1, 1999 1999.
- [24] K. Moret, D. C. Grootendorst, C. Beerenhout, and J. P. Kooman, "Conductivity pulses needed for Diascan® measurements: does it cause sodium burden?" *Nephrol. Dial. Transplant. Plus*, vol. 2, pp. 334-5, Aug 2009.
- [25] [https://www.baxter.com/assets/downloads/products\\_expertise/renal\\_therapies/Diascan\\_Brochure\\_FINAL.pdf](https://www.baxter.com/assets/downloads/products_expertise/renal_therapies/Diascan_Brochure_FINAL.pdf), last accessed March 2017

- [26] <http://fmc-au.com/pdf/machines/Blood%20Volume%20Monitor-Literature.pdf>, last accessed January 2016
- [27] D. Schneditz, H. Pogglichsch, J. Horina, and U. Binswanger, "A blood protein monitor for the continuous measurement of blood volume changes during hemodialysis," *Kidney Int*, vol. 38, pp. 342-6, Aug 1990.
- [28] C. Johner, P. W. Chamney, D. Schneditz, and M. Kramer, "Evaluation of an ultrasonic blood volume monitor," *Nephrol. Dial. Transplant.*, vol. 13, pp. 2098-103, Aug 1998.
- [29] E. Mancini, A. Santoro, M. Spongano, F. Paolini, M. Rossi, and P. Zucchelli, "Continuous on-line optical absorbance recording of blood volume changes during hemodialysis," *Artif Organs*, vol. 17, pp. 691-4, Aug 1993.
- [30] F. Paolini, E. Mancini, A. Bosetto, and A. Santoro, "Hemoscan: a dialysis machine-integrated blood volume monitor," *Int J Artif Organs*, vol. 18, pp. 487-94, Sep 1995.
- [31] J. Kron, D. Schneditz, T. Leimbach, S. Aign, and S. Kron, "A simple and feasible method to determine absolute blood volume in hemodialysis patients in clinical practice," *Blood Purif*, vol. 38, pp. 180-7, 2014.
- [32] S. Kron, D. Schneditz, T. Leimbach, J. Czerny, S. Aign, and J. Kron, "Determination of the critical absolute blood volume for intradialytic morbid events," *Hemodial Int.*, vol. 20, pp. 321-6, Apr 2016.
- [33] F. Uhlin, I. Fridolin, L. G. Lindberg, and M. Magnusson, "Estimation of delivered dialysis dose by on-line monitoring of the ultraviolet absorbance in the spent dialysate," *Am J Kidney Dis*, vol. 41, pp. 1026-36, May 2003.
- [34] F. Uhlin, I. Fridolin, M. Magnusson, and L. G. Lindberg, "Dialysis dose (Kt/V) and clearance variation sensitivity using measurement of ultraviolet-absorbance (on-line), blood urea, dialysate urea and ionic dialysance," *Nephrol. Dial. Transplant.*, vol. 21, pp. 2225-31, Aug 2006.
- [35] <http://fmc-au.com/pdf/machines/Blood%20Temperature%20Monitor-Literature.pdf>, last accessed March 2017
- [36] M. Holmer, F. Sandberg, K. Solem, E. Grigonyte, B. Olde, and L. Sornmo, "Extracting a cardiac signal from the extracorporeal pressure sensors of a hemodialysis machine," *IEEE Trans Biomed Eng*, vol. 62, pp. 1305-15, May 2015.
- [37] J. Waniewski, "Mathematical modeling of fluid and solute transport in hemodialysis and peritoneal dialysis," *J Membr Sci*, vol. 274, pp. 24-37, 2006.
- [38] Z. Liao, C. K. Poh, Z. Huang, P. A. Hardy, W. R. Clark, and D. Gao, "A numerical and experimental study of mass transfer in the artificial kidney," *J Biomech Eng*, vol. 125, pp. 472-80, Aug 2003.
- [39] J. Lu and W.-Q. Lu, "A numerical simulation for mass transfer through the porous membrane of parallel straight channels," *Int J Heat Mass Transfer*, vol. 53, pp. 2404-2413, 5// 2010.
- [40] K. Annan, "Mathematical modeling of the dynamic exchange of solutes during bicarbonate dialysis," *Math Comput Model*, vol. 55, pp. 1691-1704, 3// 2012.
- [41] M. Islam and J. Szpunar, "Study of Dialyzer Membrane (Polyflux 210H) and Effects of Different Parameters on Dialysis Performance," *Open J Nephrol*, Vol. 3 No. 3, 2013, pp. 161-167.
- [42] W. Ding, L. He, G. Zhao, H. Zhang, Z. Shu, and D. Gao, "Double porous media model for mass transfer of hemodialyzers," *Int J Heat Mass Transfer*, vol. 47, pp. 4849-4855, 10// 2004.
- [43] K. Yamamoto, M. Matsuda, A. Hirano, N. Takizawa, S. Iwashima, T. Yakushiji, et al., "Computational evaluation of dialysis fluid flow in dialyzers with variously designed jackets," *Artif Organs*, vol. 33, pp. 481-6, Jun 2009.
- [44] S. Eloit, D. De Wachter, I. Van Tricht, and P. Verdonck, "Computational flow modeling in hollow-fiber dialyzers," *Artif Organs*, vol. 26, pp. 590-9, Jul 2002.
- [45] W. Ding, W. Li, S. Sun, X. Zhou, P. A. Hardy, S. Ahmad, et al., "Three-dimensional simulation of mass transfer in artificial kidneys," *Artif Organs*, vol. 39, pp. E79-89, Jun 2015.
- [46] Gotch FA "Kinetic modeling in hemodialysis". In: Nissenson AR, Fine RN, Gentile DE, eds. *Clinical Dialysis*. 3rd ed. Norwalk, CT: Appelton and Lange 1995
- [47] M. Ursino and M. Innocenti, "Mathematical investigation of some physiological factors involved in hemodialysis hypotension," *Artif Organs*, vol. 21, pp. 891-902, Aug 1997.

- [48] W. R. Clark, J. K. Leypoldt, L. W. Henderson, B. A. Mueller, M. K. Scott, and E. F. Vonesh, "Quantifying the effect of changes in the hemodialysis prescription on effective solute removal with a mathematical model," *J Am Soc Nephrol*, vol. 10, pp. 601-9, Mar 1999.
- [49] V. A. de los Reyes, D. H. Fuertinger, F. Kappel, A. Meyring-Wosten, S. Thijssen, and P. Kotanko, "A physiologically based model of vascular refilling during ultrafiltration in hemodialysis," *J Theor Biol*, vol. 390, pp. 146-55, Feb 7 2016.
- [50] R. Hussain, F. Kappel, F. Zhu, N. W. Levin, and P. Kotanko, "Body composition and solute kinetics in hemodialysis patients: a mathematical model," *IET Communications*, vol. 6, pp. 3301-3308, 2012.
- [51] J. K. Leypoldt, C. Kablitz, M. C. Gregory, H. O. Senekjian, and A. K. Cheung, "Prescribing hemodialysis using a weekly urea mass balance model," *Blood Purif*, vol. 9, pp. 271-84, 1991.
- [52] M. Prado, L. Roa, A. Palma, and J. A. Milan, "A novel mathematical method based on urea kinetic modeling for computing the dialysis dose," *Comput Methods Programs Biomed*, vol. 74, pp. 109-28, May 2004.
- [53] M. Ursino, L. Coli, C. Brighenti, L. Chiari, A. de Pascalis, and G. Avanzolini, "Prediction of solute kinetics, acid-base status, and blood volume changes during profiled hemodialysis," *Ann Biomed Eng*, vol. 28, pp. 204-16, Feb 2000.
- [54] J. Waniewski, "Mathematical modeling of fluid and solute transport in hemodialysis and peritoneal dialysis," *J Membr Sci*, vol. 274, pp. 24-37, 2006.
- [55] J. K. Leypoldt, B. U. Agar, A. Akonur, M. E. Gellens, and B. F. Culleton, "Steady state phosphorus mass balance model during hemodialysis based on a pseudo one-compartment kinetic model," *Int J Artif Organs*, vol. 35, pp. 969-80, Nov 2012.
- [56] B. U. Agar, B. F. Culleton, R. Fluck, and J. K. Leypoldt, "Potassium kinetics during hemodialysis," *Hemodial Int*, vol. 19, pp. 23-32, Jan 2015.
- [57] S. H. Laursen, A. Buus, M. H. Jensen, P. Vestergaard, and O. K. Hejlesen, "Distribution volume assessment compartment modelling: theoretic phosphate kinetics in steady state hemodialys patients," *Int J Artif Organs*, vol. 38, pp. 580-7, Nov 2015.
- [58] M. Ursino, L. Coli, E. Magosso, P. Capriotti, A. Fiorenzi, P. Baroni, *et al.*, "A mathematical model for the prediction of solute kinetics, osmolarity and fluid volume changes during hemodiafiltration with on-line regeneration of ultrafiltrate (HFR)," *Int J Artif Organs*, vol. 29, pp. 1031-41, Nov 2006.
- [59] G. Casagrande, C. Bianchi, D. Vito, F. Carfagna, C. Minoretti, G. Pontoriero, *et al.*, "Patient-specific modeling of multicompartmental fluid and mass exchange during dialysis," *Int J Artif Organs*, vol. 39, pp. 220-7, Jul 4 2016.
- [60] B. Ene-Iordache, L. Mosconi, G. Remuzzi, and A. Remuzzi, "Computational fluid dynamics of a vascular access case for hemodialysis," *J Biomech Eng*, vol. 123, pp. 284-92, Jun 2001.
- [61] A. Caroli, S. Manini, L. Antiga, K. Passera, B. Ene-Iordache, S. Rota, *et al.*, "Validation of a patient-specific hemodynamic computational model for surgical planning of vascular access in hemodialysis patients," *Kidney Int*, vol. 84, pp. 1237-45, Dec 2013.
- [62] A. Remuzzi and S. Manini, "Computational model for prediction of fistula outcome," *J Vasc Access*, vol. 15 Suppl 7, pp. S64-9, 2014.
- [63] G. Casagrande, E. Lanzarone, F. Miglietta, A. Remuzzi, R. Fumero, and M. L. Costantino, "Determination of cardiovascular mechanics evolution in the presence of the arteriovenous fistula," *ASAIO J*, vol. 55, pp. 484-93, Sep-Oct 2009.
- [64] A. Santoro, E. Mambelli, C. Canova, A. Lopez, E. Sestigiani, and E. Mancini, "Biofeedback in dialysis," *Journal of nephrology*, vol. 16 Suppl 7, pp. S48-56, Nov-Dec 2003.
- [65] F. Locatelli, U. Buoncrisiani, B. Canaud, H. Kohler, T. Petitclerc, and P. Zucchelli, "Haemodialysis with on-line monitoring equipment: tools or toys?" *Nephrol. Dial. Transplant.*, vol. 20, pp. 22-33, Jan 2005.

- [66] G. E. Nesrallah, R. S. Suri, G. Guyatt, R. A. Mustafa, S. D. Walter, R. M. Lindsay, et al., "Biofeedback dialysis for hypotension and hypervolemia: a systematic review and meta-analysis," *Nephrol. Dial. Transplant.*, vol. 28, pp. 182-91, Jan 2013.
- [67] A. Santoro, E. Mancini, and F. Grandi, "Ultrafiltration and dialysate conductivity biofeedback in the prevention of dialysis-related hypotension," *Port J Nephrol Hypert*, 2010; 24(3): 195-200
- [68] [http://www.baxter.ca/en/healthcare\\_professionals/therapies/gambro\\_therapies/hemodialysis/hemocontrol/index.html](http://www.baxter.ca/en/healthcare_professionals/therapies/gambro_therapies/hemodialysis/hemocontrol/index.html), last accessed March 2017
- [69] [http://www.bellco.net/products-and-therapies/chronic-line/10-en\\_c-3-8/therapies.aspx#](http://www.bellco.net/products-and-therapies/chronic-line/10-en_c-3-8/therapies.aspx#), last accessed March 2017
- [70] J. J. Dasselaaar, "Relative blood volume based biofeedback during haemodialysis," *J Ren Care*, vol. 33, pp. 59-65, Apr-Jun 2007.
- [71] C. Ronco, A. Brendolan, M. Milan, M. P. Rodeghiero, M. Zanella, and G. La Greca, "Impact of biofeedback-induced cardiovascular stability on hemodialysis tolerance and efficiency," *Kidney Int*, vol. 58, pp. 800-8, Aug 2000.
- [72] C. Basile, R. Giordano, L. Vernaglione, A. Montanaro, P. De Maio, F. De Padova, et al., "Efficacy and safety of haemodialysis treatment with the Hemocontrol biofeedback system: a prospective medium-term study," *Nephrol. Dial. Transplant.*, vol. 16, pp. 328-34, Feb 2001.
- [73] V. Begin, C. Deziel, and F. Madore, "Biofeedback regulation of ultrafiltration and dialysate conductivity for the prevention of hypotension during hemodialysis," *ASAIO J*, vol. 48, pp. 312-5, May-Jun 2002.
- [74] C. F. Franssen, J. J. Dasselaaar, P. Sytisma, J. G. Burgerhof, P. E. de Jong, and R. M. Huisman, "Automatic feedback control of relative blood volume changes during hemodialysis improves blood pressure stability during and after dialysis," *Hemodial Int.*, vol. 9, pp. 383-92, Oct 2005.
- [75] C. Deziel, J. Bouchard, M. Zellweger, and F. Madore, "Impact of hemocontrol on hypertension, nursing interventions, and quality of life: a randomized, controlled trial," *Clin J Am Soc Nephrol*, vol. 2, pp. 661-8, Jul 2007.
- [76] H. W. Gil, K. Bang, S. Y. Lee, B. G. Han, J. K. Kim, Y. O. Kim, et al., "Efficacy of hemocontrol biofeedback system in intradialytic hypotension-prone hemodialysis patients," *J Korean Med Sci*, vol. 29, pp. 805-10, Jun 2014.
- [77] L. Mercadal, C. Piekarski, J. L. Renaux, T. Petitclerc, and G. Deray, "Isonatric dialysis biofeedback in hemodiafiltration with online regeneration of ultrafiltrate (HFR): rationale and study protocol for a randomized controlled study," *J Nephrol*, vol. 25, pp. 1126-30, Nov-Dec 2012.
- [78] F. Locatelli, S. Stefoni, T. Petitclerc, L. Coli, S. Di Filippo, S. Andrulli, et al., "Effect of a plasma sodium biofeedback system applied to HFR on the intradialytic cardiovascular stability. Results from a randomized controlled study," *Nephrol. Dial. Transplant.*, vol. 27, pp. 3935-42, Oct 2012.
- [79] N. M. Selby and C. W. McIntyre, "A systematic review of the clinical effects of reducing dialysate fluid temperature," *Nephrol. Dial. Transplant.*, vol. 21, pp. 1883-98, Jul 2006.
- [80] Z. J. Twardowski, "History of hemodialyzers' designs," *Hemodial Int.*, vol. 12, pp. 173-210, Apr 2008.
- [81] A. Davenport, "How can dialyzer designs improve solute clearances for hemodialysis patients?," *Hemodial Int*, 2014 Oct;18 Suppl 1:S43-7. doi: 10.1111/hdi.12223.
- [82] E. Lacson, Jr., J. Xu, R. S. Suri, G. Nesrallah, R. Lindsay, A. X. Garg, et al., "Survival with three-times weekly in-center nocturnal versus conventional hemodialysis," *J Am Soc Nephrol*, vol. 23, pp. 687-95, Apr 2012.
- [83] M. Walsh, B. Culleton, M. Tonelli, and B. Manns, "A systematic review of the effect of nocturnal hemodialysis on blood pressure, left ventricular hypertrophy, anemia, mineral metabolism, and health-related quality of life," *Kidney Int*, vol. 67, pp. 1500-8, Apr 2005.
- [84] E. Ok, S. Duman, G. Asci, M. Tumuklu, O. Onen Sertoz, M. Kayikcioglu, et al., "Comparison of 4- and 8-h dialysis sessions in thrice-weekly in-centre haemodialysis: a prospective, case-controlled study," *Nephrol. Dial. Transplant.*, vol. 26, pp. 1287-96, Apr 2011.
- [85] A. Naso, G. Scaparrotta, E. Naso, and L. A. Calo, "Intensive Home Hemodialysis: An Eye at the Past Looking for the Hemodialysis of the Future," *Artif Organs*, vol. 39, pp. 736-40, Sep 2015.
- [86] A. Power and D. Ashby, "Haemodialysis: hospital or home?," *Postgrad Med J*, vol. 90, pp. 92-7, Feb 2014.

- [87] J. W. Agar, A. Perkins, and J. G. Heaf, "Home hemodialysis: infrastructure, water, and machines in the home," *Hemodial Int*, vol. 19 Suppl 1, pp. S93-s111, Apr 2015.
- [88] C. Chazot, E. Ok, E. Lacson, Jr., P. G. Kerr, G. Jean, and M. Misra, "Thrice-weekly nocturnal hemodialysis: the overlooked alternative to improve patient outcomes," *Nephrol. Dial. Transplant.*, vol. 28, pp. 2447-55, Oct 2013.
- [89] L. Ponson, W. Arkouche, and M. Laville, "Toward green dialysis: focus on water savings," *Hemodial Int*, vol. 18, pp. 7-14, Jan 2014.
- [90] F. Tarrass, M. Benjelloun, O. Benjelloun, and T. Bensaha, "Water conservation: an emerging but vital issue in hemodialysis therapy," *Blood Purif*, vol. 30, pp. 181-5, 2010.
- [91] N. A. Hoenich, R. Levin, and C. Ronco, "Water for haemodialysis and related therapies: recent standards and emerging issues," *Blood Purif*, vol. 29, pp. 81-5, 2010.
- [92] J. W. Agar, "Review: understanding sorbent dialysis systems," *Nephrology*, vol. 15, pp. 406-11, Jun 2010.
- [93] S. R. Ash, "Sorbents in treatment of uremia: a short history and a great future," *Semin Dial*, vol. 22, pp. 615-22, Nov-Dec 2009.
- [94] M. Wester, K. G. Gerritsen, F. Simonis, W. H. Boer, D. H. Hazenbrink, K. R. Vaessen, *et al.*, "A regenerable potassium and phosphate sorbent system to enhance dialysis efficacy and device portability: a study in awake goats," *Nephrol. Dial. Transplant.*, May 24 2016.
- [95] A. Davenport, "Portable and wearable dialysis devices for the treatment of patients with end-stage kidney failure: Wishful thinking or just over the horizon?," *Pediatr Nephrol*, vol. 30, pp. 2053-60, Dec 2015.
- [96] S. Kron, R. Wenkel, T. Leimbach, S. Aign, and J. Kron, "Effects of sodium on measuring relative blood volume during hemodialysis differ by techniques," *ASAIO J*, Vol. 59, pp. 612-6, Nov-Dec 2013.
- [97] S. Kron, R. Wenkel, T. Leimbach, S. Aign, and J. Kron, "Effects of Osmotic Changes on Measuring Relative Blood Volume: Comparison of Three Hemodialysis Devices," *ASAIO J*, Vol. 62, pp. 214-5, Mar-Apr 2016.



# Chapter 2

## **Non-invasive conductivity measurement in hemodialysis**

In this chapter, a new method for the direct, continuous and non-invasive measurement of the electrical conductivity of liquids contained inside a hemodialysis bloodline is presented. This new method shows good results in the estimation of conductivity of saline solution and blood-mimicking fluid, in a range of values compatible with the conductivity of human plasma, using a very compact measurement cell. Thus, this work constitutes an important first step in the development of a conductivity measurement system for blood, which is faster and more accurate than the current state of the art.

The content of this chapter is based on the article “Non-invasive measurement of electrical conductivity of liquids in biocompatible polymeric lines for hemodialysis applications”, by Enrico Ravagli, Marco Crescentini, Marco Tartagni, and Stefano Severi. At the time of writing (March 2017) the article has been submitted to *Sensors and Actuators A - Physical* and is undergoing the review process.

## **Abbreviations**

BMF: Blood-mimicking fluid

C4D: Capacitively-Coupled Contactless Conductivity Detection

CPE: Constant Phase Element

IS: Impedance Spectroscopy

LP: Lumped Parameters

R-C: Resistance-Capacitance

R-CPE: Resistance-Constant Phase Element

## **Keywords:**

Conductivity; Constant-phase Element; Hemodialysis; Impedance Spectroscopy.

## 2.1 Introduction

The monitoring of the electrical properties of a material is an important process because such properties are related to its internal structure. Thus, changes in conductivity or permittivity can be used to detect alterations in composition. In the specific case of fluids, electrical properties are influenced by the presence of electrically charged suspensions (i.e. ions). For a mix of water and electrolytes with sufficient dilution, conductivity is determined by the concentration of the individual ionic species, weighted by ionic mobility [1]. The possibility of using electrical conductivity to estimate biological parameters has also been largely explored in biomedical engineering and science, with many different target tissues, such as blood [2-3] and skin [4].

A particularly important biomedical application for conductivity monitoring is in the field of hemodialysis for chronic patients. Hemodialysis is a periodical blood purification treatment for patients with end-stage renal failure [5-6]. During the treatment, the blood of the patient is pumped into an extracorporeal circulation system and put in contact with a liquid solution, the dialysate, through a semi-permeable membrane. Contact with dialysate allows toxins removal and electrolytes balance through diffusion and convection [7].

In this context, conductivity is important as a surrogate for sodium concentration measurements. Knowledge of the trend of sodium concentration during the treatment is useful for clinical purposes, but implementing an on-machine system for repeated blood sampling and chemical analysis is complex and expensive. Since electrical conductivity of blood plasma is mainly determined by sodium concentration, with a nearly linear relationship, conductivity monitoring is a valid substitute for sodium measurements [8]. Unfortunately, direct conductivity measurements cannot be carried out because of complications in using traditional immersion electrodes in this particular context. The first complication is the contact of the electrodes with blood, which demands for the electrodes to be either disposable or sterilized after every use. The second complication is the lack of biocompatibility of metallic electrodes, which is

required for *in vivo* measurements on patient blood.

Currently, the state-of-the-art method for plasmatic conductivity estimation during standard hemodialysis treatments is based on the theory originally developed by Polaschegg [9]. This is an indirect method that allows estimation of plasmatic conductivity by applying conductivity steps to the dialysate fluid following a dynamic protocol. Briefly:

- i) Conductivity steps are imposed on inlet dialysate by the hemodialysis machine, and conductivity is measured on both inlet and outlet dialysate.
- ii) By use of a mathematical formulation, the measured conductivities of dialysate before and after its electrolyte exchange with blood can be employed to estimate plasmatic conductivity.

This method presents some disadvantages. The protocol, as currently implemented by modern machines, requires a measurement time of about 10 minutes and is repeated automatically every 30 minutes. Its accuracy is limited (typically in the order of 0.1 mS/cm in a 13-16 ms/cm full-scale measurement range) and, due to the conductivity steps, it also causes a temporary alteration of blood electrolytes content, so conceptually it can be somehow considered invasive.

The C4D (Capacitively-Coupled Contactless Conductivity Detection) is a technique employed in electrochemistry for the detection of transition of ionic species with different mobility values through an electrophoresis capillary exposed to a constant electric field [10-12]. It is one of the many measurement techniques proposed in the literature for the estimation of material properties in a fast and contactless way [13-16]. The basis of C4D is the capacitive coupling of an AC electrical signal between exterior and interior of the line containing the fluid. Two ring electrodes placed axially outside the line (Fig. 2.1) couple the signal to the fluid. The current finds a flowing pathway through the liquid, and the pick-up signal (current) amplitude is analyzed in conjunction with the stimulation signal (voltage). The relation between stimulation voltage and pick-up current can be analyzed to determine conductivity of the flowing liquid.

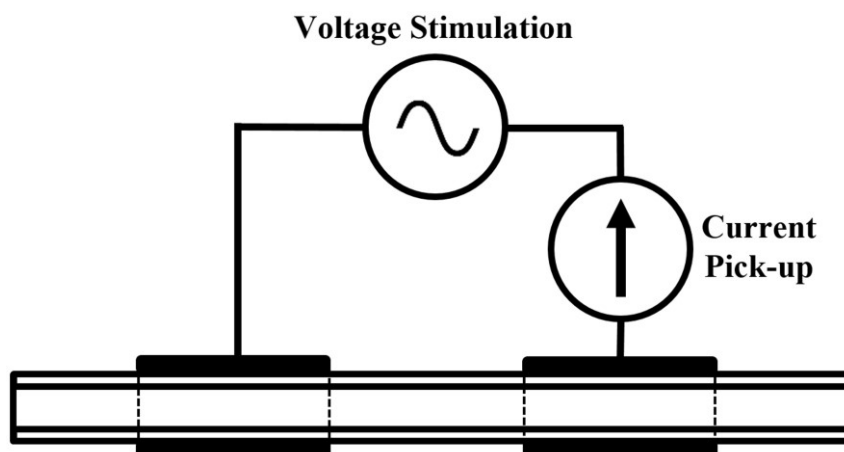


**Fig. 2.1 - C4D System**

Schematic representation of the general setup for a C4D system in voltage-stimulation configuration

The C4D technique has been applied to many different pharmaceutical and biological samples, as reported in [17-19]. Over the years, the effects of the geometry of the measurement cell and of the operating parameters of the system (i.e. frequency) have been studied [20-24]. Recently, many evolutions in the electronics and measurement aspects of C4D have also been proposed, for example the use of the lock-in principle [25-26], phase-sensitive demodulation [27] or resonance sensing [28-32]. Contactless impedance cells with geometries similar to that of C4D cells have also been used for other purposes, like flow measurements [33].

The aim of this work is to explore the possibility of developing a contactless method to estimate the conductivity of liquids contained in biocompatible polymeric line for hemodialysis applications. This method would allow faster and more frequent measurements, in addition to being non-invasive and maintaining an accuracy equal or better than the traditional method.

The method we propose is loosely based on C4D regarding the topology of the measurement cell, but differs from such technique by using all the information available from impedance spectroscopy (IS, magnitude and phase of impedance at different frequencies) for conductivity estimation. In our case a quantitative estimation of the conductivity of the liquid is given, whereas traditional C4D is only used to monitor the time of passage of different ions during electrophoresis.

In the following sections, the development and testing of a contactless conductimetry cell for biomedical use will be described. The cell was first tested with hemodialysis biopolymeric line segments filled with saline solution, to validate the measurement principle with a simple fluid. Afterwards, it was tested with blood-mimicking fluid (BMF) to study the response of the system to a more complex fluid.

Impedance spectroscopy was used for experimental characterization of the cell and for measurements. A lumped-parameters (LP) electrical model of the cell was developed, and its performances were evaluated using experimental data as reference.

## **2.2 Methods**

The measurement cell was developed to scale the application of the C4D principle from the original electrophoresis capillaries to biocompatible lines with a diameter in the order of several millimeters. The device was implemented and tested by filling a polymeric line segment with liquid samples, first of saline solution and then of BMF. Each set of solutions was composed of samples with different conductivity values. A LP model of the electrical equivalent circuit of the cell was also developed. Characterization of the electrical properties of the biopolymer was also helpful in model development. The purpose of the LP model was dual: i) experimental data interpretation on a high abstraction level; ii) easy conductivity estimation.

### **2.2.1 Cell prototype**

Our degrees of freedom in cell geometry design were partially limited by the intended purpose of use on-board of a dialysis machine, which puts an upper limit to cell size. The developed cell (Fig. 2.2) is composed of two cylindrical aluminum electrodes of length 20 mm and distance from each other of 70 mm (center-to-center), held by two PVC holders. The electrodes are round-shaped, 10

mm wide, with internal diameter of 6 mm.

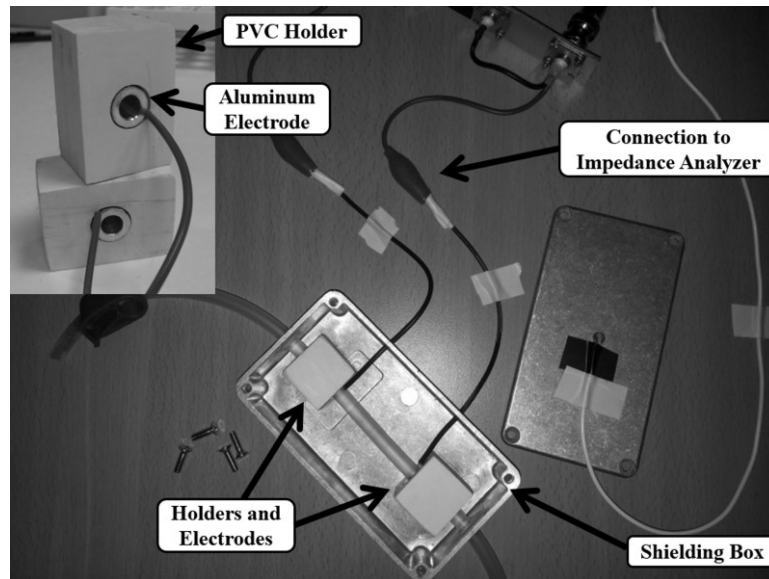


**Fig. 2.2 - Measurement Cell**

Prototype of our C4D measurement cell with a biocompatible line. Inset: detail of the cylindrical electrodes enclosed in the PVC holders.

Electrodes and holders are contained in an aluminum shielding box of approximately 115 mm x 60 mm x 30 mm, with two holes on the extremities to allow for the insertion of the polymeric line trait. The shielding box is only functional to electromagnetic isolation of the electrodes from the outside environment, and its size was chosen based on the compactness requirement for the cell. Although the cell presented here is a simple version that requires cutting and insertion of the line into the electrodes, a version based on two half-electrodes and two half-boxes to be clamped around the line, without any alteration to it, can be easily manufactured. The line used to contain fluid is a segment of a polymeric biocompatible line used for hemodialysis treatment (ArtiSet blood tubing system, Baxter, Medolla, Italy), with an external diameter of 6.5 mm and an internal diameter of 4 mm. The size of the tubing is fixed by technical requirements for hemodialysis: bloodlines from different companies have very similar sizes.

### 2.2.2 Electrical properties of the biocompatible polymer

Electrical properties of the biocompatible polymeric line were determined by

measuring the impedance of a cut sample placed between two square aluminum electrodes of known area and thickness (15 mm x 15 mm x 1.2 mm), as shown in Fig. 2.3a. An Agilent E4980A Precision LCR Meter (0.3% accuracy in the chosen configuration) was used for impedance measurements in a two-points configuration. This impedance spectroscopy for material analysis was carried out in the 0.8-200 kHz frequency range with a 2V voltage amplitude.

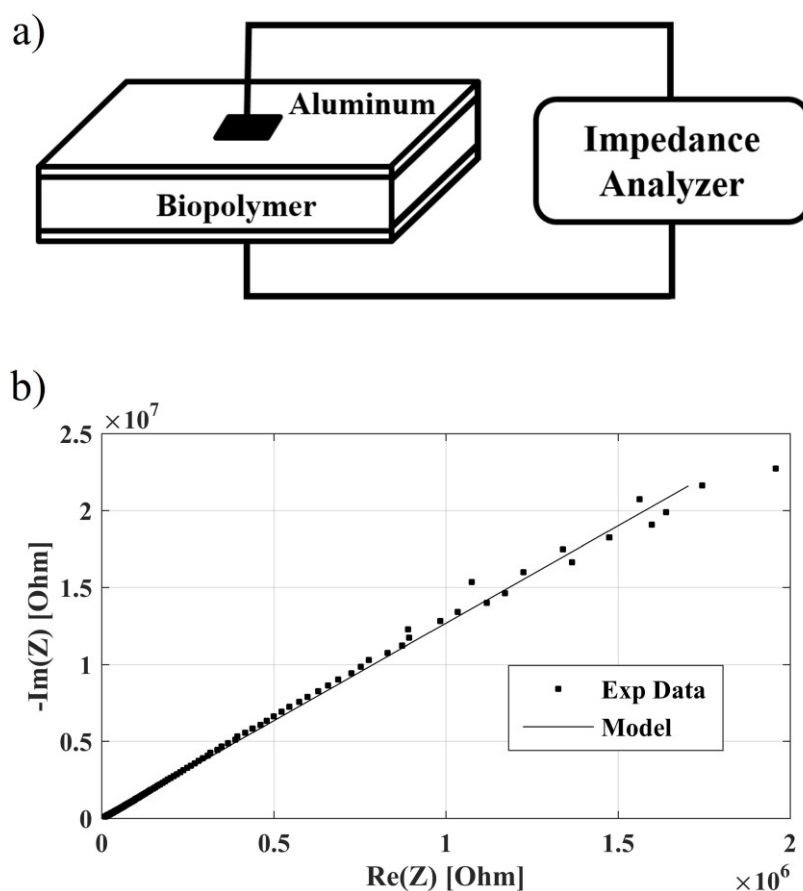


**Fig. 2.3 - Polymer characterization**

(a) Diagram of the polymer characterization process (b) Experimental results and model fitting for polymer characterization. Horizontal axis shows the real part of impedance  $\text{Re}(Z)$ , vertical axis shows the imaginary part of impedance  $\text{Im}(Z)$ . For better illustration, vertical axis is inverted.

The polymeric square was originally prepared to quantify the dielectric constant of the bloodline material on a test sample of known dimensions and size. However, the resulting data, reported in Fig. 2.3b, show that the biopolymeric material behavior is best described in the lumped-parameters domain as a constant

phase element (CPE) [34-36]. CPE is used to describe an imperfect capacitor, with a continuous distribution of time constants. This phenomenon is also called “frequency dispersion of capacitance” [36]. Its physical origin is thought to be fundamentally related to microscopic surface roughness [35], or to electrochemical behaviour at the electrode interface, but is still not completely clear [36]. In our specific case, it may also be related to the composition of the biomedical polymer. The formulation for CPE impedance is described in equation (2.1):  $K$  is the magnitude of the impedance element expressed in Ohm and  $\alpha$  is a dimensionless constant. Asymptotic behavior of the CPE impedance is resistive for  $\alpha \rightarrow 0$  and capacitive for  $\alpha \rightarrow 1$ .

$$Z_{CPE} = \frac{K}{(j\omega)^\alpha} \quad (2.1)$$

The software ZView (Scribner Associates, Inc. Southern Pines, North Carolina, USA) was used to fit spectroscopy data and estimate parameters contained in eq. (2.1), resulting in  $K=67.705 \text{ G}\Omega$  and  $\alpha= 0,94987$ . These model-fitting results refer only to the sample of the biocompatible material and not to the complete device. Fitting results are also shown in Fig. 2.3b. The value of  $\alpha$ , which is close to 1, indicates that the material is very close to being a pure dielectric, but the effect of the CPE behaviour is still significant due to the high value of  $K$ .

### 2.2.3 Preparation of solution samples

For saline solution, five samples composed of ultrapure deionized water and different quantities of sodium chloride (NaCl) were prepared. A 10 - 20 mS/cm conductivity range, which includes conductivity values typical for fluids with physiological concentration of ions (e.g. blood plasma), was explored. To this end, the required NaCl concentration for each sample was calculated according to the concepts of molar conductivity and Kohlrausch's law [1].

For BMF, four samples composed of Intralipid 20% (Fresenius Kabi Italia Srl, Isola della Scala, Italy) and different quantities of NaCl were prepared. To the

best of our knowledge, no commonly-used solution for simulating the electrical properties of whole blood exists: usually BMFs are used to reproduce its optical [37] or fluid-dynamic [38] properties. Intralipid is a fat emulsion used clinically as an intravenously-administered nutrient. It has been used in the past as blood-mimicking fluid for optical experiments [37] due to the presence of spherical scattering particles inside the solution. We choose this solution to simulate the presence of red blood cells inside our fluid. NaCl was added to Intralipid to rise its conductivity from its basic value ( $\approx 0.4$  mS/cm) to the range of 7-15 mS/cm. This range was chosen because whole blood, due to the presence of red blood cells, has a lower total conductivity compared to plasma [39].

The effective conductivity of the samples was then measured at room temperature using a Thermo Orion 150 APlus conductivity meter as gold standard, with temperature correction to normalize conductivity values to 25 °C.

#### **2.2.4 Impedance Spectroscopy**

Impedance measurements in a two-points configuration were carried out using the same instrument employed in section 2.2.2. The terminals of the instrument were connected to the electrodes of the cell and the instrument ground was connected to the external shielding box. Sweep-mode measurements for conductivity estimation were carried out in the 1 - 2 MHz frequency range, with a 2V amplitude. The frequency range was chosen because of an upper and a lower bound. The lower bound was a consequence of the nature of C4D measurements: at low frequencies, the impedance of the coupling electrodes becomes very high, making the measurement of small impedance variations more difficult. We considered 1 MHz a sufficiently high frequency to achieve good sensitivity for our target application. The upper bound is given by the intended final use of our system, which is measurement on whole blood. Blood is subject to  $\beta$ -transition, a change in impedance which occurs at sufficiently high frequencies when current starts flowing inside red blood cells instead of around them [40]. We choose 2 MHz as upper frequency limit, to work in a condition where  $\beta$ -transition is

negligible, as it may lead to more difficult modeling of the effect on hematocrit in future stages of this work.

Impedance spectroscopies were carried out after filling the segment with samples from the prepared saline and BMF solutions. During each measurement, the liquid-filled segment was sealed at both ends with mechanical clamps. The tests were carried out for increasing conductivity values, to avoid contamination from higher ionic concentration samples to low ones. For each sample, 3 measurements were taken within minutes from one another and averaged out. Data were exported and processed in MATLAB (Mathworks, Natick, USA).

### 2.2.5 Lumped-Parameters Modeling

A lumped-parameters model was developed to describe the equivalent electrical behavior of the conductimetry cell; the purpose is to use it to fit experimental results and estimate conductivity of the saline solution.

C4D systems are traditionally modeled with a basic capacitance-resistance-capacitance series circuit as the one shown in Fig. 2.4a, where the capacitances  $C_{E1}$  and  $C_{E2}$  represent the coupling between the external electrodes and the liquid through the containment line, and the resistance  $R_{LP}$  is associated to the resistivity of the liquid.

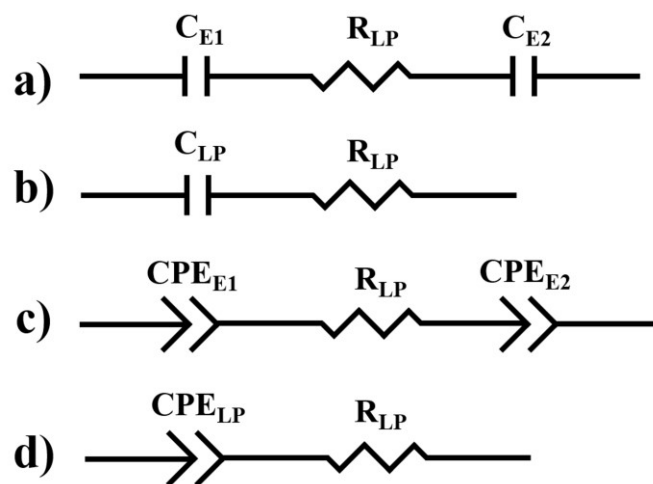


**Fig. 2.4 - Electrical equivalent models**  
 (a-b) typical C4D equivalent electrical model and its simplified version. (c-d) best equivalent model for our cell and its simplified version

The resistive element decreases its value as conductivity of the liquid increases, whereas the parameters of the coupling elements are assumed to be constant. Under the hypothesis of a sufficiently accurate manufacturing process, the two electrodes have equal capacitance and can be represented by a single equivalent capacitor  $C_{LP}$  as shown in the simplified resistance-capacitance (R-C) model of Fig. 2.4b. Mathematical formulation for the R-C model is:

$$Z_{LP}(j\omega) = R_{LP} + \frac{1}{j\omega C_{LP}} \quad (2.2)$$

In our specific case, though, the characterization of the electrical properties of the polymeric material led to the decision to replace the two capacitances  $C_{E1}$  and  $C_{E2}$  with two CPE elements, for a better description of the coupling process through polymeric line (Fig 2.4c). The CPE behavior is reasonably attributable to a non-purely dielectrical interaction between the biocompatible line and the aluminum electrode. Although this phenomenon was at first unexpected, the use of spectroscopic characterization as part of the measurement procedure allowed us to estimate conductivity of the solution, independently from the presence of CPEs instead of pure capacitances. Because coupling can be assumed to be the same for both electrodes (with negligible manufacturing differences), the model can be further simplified with the series equivalent of the two CPE elements (R-CPE model, Fig. 2.4d). The impedance of this model is:

$$Z_{LP}(j\omega) = R_{LP} + \frac{K_{LP}}{(j\omega)^{\alpha_{LP}}} \quad (2.3)$$

Spectroscopy data was fitted using the ZView software, as done in section 2.2.2 for the polymeric sample. For comparison, spectroscopy data collected with saline solution samples was fitted to both the R-C model described by eq. (2.2) and R-CPE model described by eq. (2.3), although the R-CPE model proved to be the best choice. For this reason, BMF data was directly fitted only with the R-CPE model.

### 2.2.6 Frequency range reduction analysis

As described in section 2.2.4, the frequency range for impedance measurement was chosen by considering the requirements of the C4D technique and the electric properties of blood. The modeling process in section 2.2.5 was, at first, carried out on the whole spectroscopy dataset in the 1-2 MHz range. However, the modeling process is also the foundation of our conductivity estimation method: for this reason, we analyzed the robustness of the method on narrower frequency ranges. We repeated the R-CPE modeling-based estimation process on three subsets of the original dataset using a 100 KHz range (0.1 MHz, 1/10<sup>th</sup> of the original range), to evaluate the effect of the range-narrowing process at the lower (1.0-1.1 MHz), middle (1.45-1.55 MHz) and upper end (1.9-2.0 MHz) of the dataset. This range reduction analysis was done for both the saline and BMF datasets.

## 2.3 Results

As previously described, the first set of measurements and analyses was carried out with saline solution samples. Reference conductivity  $\sigma_{\text{Sol}}$  for the five saline solution samples was 10.50, 12.99, 15.52, 17.98 and 20.6 mS/cm.

Fig. 2.5 reports impedance spectroscopy results on the complex plane. As described in section 2.2.4 and shown in the inset of Fig. 2.5, three complete frequency sweeps were carried out for each conductivity value, to assess the repeatability of the measurement process. It can be noticed that the cell response to an increase in frequency is a reduction in the impedance magnitude and the conservation of a constant phase. The reduction in the real part of impedance as a response to the increase in measurement frequency is the clearest indicator of the CPE behavior. The asymptotic value of impedance magnitude for infinite frequency is different from zero due to the presence of the saline solution's resistive effect.

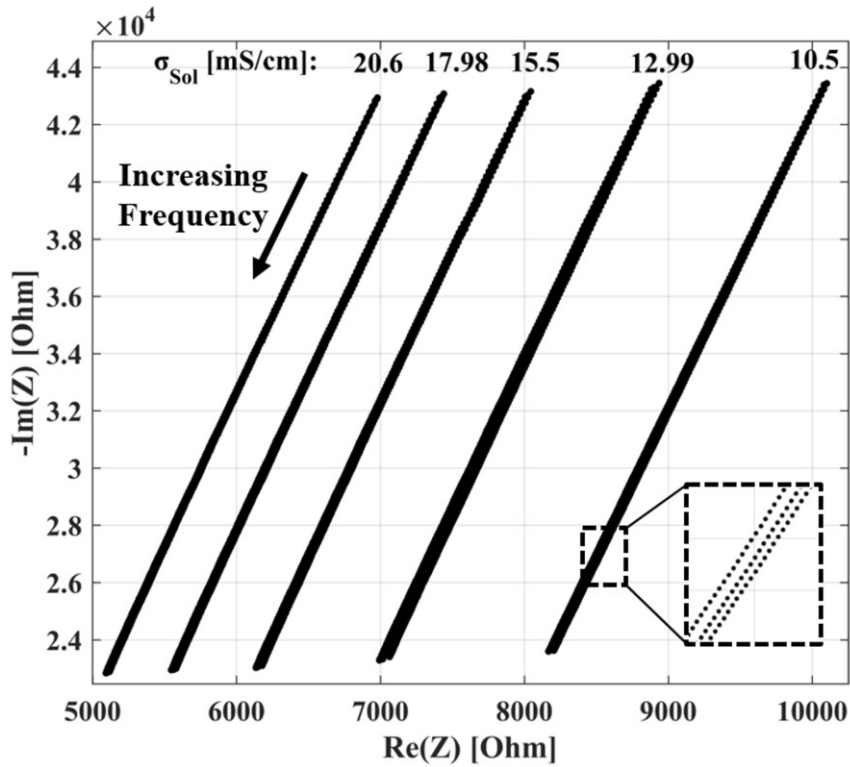


**Fig. 2.5 - Impedance spectroscopy results for saline solution samples**

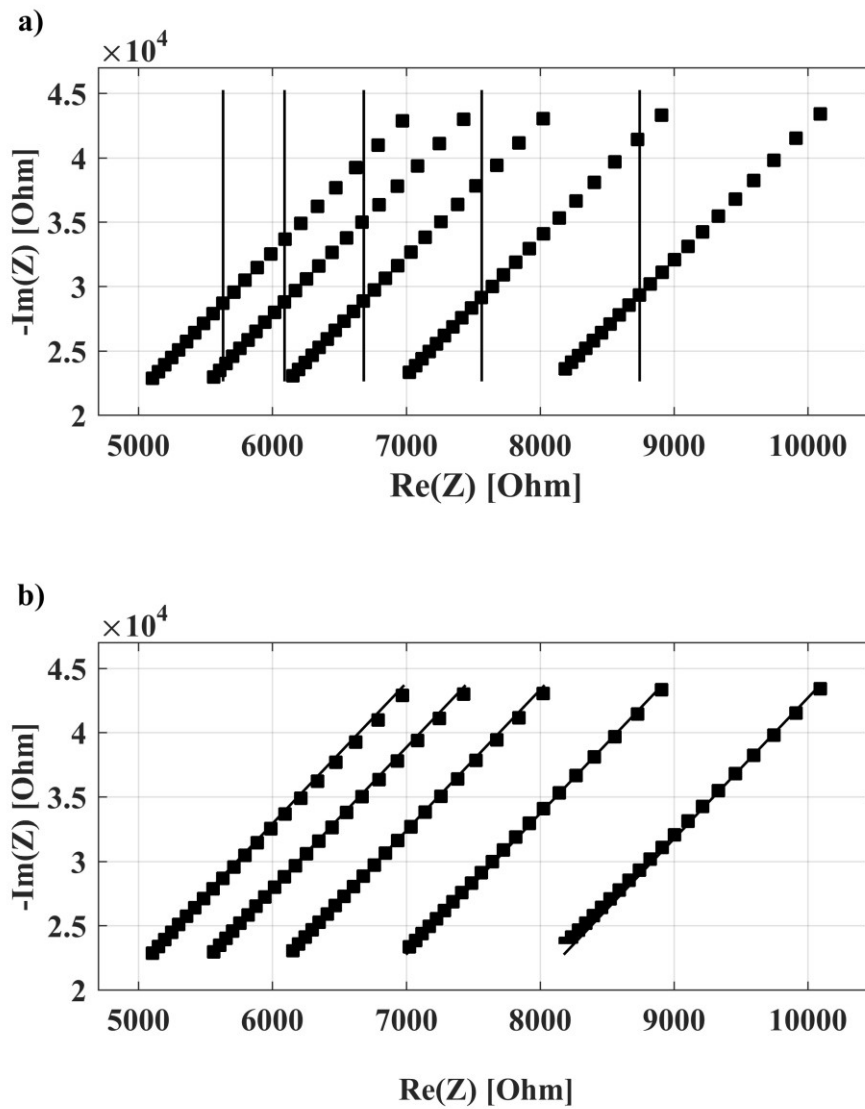
Results of experimental impedance spectroscopies in the 1-2 MHz range performed on the conductivity cell with different conductivity values of the solution. Horizontal axis shows the real part of impedance  $\text{Re}(Z)$ , vertical axis shows the imaginary part of impedance  $\text{Im}(Z)$ . For better illustration, vertical axis is inverted. Inset: detail of the three frequency sweeps carried out for each conductivity value.

Fig. 2.5 shows that the developed system can detect changes in the conductivity of fluid without direct contact with the fluid itself, effectively achieving our target. Changes in a physiological range of conductivities correspond to evident changes in the real part of the total impedance.

Result from fitting experimental spectroscopies in the complete measurement frequency range with the R-C and R-CPE model are shown in Fig. 2.6.

R-C fitting returned  $C_{\text{LP}}=3.56$  pF, referring to eq. (2.2). R-CPE fitting returned  $K_{\text{LP}}=8.9934$  T $\Omega$  and  $\alpha_{\text{LP}}=0.942$ , referring to eq. (2.3). Due to  $R_{\text{LP}}$  being the resistance associated with the current path through the liquid, its value is dependent on the value of  $\sigma_{\text{sol}}$ . Values of  $R_{\text{LP}}$  obtained when fitting data with the R-C and R-CPE models are reported in Table 2.1, which also reports estimated values with the R-CPE model when narrower frequency ranges are employed, as described in section 2.2.6.

Results of the fitting procedure are consistent with the preliminary results obtained in section 2.2.2 for the characterization process of the polymeric material.



**Fig. 2.6 - Model fitting of experimental data for saline solution samples**  
 Fitting of experimental data (dots) with lumped-parameters models (lines). (a) Fitting with R-C model. (b) Fitting with R-CPE model. In both panels, horizontal axis shows the real part of impedance  $\text{Re}(Z)$  and vertical axis shows the imaginary part of impedance  $\text{Im}(Z)$ . For better illustration, in each panel vertical axis is inverted. For the same purpose, only 1 every 10 data points is reported in figure for each spectroscopy.

TABLE 2.1  
FITTING OF RESISTANCE ELEMENT IN LUMPED-PARAMETERS MODELING FOR SALINE SOLUTION

<i>Frequency Range</i>	<i>R<sub>LP</sub> (R-C model)</i> [ $\Omega$ ]	<i>R<sub>LP</sub> (R-CPE model)</i> [ $\Omega$ ]	$\sigma_{Sol,Exp}$ [mS/cm]	$\sigma_{Sol,Est}$ [mS/cm]	$\sigma$ error (r.m.s.) [mS/cm]
<i>Complete</i> (1.0-2.0 MHz)	8746	6099	10.50	10.56	0.0566
	7565	4921	12.99	12.89	
	6683	4042	15.52	15.50	
	6091	3452	17.98	18.00	
	5631	2994	20.60	20.62	
<i>Low</i> (1-1.1 MHz)	-	6016	10.50	10.60	0.0696
	-	4830	12.99	12.88	
	-	3946	15.52	15.48	
	-	3352	17.98	17.99	
	-	2894	20.60	20.64	
<i>Middle</i> (1.45-1.55 MHz)	-	6126	10.50	10.5705	0.0545
	-	4945	12.99	12.8943	
	-	4063	15.52	15.5111	
	-	3473	17.98	18.0034	
	-	3015	20.60	20.6107	
<i>High</i> (1.9-2.0 MHz)	-	6209	10.50	10.56	0.0488
	-	5043	12.99	12.90	
	-	4170	15.52	15.52	
	-	3579	17.98	18.01	
	-	3121	20.60	20.60	

Value of  $\alpha_{LP}$  from eq. (2.3) shows only a small difference compared to the value of  $\alpha$  in eq. (2.1), and the difference between  $K_{LP}$  from eq. (2.3) and  $K$  from eq. (2.1) can be ascribed to the different geometries of the systems under analysis. The gap between the estimated  $R_{LP}$  values for the two models can be easily explained by the fact that in the R-C case, the fitting algorithm is forced to fit the CPE behavior of the AC coupling to a purely capacitive element. To do so and minimize fitting error,  $R_{LP}$  is improperly adjusted for compensation. It is clear from Fig. 2.6a that the traditional R-C model typically employed in C4D applications is not a good choice for our system because a purely capacitive coupling cannot correctly describe the frequency dispersion in the real part of impedance. Fig. 2.6b shows that the R-CPE model is a much better solution and describes very well the behavior of the cell in the chosen frequency range.

To quantify the goodness-of-fit of the R-C and R-CPE models, we used a mathematical formulation based on the deviation of model impedance values from the experimental data points. This formulation, reported in eq. (2.4), was used to

calculate relative dispersion for each frequency and conductivity value of the dataset.

$$E = \sqrt{\left(\frac{\text{Re}\{Z_{MOD}\}-\text{Re}\{Z_{EXP}\}}{\text{Re}\{Z_{EXP}\}}\right)^2 + \left(\frac{\text{Im}\{Z_{MOD}\}-\text{Im}\{Z_{EXP}\}}{\text{Im}\{Z_{EXP}\}}\right)^2} \quad (2.4)$$

Mean relative dispersion on the whole dataset was calculated for each model for the purpose of comparison of model performances in reproduction of experimental data, resulting in  $E_{C,Mean}=0.0667$  and  $E_{CPE,Mean}=0.0100$ . The resulting mean relative dispersion is 6.67 times higher for the R-C model compared to the R-CPE model. The ratio between the two dispersions demonstrates quantitatively that the R-CPE fits better the experimental data, which is already qualitatively evident from Fig. 2.6a-b.

From this point on,  $R_{LP}$  refers to the resistance element of the R-CPE model. Resistance  $R_{LP}$  is related to the conductivity of the solution by the internal cylindrical geometry of the tubing: for this reason, the relationship between admittance  $G_{LP}$ , the reciprocal of  $R_{LP}$ , and  $\sigma_{Sol}$  was investigated. Such relationship is theoretically linear. Because of the aim of the work, which is to estimate conductivity  $\sigma_{Sol}$  starting from the impedance spectroscopy results, linear regression was used to estimate conductivity  $\sigma_{Est}$  of the solution from the admittance values of  $G_{LP}$ . Fig. 2.7 summarizes the steps of the conductivity estimation process. Fig. 2.8 shows the correlation between reference conductivity  $\sigma_{Sol}$  (measured with Thermo Orion 150 APlus) and conductivity  $\sigma_{Est}$  linearly estimated from  $G_{LP}$ . Calculations yielded a root mean square (r.m.s.) error of 0.0566 mS/cm on the complete frequency range.

By applying Ohm's second law to  $R_{LP}$  and  $\sigma_{Sol}$  values, the average detection path length was found to be  $\approx 7.9$ cm. This value is slightly higher than the center-to-center distance between electrodes since the entire electrodes surface contributes to the flow of current, even if the current density is not constant over the electrode. As a result, applying the Ohm's second law to  $R_{LP}$  and  $\sigma_{Sol}$  must give a mean detection path value comprised between the start-to-start distance

(i.e. 5 cm) and the end-to-end distance (i.e. 9 cm).

The second set of measurements was carried out using the BMF described in section 2.3. Reference conductivity  $\sigma_{Sol}$  for the four BMF samples was 7.19, 9.66, 12.77, 14.15 mS/cm.

Table 2.1 reports estimated conductivity values and r.m.s. errors of the saline solution dataset for the complete and for the reduced frequency ranges.

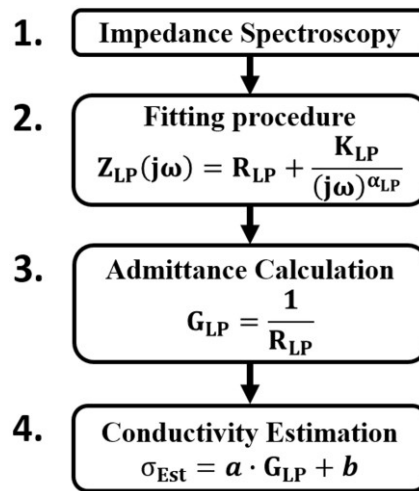


**Fig. 2.7 - Conductivity estimation**  
Steps of the model-based conductivity estimation process

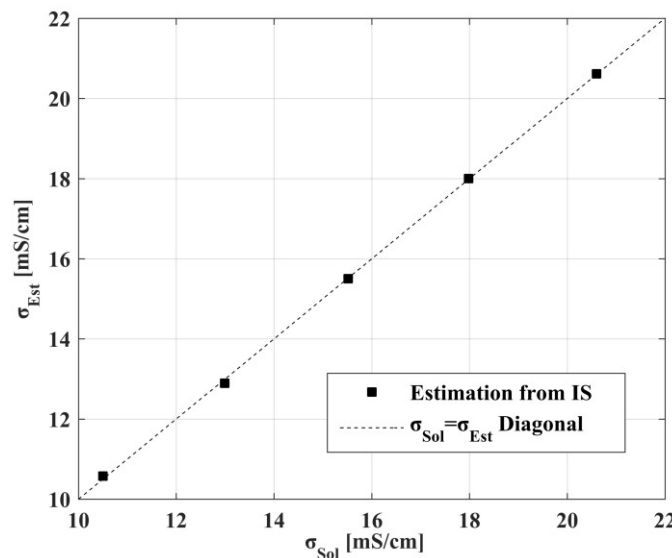


**Fig. 2.8 - Conductivity estimation results for saline solution samples**  
Correlation between experimentally measured conductivity of the saline solution ( $\sigma_{Sol}$ ) and conductivity values estimated from model admittance ( $\sigma_{Est}$ ) is reported by dots. Ideal results (estimated=experimental) are shown as reference by the slashed line.

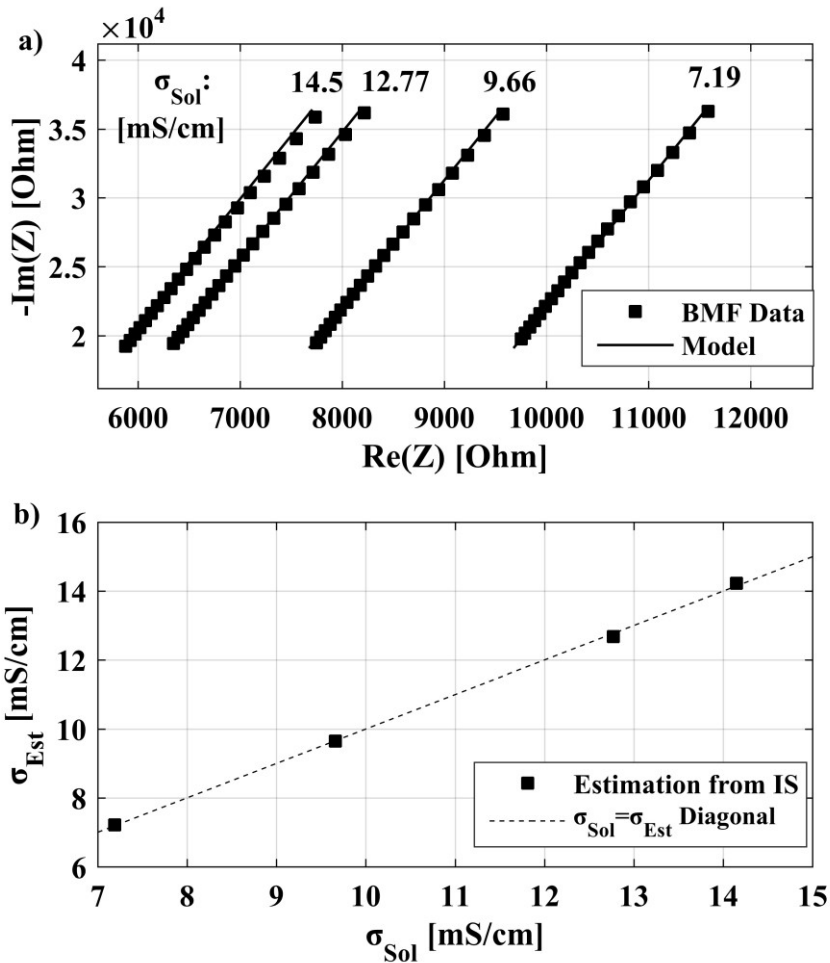


**Fig. 2.9 - Model fitting and conductivity estimation for BMF data**

(a) Fitting of BMF experimental data (dots) with the lumped-parameters R-CPE model (lines). For better illustration, only 1 every 10 data points is reported in figure for each spectroscopy. (b) Correlation between experimentally measured conductivity of BMF and conductivity values estimated from model admittance (dots), with ideal results (estimated=experimental) as reference (slashed line).

Fig. 2.9a shows impedance spectroscopy results for BMF and model-fitting results obtained with the R-CPE model. Fitting was carried out directly with the R-CPE model, given the shape of complex impedance data: the trend in response to different frequencies is similar to that of the saline solution spectroscopies reported in Fig. 2.5 and Fig. 2.6, which were shown to be better represented by the R-CPE model.

R-CPE fitting returned  $K_{\text{LP}}=78.16 \text{ G}\Omega$  and  $\alpha_{\text{LP}}=0.9310$ , referring to eq. (2.3).

The disparity between these fitting values and those extracted in measurements with saline samples will be discussed in the next section.

Values of  $R_{LP}$  for the BMF data are reported in Table 2.2, along with estimated values for narrower frequency ranges.

TABLE 2.2  
FITTING OF RESISTANCE ELEMENT IN LUMPED-PARAMETERS MODELING FOR BLOOD-MIMICKING FLUID

<i>Frequency Range</i>	$R_{LP}$ (R-CPE model) [ $\Omega$ ]	$\sigma_{Sol,Exp}$ [mS/cm]	$\sigma_{Sol,Est}$ [mS/cm]	$\sigma$ error (r.m.s.) [mS/cm]
<i>Complete</i> (1.0-2.0 MHz)	7599	7.19	7.21	0.0608
	5596	9.66	9.65	
	4216	12.77	12.68	
	3744	14.15	14.22	
<i>Low</i> (1-1.1 MHz)	7464	7.19	7.22	0.0789
	5456	9.66	9.65	
	4096	12.77	12.65	
	3616	14.15	14.25	
<i>Middle</i> (1.45-1.55 MHz)	7620	7.19	7.21	0.0594
	5617	9.66	9.66	
	4239	12.77	12.68	
	3767	14.15	14.22	
<i>High</i> (1.9-2.0 MHz)	7773	7.19	7.21	0.0453
	5770	9.66	9.66	
	4372	12.77	12.70	
	3904	14.15	14.21	

The same conductivity estimation procedure used for saline solutions, based on linear regression and schematized in Fig. 2.7, was applied to BMF data, with the results shown in Fig. 2.9b. Table 2.2 also reports estimated conductivity values and r.m.s. errors of the BMF solution for the complete and for the reduced frequency ranges.

By applying Ohm's second law to the  $R_{LP}$  and  $\sigma_{Sol}$  values for BMF, the average detection path length was found to be  $\approx 6.8$ cm.

## 2.4 Discussion

In this work, we developed a conductivity cell that allows the estimation of the conductivity of a fluid without direct contact between the liquid and the

measurement electrodes. The cell exploits the principles of capacitive coupling and impedance spectroscopy, and avoids the use of disposable electrodes or their periodical sterilization. The cell was designed to work in conjunction with biocompatible polymeric lines used for hemodialysis applications. The range of conductivities chosen for testing reflects this biomedical application: the 10-20 mS/cm range comprehends the conductivity values of medical saline solutions and human plasma in normal physiological conditions, whereas the lower 7-15 mS/cm range is closer to the physiological conductivity of whole blood, which is lower than plasma. A typical full-scale measurement range for plasmatic conductivity estimation is, as reported in the Introduction, the 13-16 mS/cm range. The exact relationship between plasma and blood conductivity is dependent on the hematocrit.

Regarding the dimensions of the system, the main boundary in cell design was, as explained in the Methods section, the compactness required to allow on-board use on hemodialysis machines. However, some words can be spent on the effects of geometrical parameters on sensors response. Cell geometry has been analyzed in several C4D papers both theoretically and experimentally (see for example [10] and [20-23]) and we can expect the results to carry over, conceptually, to our larger cell. The main geometrical effects regard electrodes. An increase in electrode length also increases coupling surface, effectively decreasing amplitude of the CPE element and its weight on total impedance of the sensors. Increasing the distance between electrodes has a two-fold effect: on one side, it increases resistance of the solution due to Ohm's second law, because the current path is longer. This is a positive effect, as it increases the weight of conductivity of the liquid on the total cell impedance, increasing sensitivity. However, given the same voltage amplitude, the picked up current in the case of longer path is weaker due to the higher resistance. This may be a problem with custom measurement circuits as it can affect the signal-to-noise ratio. Short distance between the electrodes also leads to additional current flow paths across air instead of liquid, which means that stray capacitances are present. For this reason, length and distance should both be increased when possible, but within reasonable limits.

The LP model gives a simple method for conductivity estimation from impedance measurement results. Although the quality of the lumped-parameters model is critical, the goodness-of-fit approach we developed demonstrated that the proposed cell, together with the R-CPE LP model, estimates the conductivity with a global r.m.s. error of 0.057 mS/cm on saline solution and 0.061 mS/cm on BMF, which correspond respectively to  $\approx 0.5\%$  and  $\approx 0.6\%$  of the measurement range. This accuracy is comparable to that of the laboratory conductivity meter used as gold standard and is also in line with the accuracy of the current estimation systems. This result demonstrates the effectiveness of the developed system and its practical usefulness in a clinically relevant measurement range.

Also, analysis of the conductivity estimation process on narrower subset of the chosen frequency range resulted in similar r.m.s. errors for each subset, for both saline solution and BMF. A slight trend of lower error with increasing frequency was noticed for both fluids ( $\approx 0.4\%$  error in the higher-end subset). This result shows the robustness of our modeling-based estimation processes, which can be applied using just  $1/10^{\text{th}}$  of the original frequency range.

The use of a CPE, instead of a standard capacitance, in the LP model is a key aspect for the proposed method, since the impedance spectroscopy approach allows accurate estimation of conductivity regardless of the AC coupling behavior.

The estimation of different  $K_{LP}$  and  $\alpha_{LP}$  values for the saline and BMF datasets, along with the different estimated path length (7.9 cm for saline solution and 6.7 cm for BMF) are indicators of the fact that the nature of the fluid inside the line affects the coupling process. In our specific case, particles with dielectric properties are suspended inside the solution. Although each dataset is self-consistent regarding conductivity estimation, a calibration process for CPE parameters may be needed in future stages of the work if different fluids are expected to flow inside the line.

In the last stage of the estimation process, conductivity is computed starting from admittance of the liquid. According to Ohm's second law, only a scaling coefficient is needed for this task, to account for the geometry of the conductor.

However, by using linear regression, we carried out this procedure by determining both a gain factor and an offset coefficient. The presence of the offset coefficient, which in practical terms correspond to an additional parameter in the model, provides an additional degree of freedom in fitting the experimental data, without excessively increasing the complexity of the model. In future stages of this work, the possibility of removing this parameter will be evaluated depending on its effect on sensitivity.

Our system provides a significant increase in measurement speed and repetition with respect to the traditional method. The time required for multiple averaged frequency sweeps and the consequent model-fitting procedure is less than one minute, while the Polaschegg protocol usually requires 10-minutes so as to get a good estimate. Moreover, the traditional method cannot be used too frequently because it perturbs blood electrolytes concentrations: our method, being non-invasive, is limited in repetition only by the sampling time of the individual measurement.

The accuracy of the proposed conductivity cell can be enhanced using a 4-point approach but it leads to an increase in complexity, economic cost and physical space occupied by the cell. The accuracy reached by our 2-point system is sufficient for the biomedical target application, and an increase in volume would have a negative impact on the compactness of the sensor bar of the hemodialysis machine. From a cost/benefit standpoint, it is better to improve the accuracy through a calibration procedure rather than complicating the system.

## **2.5 Conclusions**

In conclusion, the proposed system is a promising tool in hemodialysis conductivity estimation, with the important properties of non-invasiveness, compactness and direct fast continuous estimation.

Future objectives regarding this work include the development of a portable device to carry out impedance spectroscopy in the required frequency range and the modeling and experimental investigation of the effect on measurements of

transition from saline solutions and BMF to real blood. An in-depth electrochemical analysis may also be useful to characterize in more detail the possible interaction effects at the polymer/liquid interface.

In this chapter, a new measurement technology, capable of monitor plasmatic conductivity directly on the bloodline, was proposed. In the next chapter, a different approach will be introduced: Chapter 3 shows how it is possible to act on pre-existing sensors to improve the quality of measurements.

## 2.6 References

- [1] R. H. Stokes and R. A. Robinson, *Electrolyte Solutions*, Second Revised Edition, Dovers Publications, 2002.
- [2] S. Zheng, M. S. Nandra, C.-Y. Shih, W. Li, and Y.-C. Tai, "Resonance impedance sensing of human blood cells," *Sensor Actuat A-Phys*, vol. 145–146, pp. 29-36, 7, 2008.
- [3] M. Wolf, R. Gulich, P. Lunkenheimer, and A. Loidl, "Broadband dielectric spectroscopy on human blood," *Biochim Biophys Acta*, vol. 1810, pp. 727-40, Aug 2011.
- [4] J. Rosell, J. Colominas, P. Riu, R. Pallas-Areny, and J. G. Webster, "Skin impedance from 1 Hz to 1 MHz," *IEEE Trans Biomed Eng*, vol. 35, pp. 649-51, Aug 1988.
- [5] <http://www.advancedrenaleducation.com/article/hemodialysis>, last accessed on 08 January 2016
- [6] A. R. Nissenson and R. N. Fine, *Clinical Dialysis*, Fourth Edition. McGraw-Hill, 2005.
- [7] C. Ronco, P. M. Ghezzi, A. Brendolan, C. Crepaldi, and G. La Greca, "The haemodialysis system: basic mechanisms of water and solute transport in extracorporeal renal replacement therapies," *Nephrol Dial Transpl*, vol. 13 Suppl 6, pp. 3-9, 1998.
- [8] F. Locatelli, S. Di Filippo, and C. Manzoni, "Relevance of the conductivity kinetic model in the control of sodium pool," *Kidney Int Suppl*, vol. 76, pp. S89-95, Aug 2000.
- [9] H. D. Polaschegg, "Automatic, noninvasive intradialytic clearance measurement," *Int J Artif Organs*, vol. 16, pp. 185-91, Apr 1993.
- [10] P. Kuban and P. C. Hauser, "Ten years of axial capacitively coupled contactless conductivity detection for CZE--a review," *Electrophoresis*, vol. 30, pp. 176-88, Jan 2009.
- [11] P. Kuban and P. C. Hauser, "Contactless conductivity detection for analytical techniques: developments from 2010 to 2012," *Electrophoresis*, vol. 34, pp. 55-69, Jan 2013.
- [12] P. Kuban and P. C. Hauser, "Contactless conductivity detection for analytical techniques-developments from 2012 to 2014," *Electrophoresis*, vol. 36, pp. 195-211, Jan 2015.
- [13] P. Muller, "Contactless determination of the conductivity in semi-insulators," *Phys. Status Solidi (a)*, vol. 78, pp 41-51, 1983
- [14] R. Stibal , J. Windscheif and W. Jantz, "Contactless evaluation of semi-insulating GaAs wafer resistivity using the time-dependent charge measurement," *Semicond. Sci. Technol.*, vol. 6, pp 955-1001, 1991
- [15] R. Stibal, U. Kretzer and W. Jantz, "Contactless electron mobility evaluation of semi-insulating GaAs and InP wafers," *Digest of GaAs MANTECH (San Diego)*, p 75, 2002
- [16] J. Krupka, "Contactless methods of conductivity and sheet resistance measurement for semiconductors, conductors and superconductors," *Meas. Sci. Technol.*, vol 24 (2013) 062001
- [17] A. A. Elbashir and H. Y. Aboul-Enein, "Applications of capillary electrophoresis with capacitively coupled contactless conductivity detection (CE-C4D) in pharmaceutical and biological analysis," *Biomed Chromatogr*, vol. 24, pp. 1038-44, Oct 2010.
- [18] A. A. Elbashir and H. Y. Aboul-Enein, "Recent advances in applications of capillary electrophoresis with capacitively coupled contactless conductivity detection (CE-C(4)D): an update," *Biomed Chromatogr*, vol. 26, pp. 990-1000, Aug 2012.
- [19] A. A. Elbashir and H. Y. Aboul-Enein, "Recent applications and developments of capacitively coupled contactless conductivity detection (CE-C4D) in capillary electrophoresis," *Biomed Chromatogr*, vol. 28, pp. 1502-6, Nov 2014.
- [20] P. Tuma, F. Opekar, and K. Stulik, "A contactless conductivity detector for capillary electrophoresis: effects of the detection cell geometry on the detector performance," *Electrophoresis*, vol. 23, pp. 3718-24, Nov 2002.
- [21] P. Kuban and P. C. Hauser, "Fundamental aspects of contactless conductivity detection for capillary electrophoresis. Part I: Frequency behavior and cell geometry.," *Electrophoresis*, vol. 25, pp. 3387-97, Oct 2004.
- [22] P. Kuban and P. C. Hauser, "Fundamental aspects of contactless conductivity detection for capillary electrophoresis. Part II: Signal-to-noise ratio and stray capacitance," *Electrophoresis*, vol. 25, pp. 3398-405, Oct 2004.

- [23] P. Kuban and P. C. Hauser, "Effects of the cell geometry and operating parameters on the performance of an external contactless conductivity detector for microchip electrophoresis," *Lab Chip*, vol. 5, pp. 407-15, Apr 2005.
- [24] J. G. A. Brito-Neto, J. A. Fracassi da Silva, L. Blanes, and C. L. do Lago, "Understanding Capacitively Coupled Contactless Conductivity Detection in Capillary and Microchip Electrophoresis. Part 2. Peak Shape, Stray Capacitance, Noise, and Actual Electronics," *Electroanal*, vol. 17, pp. 1207-1214, 2005.
- [25] L. Honghua, C. Jianjun, Y. Jun, L. Yu, and Y. Jinqiao, "Micro-Conductivity Rapid Detection Research of Electrophoresis Chip Based on Orthogonal Vector Lock-In Amplifier on FPGA," in *Proc. CiSE 2009*, pp. 1-4.
- [26] L. Honghua, L. Yu, Y. Jinqiao, and H. Yong, "Study of orthogonal vector lock-in amplifier in contactless conductivity detector of electrophoresis microchip," in *Proc. ICCASM 2010*, pp. V3-203-V3-207.
- [27] W. Baoliang, C. Majing, J. Haifeng, H. Zhiyao, and L. Haiqing, "Capacitively coupled contactless conductivity detection based on phase-sensitive demodulation principle," in *Proc. IEEE ICCA 2013*, pp. 547-550.
- [28] Z. Huang, W. Jiang, X. Zhou, B. Wang, H. Ji, and H. Li, "A new method of capacitively coupled contactless conductivity detection based on series resonance," *Sensor Actuat B-Chem*, vol. 143, pp. 239-245, 2009.
- [29] Z. Huang, J. Long, W. Xu, H. Ji, B. Wang, and H. Li, "Design of capacitively coupled contactless conductivity detection sensor," *Flow Meas Instrum*, vol. 27, pp. 67-70, 2012.
- [30] F. Sanfu, W. Baoliang, J. Haifeng, H. Zhiyao, and L. Haiqing, "A contactless conductivity sensor based on capacitively coupled principle," in *Proc. ICECE 2011*, pp. 9-11.
- [31] H. Ji, Z. Li, B. Wang, Z. Huang, H. Li, and Y. Yan, "Design and implementation of an industrial C4D sensor for conductivity detection," *Sensor Actuat A-Phys*, vol. 213, pp. 1-8, 2014.
- [32] H. Ji, Y. Lyu, B. Wang, Z. Huang, H. Li, and Y. Yan, "An improved capacitively coupled contactless conductivity detection sensor for industrial applications," *Sensor Actuat A-Phys*, vol. 235, pp. 273-280, 2015.
- [33] F. Opekar, P. Tüma, and K. Štulík, "Contactless impedance sensors and their application to flow measurements," *Sensors (Switzerland)*, vol. 13, n. 3, pp. 2786-2801, 2013.
- [34] H. Morgan and N. G. Green, "AC Electrokinetics: colloids and nanoparticles," Research Studies Press LTD., 2003.
- [35] G. J. Brug, A. L. G. van den Eeden, M. Sluyters-Rehbach, and J. H. Sluyters, "The analysis of electrode impedances complicated by the presence of a constant phase element," *J Electroanal Chem*, vol. 176, pp. 275-295, 1984/09/25 1984.
- [36] P. Zoltowski, "On the electrical capacitance of interfaces exhibiting constant phase element behaviour," *J Electroanal Chem*, vol. 443, pp. 149-154, Oct 1998.
- [37] H.J. van Staveren, C.J. Moes, J. van Marie, S.A. Prah, M.J. van Gemert, "Light scattering in Intralipid-10% in the wavelength range of 400-1100 nm," *Appl Opt*, vol. 30, issue 31, pp. 4507-14.
- [38] H. Samavat and J. A. Evans, "An ideal blood mimicking fluid for doppler ultrasound phantoms," *J Med Phys*, vol. 31, issue 4, pp. 275-278, Oct-Dec 2006.
- [39] K.R. Visser, "Electric conductivity of stationary and flowing human blood at low frequencies," *Med Biol Eng Comput*, vol. 30, issue 6, pp. 636-4, Nov 1992.
- [40] M. Wolf, R. Gulich, P. Lunkenheimer, A. Loidl, "Broadband Dielectric Spectroscopy on Human Blood," *Biochim Biophys Acta*, 1810(8), pp. 727-40, Aug 2011

# Chapter 3

## **Estimation of relative blood volume and plasmatic sodium concentration during hemodialysis**

In this chapter, a new system for the conjoined estimation of two important hemodialysis-related physiological variables is presented. The system employs a mathematical estimator based on the widely known Kalman filter theory to merge data from multiple sensors, both newly-designed and already on-board, with modeling knowledge about the hemodialysis process. The estimation accuracy for both variables proved to be comparable with that of reference data and, in general, high enough for relevance in a clinical context.

The inclusion of plasmatic sodium as a state variable in our estimator constitutes an addition or alternative to the approach presented in Chapter 2 regarding direct measurement of plasmatic conductivity on the bloodline tubing, given that sodium is one of the main determinants of plasmatic conductivity.

The content of this chapter is based on the article “A New Method for Continuous Relative Blood Volume and Plasmatic Sodium Concentration Estimation during Hemodialysis”, by Enrico Ravagli, Mattias Holmer, Leif Sornmo, and Stefano Severi. At the time of writing (March 2017) the article is in preparation for submission to a scientific journal of the biomedical engineering field.

## **Abbreviations**

$\Delta$ RBV: Relative blood volume loss

$\sigma_{PI}$ : Plasmatic conductivity

CKI: Chronic kidney injury

D: Dialysance

Hgb: Hemoglobin

RBC: Red blood cell

UF: Ultrafiltration

## **Keywords:**

Hemodialysis; Blood; Optical sensor; Optical measurements; Kalman filter;  
Relative blood volume; Sodium.

### 3.1 Introduction

Hemodialysis is a therapy employed for treating patients with chronic kidney injury (CKI) [1-2], usually performed 3–4 times a week and lasting 3–5 hours. The treatment has three main goals of which the first is to remove excess body water accumulated between sessions. This goal is achieved by ultrafiltration (UF), a process for the removal of liquid from blood. The second goal is to remove uremic toxins, also accumulated between subsequent sessions. The third goal is to restore the proper balance of electrolytes in the blood, so as to maintain the body homeostasis. Hemodialysis is based on the two phenomena of diffusion and convection, which allow mass transfer of water and solutes across the membrane of the hemodialysis filter (hemodialyzer) [3] is achieved. The hemodialyzer is a cylindrical bundle of hollow fibers designed to maximize the exchange surface area. Inside, blood and dialysis fluid (dialysate) flow in counter-current on opposite sides of the membrane [4].

In modern hemodialysis, much emphasis has been placed on the development of non-invasive methods for the collection of physiological information, carried out either by applying sensors directly on the patient [5] or by accessing the hemodialysis machine [6–7] during the treatment. In addition to being important for patient safety and for clinical knowledge gathering, continuous or semi-continuous monitoring of physiological parameters plays a key role as input to biofeedback systems [8–11].

Examples of physiological parameters subject to investigation are relative blood volume loss ( $\Delta RBV$ ), dialysance ( $D$ ) and plasmatic electrical conductivity ( $\sigma_{PI}$ ).  $\Delta RBV$  quantifies the effect of UF and vascular refilling, and is continuously monitored by optical [12–14] or ultrasonic [14–16] means. The parameter  $D$  quantifies dialysis efficiency, and can change during treatment.  $\sigma_{PI}$  is a surrogate for plasmatic sodium concentration  $Na_{PI}$ , which currently cannot be measured in a direct, continuous and non-invasive way. Both  $D$  and  $\sigma_{PI}$  are estimated at fixed time intervals during treatment by applying conductivity steps to the inlet dialysate and measuring the outlet dialysate conductivity response [17–18].

Optical  $\Delta$ RBV estimation is based on the absorbance of hemoglobin (Hgb), which is almost completely contained inside the red blood cells (RBCs). In simple optical sensors, a LED and a photodiode are used to detect absorbance changes linked to variations in RBC concentration. The number of RBCs is nearly constant during treatment, so hemoconcentration is mainly caused by a water removal due to UF that is larger than the plasma-refilling rate. Recently, it was reported that  $\Delta$ RBV estimation by optical sensors is afflicted by a cross-sensitivity to changes in concentration of electrolytes [19-20]. Drastic changes in dialysate sodium concentration can lead to under- or overestimation of  $\Delta$ RBV. Such changes can be explained by considering the action of osmolarity on RBC volume. Sodium, being one of the highest-concentrated solutes in both dialysate and plasma, is a main driver of osmolarity. Dialysate sodium variations propagate to plasma due to diffusion across the hemodialyzer membrane. Consequently, a water shift takes place across the membrane of RBCs to balance inner and outer osmolarity, thereby changing their volume. This volume variation alters local Hgb concentration and leads to a modification of the absorbance and scattering properties of blood. Although the relationship between hemoconcentration, osmolarity and the optical properties of blood has already been investigated [21], the influence of osmolarity on  $\Delta$ RBV estimation is still an important issue to deal with, in order to get a correct estimate during the dialysis session.

In whole blood, light propagation along different trajectories takes different names: transmittance, reflectance, scattering. The fact that propagation in different directions depends on both hemoconcentration and osmolarity constitutes the biophysical principle underlying the present work.

Our aim is to develop a method for an accurate estimation of blood composition during hemodialysis treatment, represented by  $\Delta$ RBV and  $N_{aPl}$ , which we consider to be a simple, yet highly descriptive set of physiological parameters. To accomplish our aim, we have designed an optical measurement system that uses plastic fiber optics to collect light propagation data at multiple angles. The data produced by this system is then augmented with data obtained from built-in sensors of the hemodialysis machine. Another novelty of the present study is the

formulation of a state-space model, which is employed to determine  $\Delta RBV$  and  $Na_{PI}$  using the optimal mean square error estimator, i.e. the Kalman filter.  $\Delta RBV$  and  $Na_{PI}$  are accurately estimated in real time throughout the treatment session.

Section 3.2 describes the new optical measurement system and the protocol used to collect experimental data. This section also describes the differential equations underlying the state-space model as well as the Kalman filter. Section 3.3 presents the results in terms of estimation errors of  $\Delta RBV$  and  $Na_{PI}$ , followed by a discussion in section 3.4.

## **3.2 Methods**

### **3.2.1 Optical measurement system**

Traditional optical sensors for  $\Delta RBV$  monitoring are composed of an infrared LED and a photodiode receiver placed either across or on the same side of the extracorporeal blood tube. The peak wavelength of the emitter is usually set to 800–810 nm, corresponding to that point of the Hgb absorption spectra where absorption is not dependent on oxygenation. The photodiode collects either reflected or transmitted light depending on its position. In certain implementations, an optically transparent flow-through cell (cuvette) may be employed to improve measurement accuracy. Figure 3.1a displays a simplified illustration of the traditional design where both reflection and transmission geometries are represented.

The new measurement system extends the architecture of the traditional design to collect light at different geometrical angles with respect to the emitter, allowing for discrimination between reflected, scattered and transmitted light. A loss in transmitted light due to an increase in scattering is not falsely detected as an increase in absorbance, if, at the same time, the scattered light is picked up by a different receiver.

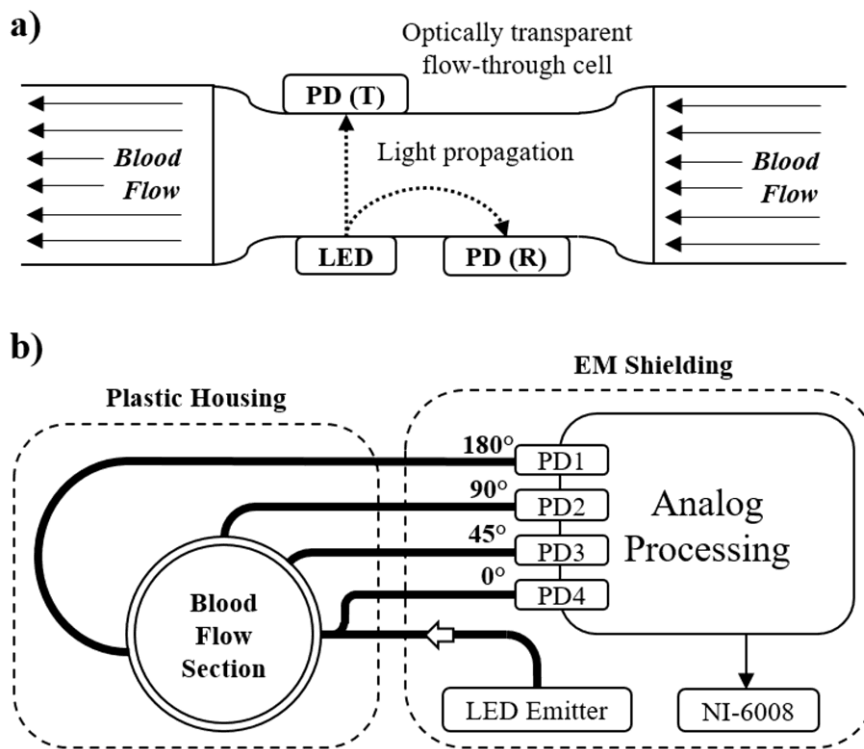


**Fig. 3.1 - Optical measurements on the hemodialysis bloodline**

(a) Two traditional design geometries for optical RBV monitoring. PD (T) and PD (R) represent photodiode placement in transmission and reflection geometries, respectively. (b) Schematic representation of the new measurement system. PD1 to PD4 are the light-collecting photodiodes. NI-6008 is the acquisition board.

During preliminary tests, a preliminary measurement setup with light collection channels at 0°, 45°, 90°, 135° and 180° was used. Preliminary tests consisted in optical measurements carried out during in-vitro dialysis sessions with animal blood, with perturbation of  $\Delta RBV$  and  $N_{aPl}$ . The specific details of the preliminary experiments are reported in the next subsection (3.2.2), since the same kind of protocol was used for the experiments described in this chapter. In the final setup, it was chosen to place light collection channels at 0°, 45°, 90° and 180° only, as shown in Fig. 3.1b. The 135° channel was deemed unnecessary after analysis of the preliminary data (example shown in the Results section).

All channels are placed radially along the normal section of the blood flow, except for the reflection channel (0°), which is slightly shifted along the flow direction to allow placement of the emission fiber. Both emitted and collected

light is coupled to and from the bloodline using plastic fiber optics (ESKA GH4001, Mitsubishi Rayon).

A mechanical open-and-close housing was built for compatibility with the Artiset bloodline (Baxter, Medolla, Italy), employing high-absorption material for the part of the housing enclosing the bloodline's cuvette. The housing guarantees tight coupling between the fiber optics channels and the surface of the cuvette.

A multiple wavelength LED emitter (MTMD6788594SMT6, Marktech Optoelectronics, NY, USA) was used for light emission, coupled to fiber surface with a custom, 3D-printed mechanical interface. The emitter includes 5 LEDs on the same chip, with peak wavelengths in the red/infrared region, covering a spectral band in the range of  $\approx 650\text{-}1000$  nm with some gaps. As already explained, traditional Hgb sensors employ a  $\approx 800\text{-}810$  nm light source. However, we choose this source with multiple wavelength for compatibility with another experiment which was carried out simultaneously with the light propagation measurements and involved the analysis of spectral absorbance of blood. Such experiment did not return significant results and it is not reported in this thesis. The choice of a source with multiple peak wavelengths could, theoretically, lead to inaccurate measurements. After careful consideration, it was decided to employ the wideband source anyway, for reasons reported in the Discussion section.

Photodiodes with specific fiber-coupling mechanics (IFD91, Industrial Fiber Optics, Tempe, USA) were chosen for light collection channels, corresponding to PD1–4 in Fig. 3.1b. The photodiodes were housed on a printed circuit board along with analog circuitry for transimpedance amplification, lowpass filtering and gain-stage amplification. The cutoff frequency of the lowpass filter was set to 30 Hz. The gain was set to channel-specific values, based on preliminary testing and calibration. The analog outputs were sampled at a rate of 100 Hz with 12-bit resolution using an NI USB-6008 DAQ card (National Instruments Italy Srl, Milano, Italy) and recorded by a custom LabView Virtual Instrument.

The multi-LED emitter, the signal conditioning board and the DAQ card were assembled together on a 3D-printed housing and placed inside a grounded metallic box for electro-magnetic shielding, provided with openings for fiber

optics, data connection and power supply.

### 3.2.2 Experimental sessions

An experimental protocol for in-vitro hemodialysis sessions with perturbations of  $\Delta RBV$  and/or  $Na_{PI}$  was designed to gather robust and representative data for the development and validation of the proposed estimation method.

12 in-vitro hemodialysis sessions were carried out using fresh heparinized bovine blood and an Artis hemodialysis machine (Baxter, Medolla, Italy). Before each session, hematocrit was measured with the capillary centrifugation method and the blood was diluted with saline solution to achieve 30% hematocrit. For each session, the starting volume of the blood was  $V_{B,0}=5l$ . The blood flow rate  $J_B$  and dialysate flow rate  $J_D$  were set to typical clinical values, i.e.  $J_B=300$  ml/min and  $J_D=500$  ml/min.

During clinical hemodialysis, water removal from the patient's blood pool is partially compensated by refilling—a phenomenon in which liquid shifts from other body compartments to the circulatory system to maintain physiological blood pressure. Refilling is simulated in the sessions by using a peristaltic pump and a container of fresh dialysis fluid, with a chemical composition similar to plasma; see Fig. 3.2a for a schematic diagram of the setup.

Relative blood volume loss was implemented by setting the ultrafiltration rate to  $J_{UF}=0.8$  L/h and the refilling rate to  $J_{Ref}=0.63$  L/h. The difference between these flows allowed reaching a physiological end-session  $\Delta RBV$  of  $\simeq 10\%$ .

Changes in  $Na_{PI}$  were implemented by applying steps to the inlet dialysate sodium concentration  $Na_{Dial,In}$ . Changes in  $Na_{Dial,In}$  propagate to  $Na_{PI}$  by diffusion across the membrane of the hemodialyzer in a manner that can be approximated as a first-order response. The concentration was initially set to 140 mM, and then two steps of  $\pm 7$  mM were applied before returning to 140 mM. Each concentration value was maintained for 45 min. The order of the positive and negative steps is changed between sessions. The protocol is illustrated in Fig. 3.2b.

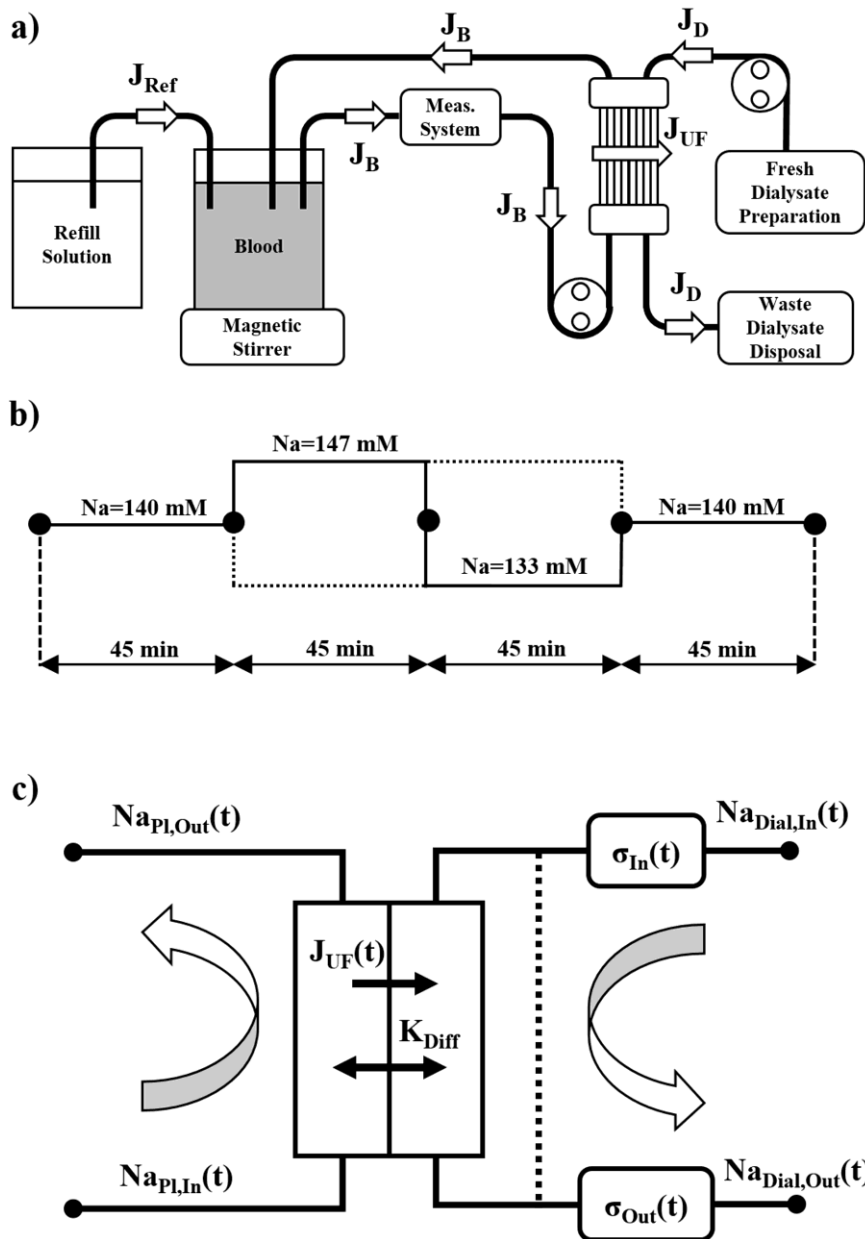


**Fig. 3.2 - The experimental setup and protocol**

(a) Diagram of the experimental setup. (b) Sodium step protocol for the inlet dialysate  $Na_{Dial,In}$ . The dotted line shows the dual protocol with inverted steps. The large black dots indicate the times for blood gas sampling. (c) Diagram of the hemodialyzer with inlet/outlet ports for blood and dialysate. Conductivity cells measure the inlet ( $\sigma_{In}$ ) and outlet ( $\sigma_{Out}$ ) dialysate electrical conductivity. The dotted black line represents the bypass condition.

Each session was composed of a 1-h adjustment phase followed by a 3-h experimental phase. The adjustment phase was designed to achieve equilibrium

between dialysate and blood in an effort to improve reproducibility of the experimental sessions, since each fresh volume of bovine blood comes with very different plasmatic concentrations of electrolytes. During the adjustment phase  $\text{Na}_{\text{Dial,In}}$  is maintained constant. In this way, the blood reaches standard initial conditions before the start of the actual experiment. The achievement of concentration balance for electrolytes is accelerated by setting  $J_{\text{UF}}=J_{\text{Ref}}=0.8$  L/h in this phase, and thus blood volume is kept constant. For notation purposes,  $t=0$  indicates the start of the 3-h experimental phase. 8 sessions out of the total of 12 were carried out with UF, refilling and sodium steps. 2 of the 12 sessions were carried out with  $J_{\text{UF}}=J_{\text{Ref}}=0$  to evaluate the isolated effects of  $\text{Na}_{\text{PI}}$  variations on the measurement system. The remaining 2 sessions were carried out with constant  $\text{Na}_{\text{Dial,In}}$  concentration to evaluate the isolated effect of  $\Delta\text{RBV}$ . Of the last two sessions, one was carried out with  $\text{Na}_{\text{PI}}(0)=\text{Na}_{\text{Ref}}=140$  mM, whereas the other with  $\text{Na}_{\text{PI}}(0)=\text{Na}_{\text{Ref}}=145$  mM to simulate a realistic case with a hyper-natremic patient.

Samples for blood gas analysis were taken at the start and end of the session and at each 45 min in-between (indicated as black dots in Fig. 3.2b). A Stat Profile pHox Ultra blood gas analyzer (Nova Biomedical, Waltham MA, USA) was used to determine electrolyte concentration. At the end of each session, the internal session log of the hemodialysis machine was downloaded to access internal sensor data (ultrafiltration rate  $J_{\text{UF}}$ , dialysate inlet conductivity  $\sigma_{\text{In}}$ , dialysate outlet conductivity  $\sigma_{\text{Out}}$ ), see Fig. 3.2c.

### 3.2.3 Data pre-processing

For all signals, moving average filtering was the technique of choice for signal smoothing. In each case, an appropriate window length was chosen, in order to remove as much noise as possible without introducing significant delay. Median filtering was the technique of choice for removal of very short spike-like artifacts, present in some of the recorded signals.

Data recorded from the optical measurement system were subjected to median filtering with a 10-samples window followed by moving average smoothing with

a 5000-samples window. Data from the 3-h experimental phase was then converted to relative optical power variations according to:

$$\Delta RP_i(t) = \frac{V_{Out,i}(t) - V_{Out,i}(0)}{V_{Out,i}(0)} \quad i = 1,2,3,4 \quad (3.1)$$

where  $V_{Out,i}(t)$  is the recorded analog voltage output and  $i$  indicates output channel.

The signals  $J_{UF}(t)$ ,  $\sigma_{In}(t)$  and  $\sigma_{Out}(t)$  were recorded by the session logger of the machine at  $F_S=0.1$  Hz. As for the optical data, only data from the 3-h experimental phase was analysed. The signal  $J_{UF}(t)$  underwent median filtering with a 5-sample window, whereas  $\sigma_{In}(t)$  and  $\sigma_{Out}(t)$  were smoothed by moving average filtering with a 5-sample window.

Throughout the session, the hemodialysis machine is temporarily switched to bypass mode, either for safety reasons or for the purpose of internal recalibration. During bypass, ultrafiltration is suspended and the hydraulic connection of dialysate to the hemodialyzer is short-circuited, see Fig. 3.2c, meaning that data from the conductivity cells ( $\sigma_{In}(t)$ ,  $\sigma_{Out}(t)$ ) is not useful. Using the session log, a binary signal indicating whether conductivity data is available at any given time was built for each session.

Blood gas analysis was used to determine the experimental plasmatic sodium concentration  $Na_{Pl,Exp}(t)$  at  $t=0, 45, 90, 135$  and  $180$  min. Three analyses were carried out on each sample to get an average value, but the first measurement in each group of three always showed negative bias, whereas the other two were consistent among them. For this reason, the value of  $Na_{Pl,Exp}(t)$  was, for each blood sample, computed as the average of the second and third measurements. A possible explanation is that the first measurement is the one that is carried out after a period of inactivity of the analyzer and operating conditions of the instrument might be slightly different.

The signals  $\Delta RBV(t)$  and  $Na_{PI}(t)$  were built from experimental data to act as a reference for the blood state estimator. The basis for signal construction is the one-compartment model of the blood pool depicted in Fig. 3.3.

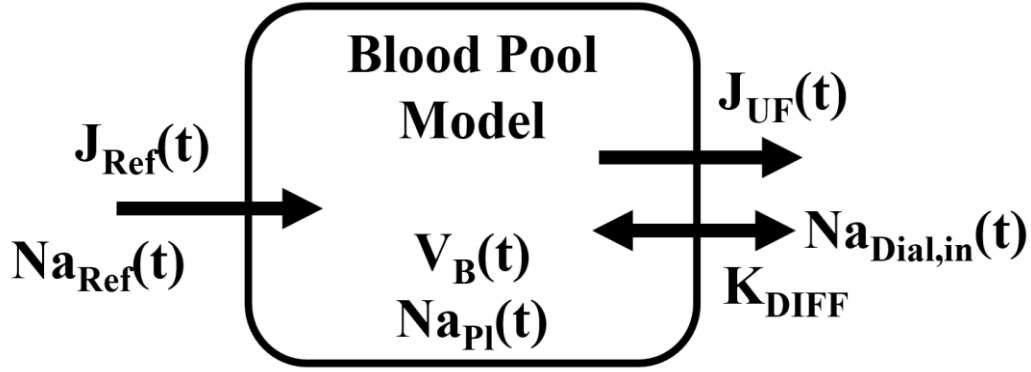


Fig. 3.3 - The blood pool model used for the computation of reference signals

$$V_B(t) = V_{B,0} + \int_0^t (-J_{UF}(\tau) + J_{Ref}(\tau))d\tau \quad (3.2)$$

$$\Delta RBV(t) = \frac{V_B(t) - V_{B,0}}{V_{B,0}} = \frac{\int_0^t (-J_{UF}(\tau) + J_{Ref}(\tau))d\tau}{V_{B,0}} \quad (3.3)$$

$$\Delta \dot{RBV}(t) = \frac{-J_{UF}(t) + J_{Ref}(t)}{V_{B,0}} \quad (3.4)$$

$$Na_{PI}(t) = \frac{K_{DIFF} \cdot (Na_{Dial,In}(t) - Na_{PI}(t)) + J_{REF}(t) \cdot (Na_{Ref}(t) - Na_{PI}(t))}{V_B(t)} \quad (3.5)$$

Equation (3.2) defines the relationship between absolute blood volume  $V_B(t)$  and flow rates. Equation (3.3) defines relative blood volume  $\Delta RBV(t)$  on the basis of absolute blood volume  $V_B(t)$ . Equation (3.4) describes  $\Delta RBV(t)$  in differential form. In (3.2-3.4),  $V_{B,0}$  and  $J_{Ref}(t)$  are experimentally known whereas  $J_{UF}(t)$  is extracted from the session log of the hemodialysis machine.

$Na_{PI}(t)$  was computed according to eq. (3.5), where  $Na_{Dial,In}(t)$  and  $J_{Ref}(t)$  are experimentally determined. It is relevant to point out that since equation (3.5) is a

concentration equation and not a mass balance equation, no term pertaining to ultrafiltration is needed. Ultrafiltration drags a specific mass of plasmatic sodium across the filter together with its associated liquid volume. Thus, there is no concentration change.

$V_B(t)$  is computed from eq. (3.2) and  $K_{Diff}$ , the membrane diffusion coefficient for sodium, is set to the typical value of 250 ml/min. Computation of  $Na_{PI}(t)$  requires an initial value, here set equal to the value measured by blood gas analysis at the onset of the experimental phase, see Fig. 3.2b. Preliminary attempts to compute  $Na_{PI}(t)$  revealed the presence of a session-specific offset associated with inter-session events, like instrument recalibration and sodium electrode replacement. Therefore, a baseline adjustment was applied when computing  $Na_{PI}(t)$  to account for this offset.

After pre-processing, all signals were resampled to  $F_s'=1$  Hz so that all signals of the dataset had identical sampling rate.

### 3.2.4 State space modeling and estimation

The state-space approach was chosen for estimation of  $\Delta RBV(t)$  and  $Na_{PI}(t)$ , treated as state variables that completely describe the system under observation. A set of modeling equations describe the evolution of the state variables and the input/output relationship. The estimation was accomplished using a Kalman filtering technique.

Classification of sensor data as being either input or output depends on whether the specific variable monitored by each sensor perturbs the system state or is determined by it. The inlet dialysate sodium concentration  $Na_{Dial,In}(t)$  and the inlet dialysate conductivity  $\sigma_{In}(t)$  constitute the input variables. The hemodialysis machine maintains the effective value of  $Na_{Dial,In}(t)$  within clinically acceptable boundaries of the value set by the operator. Due to the general properties of electrolyte solutions [22], and the fact that sodium is the most concentrated electrolyte in plasma and dialysate, a good correlation can be found between the two fluids' electrical conductivity and sodium concentration [23-24]. This

assumption is exploited in some of the following design choices. The output sensor data consists of the optical outputs  $\Delta RP_1(t)$  to  $\Delta RP_4(t)$  and the outlet conductivity  $\sigma_{Out}(t)$ .

$$\Delta RBV(t) = 0 \quad (3.6)$$

$$Na_{Pl}(t) = \frac{Na_{Dial,In}(t) - Na_{Pl}(t)}{\tau_{Diff}} \quad (3.7)$$

The ordinary differential equations (3.6) and (3.7) model the blood pool dynamics, and were developed by removing the terms with parameters unknown during clinical practice ( $V_{B,0}$ ,  $J_{Ref}$ ,  $Na_{Ref}$ ) from (3.4) and (3.5). One critical part of the estimation procedure is the handling of non-modeled terms: thanks to the properties of the Kalman filter, the lack of some terms of (3.4-3.5) not included in (3.6–3.7) can be accounted for as noise in process modeling. This way, although refilling properties and starting blood volume are not known exactly, their influence on the reliability of the estimation is taken into account.

While (3.4) would be a better theoretical description,  $V_{B,0}$  and  $J_{Ref}(t)$  are not known in clinical routine. By employing the approximate version in (3.6), no time-dependent evolution of  $\Delta RBV$  is predicted, but the Kalman filter technique includes a measurement-based correction step that is applied to the model prediction. This correction is applied to the static  $\Delta RBV$  value at each time step, thus making  $\Delta RBV$  a quasi-static variable.

Equation (3.7) approximates (3.5): the parameters of the refilling process are not clinically available during treatment, so only sodium diffusion is modeled by employing a diffusion time constant  $\tau_{Diff}$  to describe how plasmatic sodium is related to  $Na_{Dial,In}(t)$ .  $\tau_{Diff}$  can be viewed as an estimate of  $V_B(t)/K_{Diff}$  from (3.5). For  $K_{Diff}=250$  ml/min (realistic for sodium) and  $V_B=5$  l (a time-independent average value), we have that  $\tau_{Diff}\approx 1200$  s. By fitting a first-order step response of outlet conductivity  $\sigma_{Out}(t)$  to experimental data, an estimate of  $\tau_{Diff}\approx 1000$ s was obtained. Therefore, an intermediate value of  $\tau_{Diff}\approx 1100$ s was used in the filter

model.

$$\Delta RP_i(t) = G_{Opt,i,1} \cdot \Delta RBV(t) + G_{Opt,i,2} \cdot Na_{Pl}(t) + G_{Opt,i,3} \quad (3.8)$$

$$\begin{bmatrix} \Delta RP_1(t) \\ \Delta RP_2(t) \\ \Delta RP_3(t) \\ \Delta RP_4(t) \end{bmatrix} = G_{Opt} \cdot \begin{bmatrix} \Delta RBV(t) \\ Na_{Pl}(t) \\ 1 \end{bmatrix} \quad (3.9)$$

A linear formulation was chosen for  $\Delta RP_i(t)$  and is described in eq. (3.8), where  $i=1,\dots,4$  indicates the output channel. The 4x3 matrix  $G_{Opt}$  in eq. (3.9) contains weighting coefficients for all channels, estimated by multivariate regression analysis.

$$\sigma_{Out}(t) = \sigma_{in} \cdot \left(1 - \frac{D}{J_D}\right) + \sigma_{Pl} \cdot \frac{D}{J_D} \quad (3.10)$$

$$\sigma_{Out}(t) = G_{Mix} \cdot \sigma_{Pl}(t) + (1 - G_{Mix}) \cdot \sigma_{In}(t - \tau_{Delay}) \quad (3.11)$$

$$\sigma_{Pl}(t) = G_{Na,Gain} \cdot Na_{Pl}(t) + G_{Na,Offset} \quad (3.12)$$

The last output element, i.e., the outlet dialysate conductivity  $\sigma_{Out}(t)$ , is modeled as a weighted average of the inlet and plasmatic conductivities [18, 25]. In eq. (3.10), adapted from [25],  $\sigma_{Out}$  is a weighted average based on the dialysance  $D$  and the dialysate flow rate  $J_D$ . We adopted the simpler formulation in eq. (3.11), where  $G_{Mix}=D/J_D$ . As mentioned in section 3.2.2,  $J_D$  is fixed to 500 ml/min in our experiments. Given an average value of  $D=250$  ml/min, it leads to a value of 0.5 for the mixing constant  $G_{mix}$ . After preliminary analysis of dialysate conductivity data, a term  $\tau_{delay}$  was included in eq. (3.11), to account for an observed delay in the response of outlet dialysate conductivity  $\sigma_{Out}(t)$  to changes in the conductivity  $\sigma_{In}(t)$  of inlet dialysate. A value of  $\tau_{delay}=140$  s was estimated by measuring the step response delay of  $\sigma_{Out}(t)$  in the sessions where sodium concentration steps

were applied. The most probable explanation for this brief delay is that modifications to the composition of inlet dialysate require some time to propagate across the hydraulic circuit.

The plasmatic conductivity  $\sigma_{PI}(t)$  is modeled in eq. (3.12) as a linear function of plasmatic sodium concentration  $Na_{PI}(t)$ . The coefficients  $G_{Na,Gain}$  and  $G_{Na,Offset}$  were estimated by linear regression starting from experimental data.

Figure 3.4a illustrates the relationship between input signals, state variables and output signals.

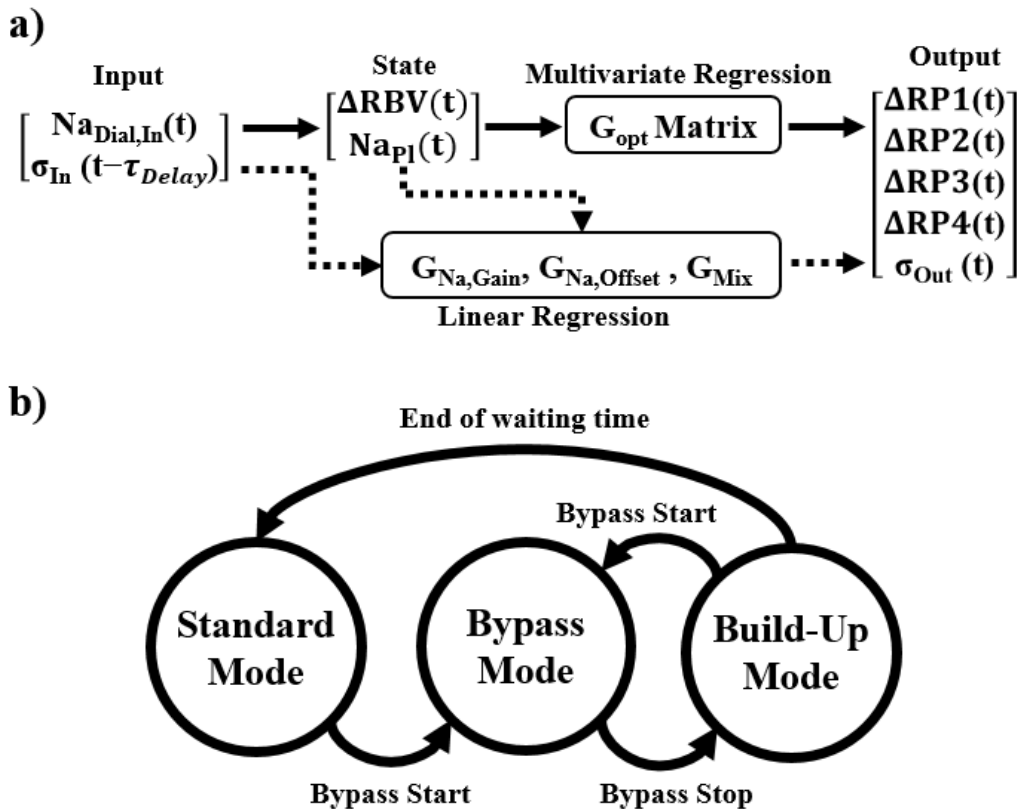


**Fig. 3.4. - Diagrams of the mathematical estimator**

(a) Relationship between input signals, state variables and output signals. The dotted lines represent connections which are unreliable during bypass mode. (b) The transition between different filter versions for bypass condition management.

As described in section 3.2.3 and illustrated in Fig. 3.2c, the hemodialysis machine periodically goes into bypass mode. Certain changes in the modeling equations are needed to reflect such temporary alterations of the physical system.

The temporary stop in UF means  $J_{UF}(t)=0$ , and, given the lack of information about  $J_{Ref}(t)$  during clinical practice, equation (3.6) is still the best available approximation for  $\Delta RBV$  modeling. For this reason, equation (3.6) is not replaced.

$$Na_{pl}(t) = 0 \quad (3.13)$$

The hydraulic disconnection of the hemodialyzer during bypass implies that diffusion is suspended, here modeled by replacing eq. (3.7) with eq. (3.13). This temporary replacement is also reflected by modifications to the process noise for  $Na_{pl}(t)$ . During bypass, data from the conductivity cells is not useful due to the different hydraulic path of the dialysate. This is reflected by setting the sensitivity of the filter related to  $\sigma_{In}(t)$  and  $\sigma_{Out}(t)$  to zero during bypass. Figure 3.4b depicts the transition model regulating switching of the Kalman filter between standard mode, bypass mode and build-up mode. During build-up mode, the alterations of the filter structure associated with the bypass conditions are maintained for an additional period of time  $\tau_{Delay}$ , to allow the accumulation of the necessary delay of  $\sigma_{In}(t)$  before returning to default filter operations.

Equations (3.14–3.18) are given as a function of the generic time step  $k$  and define the Kalman filter employed in the present work. A time step of 1s was chosen.

Although an exhaustive explanation of the theoretical aspects of the Kalman filter is out of the scope of this work, a brief explanation of the filter's working principle will be given. For more detailed information, see e.g. [26-28].

$$x_k^- = f(x_{k-1}^+, u_k) \quad (3.14)$$

$$P_k^- = A \cdot P_{k-1}^+ \cdot A^T + Q \quad (3.15)$$

$$E_k = P_k^- \cdot H^T \cdot (H \cdot P_k^- \cdot H^T + R)^{-1} \quad (3.16)$$

$$x_k^+ = x_k^- + E_k \cdot (z_k - g(x_k^-, u_k)) \quad (3.17)$$

$$P_k^+ = (I - E_k \cdot H) \cdot P_k^- \quad (3.18)$$

The Kalman filter works by estimating the value of its state variables with continuous prediction-correction. At each time step, the value of the state variables is predicted by a function  $f(\cdot, \cdot)$  which takes into account the previous (or initial) state  $x_{k-1}^+$  and one or more inputs contained in the input vector  $u_k$ . Predicted state variables are memorized in vector  $x_k^-$ . Inputs are defined as known quantities able to perturb the system's state: they usually correspond to control mechanisms which are also monitored by sensors. After computation of  $x_k^-$  in equation (3.14), covariance  $P_k^-$  is predicted in equation (3.15). It depends on the previously estimated covariance  $P_{k-1}^+$ , on  $A$ , which is the linearized version of  $f(\cdot, \cdot)$ , and on the so-called process noise covariance  $Q$ . Eqs. (3.14) and (3.15) together represent the prediction step.

Afterwards, the correction step begins by computing the so-called error gain  $E_k$ , which is dependent on predicted state covariance  $P_k^-$ , on the linearized version of the relationship between state variables and outputs ( $H$ , linearization of  $g(\cdot, \cdot)$ ), and on measurement noise covariance  $R$ . Outputs are defined as measurable quantities whose value is influenced by the state of the system, in a way which is modelled by a specific relation. Measured outputs are contained in the observation vector  $z_k$ . Equation (3.16) shows how error gain is determined. Then, the difference between the output values predicted by  $g(\cdot, \cdot)$  and the measured outputs contained in  $z_k$  is multiplied by the error gain and added to  $x_k^-$ , as shown in equation (3.17), to obtain the corrected estimate  $x_k^+$ . The last step is to update state covariance, obtaining  $P_k^+$ . Equations (3.16–3.18) together represent the measurement-based correction step. Reported below are the detail of our specific implementation of the Kalman filter.

Input vector  $u_k$  is a 2x1 vector which includes  $N_{aDial,ln}[k]$  and  $\sigma_{ln}[k]$ . The vectors  $x_k^-$  and  $x_k^+$  are both 2x1 and contain the predicted and corrected values of the state variables  $\Delta RBV[k]$  and  $N_{aPI}[k]$ .  $x_k^-$  is the predicted system state at step  $k$ , and is a function  $f(\cdot, \cdot)$  of  $x_{k-1}^+$  and  $u_k$ . The elements of initial vector  $x_0^+$  were set to  $\Delta RBV=0$  and  $N_{aPI}=140$  mM.

Function  $f(\cdot, \cdot)$  is defined by the discretized versions of eqs. (3.6) and (3.7) in standard mode, and by the discretized eqs. (3.6) and (3.13) in bypass mode.

Discretization of eqs. (3.6), (3.7) and (3.13) was implemented with the forward Euler method, given by

$$\Delta RBV[k] = \Delta RBV[k - 1] \quad (3.19)$$

$$Na_{pl}[k] = Na_{pl}[k - 1] \cdot \left(1 - \frac{1}{\tau_{Diff}}\right) + \frac{1}{\tau_{Diff}} \cdot Na_{Dial,In}[k] \quad (3.20)$$

$$Na_{pl}[k] = Na_{pl}[k - 1] \quad (3.21)$$

respectively. Process noise covariance is described by the 2x2 matrix Q. Matrix A is the 2x2 Jacobian linearization of  $f(\cdot, \cdot)$  with respect to  $\Delta RBV$  and  $Na_{pl}$ .

A standard  $Q_{std}$  matrix is used during standard filter operation, replaced by  $Q_{bypass}$  during bypass mode. Both versions of Q are diagonal matrices whose elements are precomputed as described in previous paragraphs, on the basis of realistic maximum values for the non-modeled terms of the process equations. Error gain  $E_k$  is a 2x5 matrix computed according to eq. (3.16).

Measurement noise is characterized by the 5x5 covariance matrix R, taken so as to be a pre-determined diagonal matrix. The diagonal values of R, associated with optical measurements, were set equal to the root-mean-square fitting residuals of eq. (3.9). The diagonal value of R associated with  $\sigma_{Out}$  modeling was chosen on the basis of realistic deviations of D from the average value considered for eq. (3.11).

The observation vector  $Z_k$  is a 5x1 column vector of experimentally measured system output, composed of the optical output  $\Delta RP_1[k]$  to  $\Delta RP_4[k]$  and outlet conductivity  $\sigma_{Out}[k]$ .  $g(x_k^-, u_k)$  is a 5x1 column vector of predicted output calculated according to state-output function  $g(\cdot, \cdot)$ . The function  $g(\cdot, \cdot)$  is determined by the time-discrete versions of eqs. (3.9) and (3.11), given by

$$\begin{bmatrix} \Delta RP_1[k] \\ \Delta RP_2[k] \\ \Delta RP_3[k] \\ \Delta RP_4[k] \end{bmatrix} = G_{opt} \cdot \begin{bmatrix} \Delta RBV[k] \\ Na_{pl}[k] \\ 1 \end{bmatrix} \quad (3.22)$$

$$\sigma_{Out}[k] = G_{Mix} \cdot \sigma_{Pl}[k] + (1 - G_{Mix}) \cdot \sigma_{In}[k - k_{Delay}] \quad (3.23)$$

respectively. In eq. (3.23),  $k_{Delay}$  is the discrete version of  $\tau_{Delay}$  and  $\sigma_{Pl}[k]$  is computed according to

$$\sigma_{Pl}[k] = G_{Na,Gain} \cdot Na_{Pl}[k] + G_{Na,Offset} \quad (3.24)$$

which is the discretized version of eq. (3.12).

The matrix H from eqs. (3.16) and (3.18) is the 5x2 Jacobian linearization of  $g(\cdot, \cdot)$  with respect to  $\Delta RBV$  and  $Na_{Pl}$ . Two versions of H exist:  $H_{std}$  and  $H_{bypass}$ . During default machine operations  $H_{std}$  is used. During bypass,  $H_{std}$  is replaced with  $H_{bypass}$  to ensure that the measurement-based correction step is insensitive to  $\sigma_{In}[k]$  and  $\sigma_{Out}[k]$ .

The matrices  $P_k^-$  and  $P_k^+$  are the predicted and corrected 2x2 estimation covariance matrices, respectively. Both matrices are computed at each step k, according to eqs. (3.15) and (3.18), initiated by a diagonal matrix  $P^+$  with the initial uncertainties of  $\Delta RBV$  and  $Na_{Pl}$  set to 0 and 4 mM, respectively. Zero uncertainty on starting  $\Delta RBV$  is given by the fact that  $\Delta RBV$  is a relative variation and its starting value is always known and equal to 0. The initial uncertainty for  $Na_{Pl}$  is based on the assumption of a 136–144 mM physiological range for patients at treatment start.

Computation of  $P^+$  is an important feature of the Kalman filter, given that it represents covariance of the state variables. As shown by eqs. (3.15) and (3.18), the estimation covariance is influenced by the covariance of the modeling and measurement processes. On this basis, P is a useful additional source of information about the uncertainty of the estimation: we choose to use the square root of the diagonal elements  $P_{11}$  and  $P_{22}$  from  $P^+$  in eq. (3.18) as an indicator of uncertainty, resulting in confidence intervals of  $\Delta RBV \pm \sqrt{P_{11}}$  and  $Na_{Pl} \pm \sqrt{P_{22}}$ .

### 3.3 Results

Figure 3.5 shows optical data recorded during one of the preliminary in-vitro sessions, with alteration of RBV and  $\text{Na}_{\text{Dial,In}}$ . In figure, the trend of relative optical intensity throughout the session is shown for each of the fiber channels available in the preliminary setup: it can be noticed that the  $135^\circ$  channel has an output which is very similar to that of the  $180^\circ$  channel, apart from a scaling factor. For this reason, it was not included from the final measurement system. The remaining part of this sections deals with the results of the experiments carried out with the final setup.

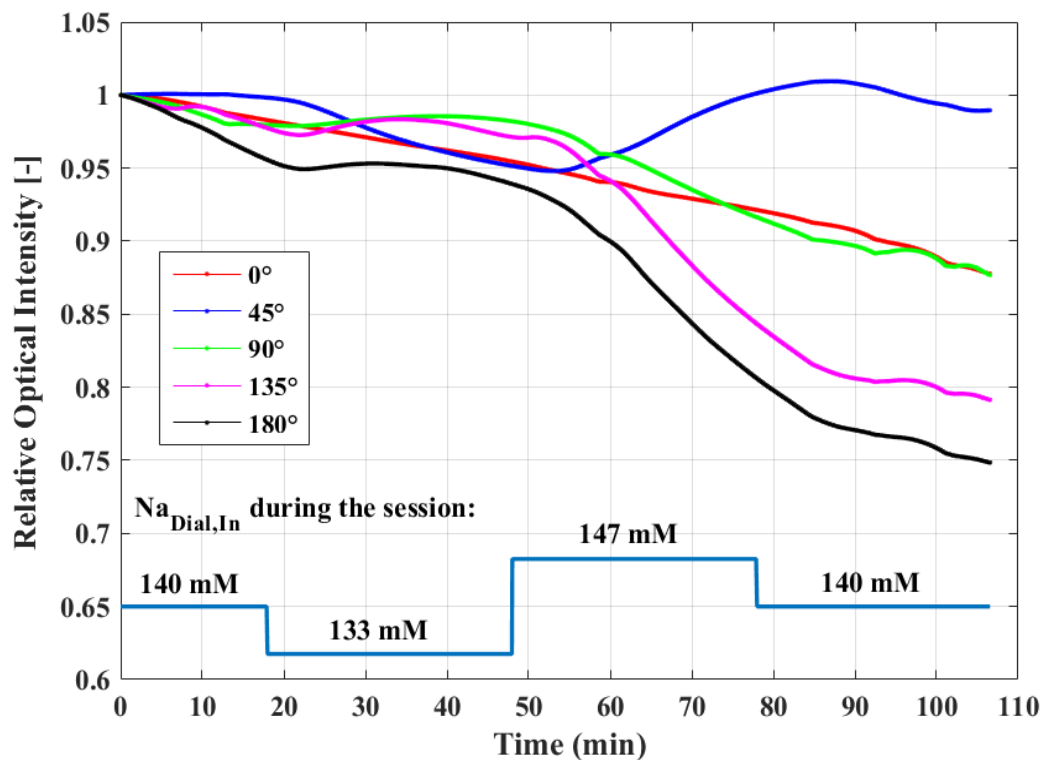


**Fig. 3.5. – Preliminary optical data**

Data collected using a preliminary version of the fiber optics measurement system during an in-vitro session with the protocol described in the Methods section. Also reported in figure are the dialysate sodium concentration steps and the color-coded legend for the fiber channel outputs.

As described in section 3.2.4, the parameters  $G_{\text{Opt}}$  in eq. (3.9) and  $G_{\text{Na,Gain}}$  and  $G_{\text{Na,Offset}}$  in eq. (3.12) are not based on modeling assumptions, but fitted to

experimental data. For this reason, the performance of the system was evaluated in two ways. To determine best performance, the estimation error was computed using a version of the Kalman filter with empirical parameters fitted to the whole dataset. Additionally, to assess the robustness of the estimator, a leave-one-out procedure was employed on the 12-sessions dataset: for each iteration, 11 sessions were employed for fitting and 1 for testing.

The estimation error was calculated for both  $\Delta RBV$  and  $N_{aPI}$  as the absolute difference between the reference data and the estimates. The mean and maximum errors were first computed for each session; then the inter-session mean  $\pm$  standard deviation was calculated for both quantities. The results are reported in Table 3.1.

TABLE 3.1  
RESULTS OF THE ESTIMATION PROCESS

<i>Estimation Conditions</i>	<i>Error</i>	<i>Mean<math>\pm</math>SD</i>	<i>Max<math>\pm</math>SD</i>
<i>Complete Dataset</i>	$\Delta RBV$ [%]	0.97 $\pm$ 0.73	1.90 $\pm$ 0.95
	$N_{aPI}$ [mM]	0.47 $\pm$ 0.19	2.35 $\pm$ 1.38
<i>Leave-One-Out</i>	$\Delta RBV$ [%]	0.99 $\pm$ 0.65	2.10 $\pm$ 0.97
	$N_{aPI}$ [mM]	0.51 $\pm$ 0.15	2.54 $\pm$ 1.33

The Kalman filter, tuned with data from the whole dataset, showed good performance when estimating  $\Delta RBV$  and  $N_{aPI}$ .

The estimation errors evaluated with the leave-one-out procedure present only small differences compared to evaluation on the whole dataset, especially if the large standard deviations are taken into account. This result indicates that the fitting procedure is not sensitive to data from one session in particular, and demonstrates the reliability of the proposed filter architecture.

Figure 3.6 exemplifies state estimation results in the best case, when parameters of the estimator are computed using data from the complete dataset.

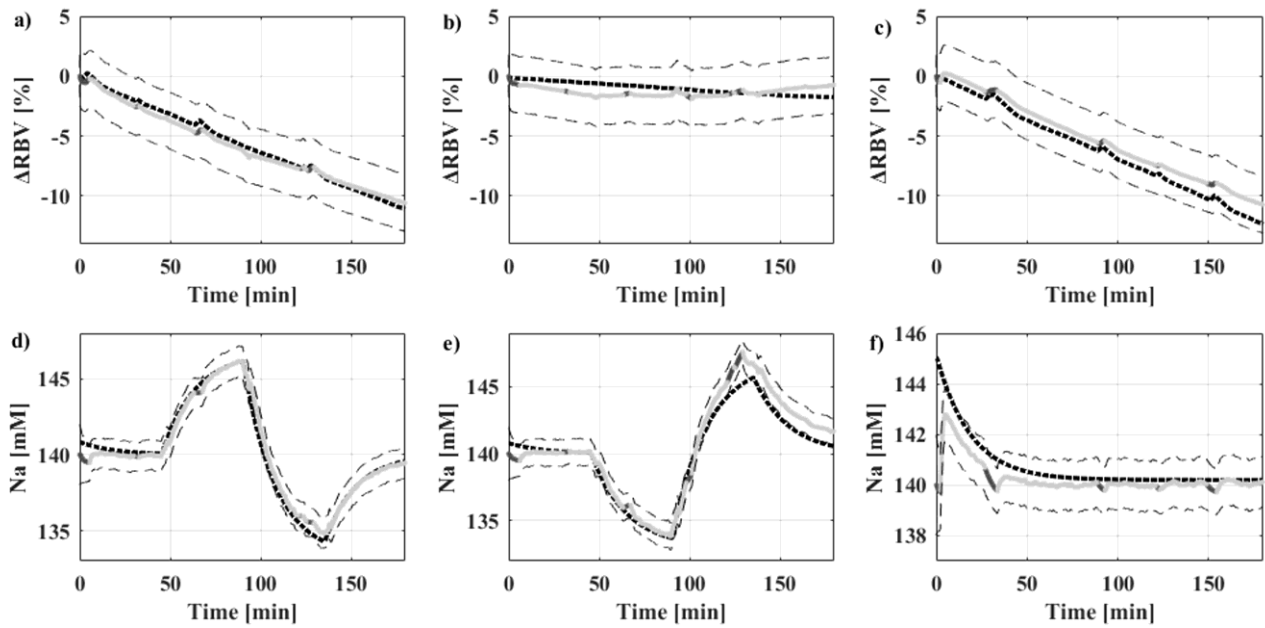


**Fig. 3.6 - Examples of estimation results**

(a), (b), (c)  $\Delta RBV$  estimation for three different experimental sessions. (d), (e), (f)  $Na_{p1}$  estimation for the same experiments. In all diagrams, the dotted black line displays the reference data. The light grey solid line displays the Kalman-based state variable estimation. The dashed black lines display the estimation confidence interval. The dark grey solid lines display the intervals of the estimation performed in bypass mode.

The estimates of  $\Delta RBV$  and  $Na_{p1}$  are presented for an experiment with both blood volume loss and sodium concentration steps (Fig. 3.6a and 3.6d respectively), for an experiment with blood volume loss close to zero (Figs. 3.6b and 3.6e) and for an experiment in which a starting hypernatremic patient condition is simulated (Figs. 3.6c and 3.6f). The switch from standard filter operation to bypass mode is represented by the temporary transition to dark grey solid lines. Figs. 3.6a–c show results on the estimation of blood volume loss. Although some difference remains between estimated and reference blood volume loss, the trend of  $Na_{p1}$  does not show any recognizable influence on the  $\Delta RBV$  signal. This feature is observable in all experimental sessions and indicates that the target of an osmolarity-insensitive  $\Delta RBV$  estimation is reached. Figure 3.6f is an example of the reliable behaviour of our estimator, even when the starting conditions are less-than-optimal: the starting plasmatic sodium concentration of our simulated patient is much higher than the starting estimate of the Kalman filter (145 vs 140 mM). Nonetheless, the estimator can drive the estimate of  $Na_{p1}$

in the direction of the experimental value. After less than 10 min from session onset, the estimated confidence interval, given by  $N_{\text{aPI}} \pm \sqrt{\hat{P}_{22}}$ , already includes reference data. Such a short time period is largely compatible with clinical usefulness for  $N_{\text{aPI}}$  estimation.

The  $P^+$  matrix, being updated at each step, is bound to converge to a steady-state value due to the properties of the Kalman filter algorithm. It is clear from the dynamics of boundary intervals of the estimates shown in Fig. 3.6 that  $P^+$  reaches steady-state very quickly, in the first few minutes of filter operation ( $\approx 2$  min).

### 3.4 Discussion

A method for improved relative blood volume loss estimation during hemodialysis was proposed. The method integrates modeling knowledge of the blood pool, dialysate conductivity data and information from a new optical measurement system. Contrary to traditional sensors, the method can estimate relative blood volume loss in a way that is insensitive to even drastic variations in osmolarity. In addition, plasmatic sodium concentration, one of the main drivers of osmolarity in plasma, can be estimated at the same time.

The results, based on in-vitro hemodialysis sessions, demonstrate the viability of the chosen approach: the estimation errors related to blood volume and sodium, reported in Table 3.1, are both on the order of magnitude of the accuracy of reference data.

For example, the mean  $\Delta\text{RBV}$  error of 0.97% is a good result, considering that 1%  $\Delta\text{RBV}$  for  $V_{\text{B},0}=5\text{l}$  corresponds to 50 ml, being a very small quantity of blood. Such a small quantity is highly compatible with the uncertainty in the experimental preparation of the starting blood pool. Regarding  $N_{\text{aPI}}$ , it is known to clinicians that blood gas analysers show large bias and inaccuracy. Nonetheless, blood gas analysers remain one of the most widespread instruments for repeated fast measurements of blood electrolytes, and it was the one available to us at this stage of the work. An example of blood gas analysis bias has been recently reported in [29]. Both the mean and maximum  $N_{\text{aPI}}$  estimation errors are lower

than the reported bias, which is  $\approx 3\text{mM}$ . In general terms, we can say that all the results reported in Table 3.1 are composed of two contributions, one dependent on the accuracy of reference data and one which depends on the quality of the estimator. The limited accuracy of reference data may also influence the quantification of the estimator's performance in a second, less obvious way, by leading to inaccurate state-output relationship estimation. For such reasons, we can assume that the estimator's performance is actually even better than reported in Table 3.1.

The estimation of blood volume loss is insensitive to drastic changes in osmolarity, thus fulfilling one of the aims listed in Introduction.

The results on the estimation of plasmatic sodium concentration are also very important: sodium has a significant role in many physiological processes, like osmotic equilibrium and electrophysiological activity, which makes it a variable of clinical interest. However, further investigation is needed to understand whether the accuracy reached for plasmatic sodium estimation can be maintained in a physiological context where different factors will influence osmolarity. Another aspect is whether blood osmolarity itself can replace plasmatic sodium concentration as a state variable.

The size of the acquired dataset, together with the fact that both isolated and combined effects on blood volume and plasmatic sodium are included, speak in favour of the general robustness and viability of the proposed approach. Another advantage is that this approach is inexpensive as it relies on a simple optical measurement system with an additional cost on the order of tens of euros, beyond existing cost for the sensors already integrated in the machine.

Regarding the choice of a multiple-wavelengths light source over a single-wavelength source, it was explained in the Methods section that it could theoretically be a source of inaccuracy: that would be, because of the influence of blood oxygenation on light absorbance in the red region, and because of the possibly different relationship between physiological and optical properties at different wavelengths. However, there are many reasons to think such problems did not affect the reported experimental work significantly. First, the dead bovine

blood pool has no active mechanisms to change its oxygenation levels. Second, the 1-h adjustment phase should allow blood to stabilize its oxygen level, at least partially, by exchange with the environment and possibly with the degassed dialysate fluid. Third, the effects of osmolarity on the optical properties of blood reported in [21] are averaged over a wide spectral band and still detectable, so our choice of light source does not have a critical impact on estimation. In the future, it is planned to multiplex the multi-LED emitter to specific wavelengths or to directly replace it with an 800 nm emitter.

A critical point of the estimation method is its reliance on a four-channel optical measurement system. Conceptually, at least two channels are needed to discriminate between two state variables. Additional channels should improve robustness of the estimation, but may prove redundant depending on the inter-channel correlation and their position on the cuvette's circumference.

An analysis will be carried out in the future to determine how the performance of the estimation process changes in relation to how many and which channels are employed. The analysis will be carried out with a furtherly improved and more accurate version of the measurement setup, in order to obtain a reliable evaluation of the necessary channels.

Other aspects to focus on include the analysis of changes in operational parameters like blood and dialysate flow rates, and hemodialyzer properties.

The choice of  $\text{Na}_{\text{PI}}$  as a state variable in place of osmolarity deserves to be discussed. Theoretically, blood osmolarity is influenced by all solutes present in plasma unable to cross the RBC membrane. Solute influence osmolarity in different degrees depending on concentration: the main drivers are electrolytes, glucose and urea. Despite this, there is reason to believe that osmolarity and  $\text{Na}_{\text{PI}}$  are highly correlated in our experiments. At the start of the experiment, the blood is in osmotic equilibrium with dialysate due to the presence of the adjustment phase. Sodium concentration in dialysate is determined by real-time dilution of the content of an electrolytes bag. This means that the concentration of all electrolytes in dialysate will roughly follow the same trend throughout the session, and consequently the exchange with the blood pool will be similar. This,

combined with the fact that the bag also contains glucose, and that urea is completely removed from the blood pool during the adjustment phase, supports our choice of monitoring  $\text{Na}_{\text{PI}}$  instead of osmolarity. In future research, it may prove useful (and even necessary) to switch from  $\text{Na}_{\text{PI}}$  to osmolarity as second state variable.

A topic of discussion is the connection between reference data and estimates. As described in the Methods section, UF and blood gas data, together with knowledge of the experimental conditions, have been employed to build continuous  $\Delta\text{RBV}$  and  $\text{Na}_{\text{PI}}$  signals, for use as reference data and for parametric fitting. The simple blood pool model we employed is described in eqs. (3.4–3.5). A simple model has also been used in (3.6–3.7) to build the internal blood pool model suitable for the Kalman filter. It should be pointed out that, given that the two models share some similarities, evaluation of filter performance may be biased toward over-estimation. This issue can, however, be dismissed based on the following two points. The first point is that the model similarities are very limited: in fact, the internal filter model does not contain any of the patient-specific parameters from the reference model. The second point is that the model used by the Kalman filter requires knowledge about the system under observation. For this reason, it is logical that it should be based on an approximation of the blood pool model employed for reference data, which is a simple but sound description of the biophysical nature of our simulated patient. Future investigations should determine whether the transition from a simple in-vitro blood pool model to real patients requires a more advanced model.

### **3.5 Conclusions**

The integration of model knowledge and data from multiple sensors is a viable approach to accurate osmolarity-insensitive estimation of relative blood volume loss during hemodialysis. The analysis of light propagation in blood using at least two different geometrical positions is a fundamental part of the proposed method. The estimation of plasmatic sodium concentration is a useful by-product of the

state-space estimation approach. Kalman filtering is an appropriate technique to handle the integration of all available knowledge into one single estimation process.

Part of the data collected during the experiments described in this chapter was also used to develop a new mathematical model of the hemodialysis process. The new model has some innovative aspect, in comparison to previous models, and is the object of the next chapter.

## 3.6 References

- [1] A. R. Nissenson and R. N. Fine, *Clinical Dialysis*, 4th Ed. McGraw-Hill, 2005.
- [2] J.A. Sargent and F.A. Gotch, "Principles and biophysics of dialysis," in *Replacement of Renal Function by Dialysis*, W. Drukker, F.M. Parsons, J.F. Maher (Eds.), Springer, 1983
- [3] C. Ronco, P. M. Ghezzi, A. Brendolan, C. Crepaldi, and G. La Greca, "The haemodialysis system: basic mechanisms of water and solute transport in extracorporeal renal replacement therapies," *Nephrol. Dial. Transplant.*, Vol. 13, Suppl 6, pp. 3–9, 1998.
- [4] T. Boure and R. Vanholder, "Which dialyser membrane to choose?," *Nephrol. Dial. Transplant.*, Vol. 19, pp. 293–296, Feb 2004.
- [5] K. Solem, B. Olde, and L. Sörnmo, "Prediction of intradialytic hypotension using photoplethysmography," *IEEE Trans. Biomed. Eng.*, Vol. 57, pp. 1611-9, Jul 2010.
- [6] I. Fridolin, D. Karai, S. Kostin, and R. Ubar, "Accurate dialysis dose evaluation and extrapolation algorithms during online optical dialysis monitoring," *IEEE Trans. Biomed. Eng.*, Vol. 60, pp. 1371-7, May 2013.
- [7] M. Holmer, F. Sandberg, K. Solem, E. Grigonyte, B. Olde, and L. Sörnmo, "Extracting a cardiac signal from the extracorporeal pressure sensors of a hemodialysis machine," *IEEE Trans. Biomed. Eng.*, Vol. 62, pp. 1305-15, May 2015.
- [8] S. Stiller, E. Bonnie-Schorn, A. Grassmann, I. Uhlenbusch-Korwer, and H. Mann, "A critical review of sodium profiling for hemodialysis," *Semin. Dial.*, Vol. 14, pp. 337-47, Sep-Oct 2001.
- [9] F. Locatelli, U. Buon cristiani, B. Canaud, H. Kohler, T. Petitclerc, and P. Zucchelli, "Haemodialysis with on-line monitoring equipment: tools or toys?," *Nephrol. Dial. Transplant.*, Vol. 20, pp. 22-33, Jan 2005.
- [10] J. J. Dasselaaar, "Relative blood volume based biofeedback during haemodialysis," *J. Ren. Care*, Vol. 33, pp. 59-65, Apr-Jun 2007.
- [11] F. Javed, A. V. Savkin, G. S. Chan, J. D. Mackie, and N. H. Lovell, "Identification and control for automated regulation of hemodynamic variables during hemodialysis," *IEEE Trans. Biomed. Eng.*, Vol. 58, pp. 1686-97, Jun 2011.
- [12] F. Paolini, E. Mancini, A. Bosetto, and A. Santoro, "Hemoscan: a dialysis machine-integrated blood volume monitor," *Int. J. Artif. Organs*, Vol. 18, pp. 487-94, Sep 1995.
- [13] I. Yoshida, K. Ando, Y. Ando, S. Ookawara, M. Suzuki, H. Furuya, et al., "A new device to monitor blood volume in hemodialysis patients," *Ther. Apher. Dial.*, Vol. 14, pp. 560-5, Dec 2010.
- [14] J. J. Dasselaaar, R. M. Huisman, D. E. J. PE, and C. F. Franssen, "Relative blood volume measurements during hemodialysis: comparisons between three noninvasive devices," *Hemodial. Int.*, Vol. 11, pp. 448-55, Oct 2007.
- [15] D. Schneditz, H. Poggliitsch, J. Horina, and U. Binswanger, "A blood protein monitor for the continuous measurement of blood volume changes during hemodialysis," *Kidney Int.*, Vol. 38, pp. 342-6, Aug 1990.
- [16] C. Johner, P. W. Chamney, D. Schneditz, and M. Kramer, "Evaluation of an ultrasonic blood volume monitor," *Nephrol. Dial. Transplant.*, Vol. 13, pp. 2098-103, Aug 1998.
- [17] H. D. Polaschegg, "Automatic, noninvasive intradialytic clearance measurement," *Int. J. Artif. Organs*, Vol. 16, pp. 185-91, Apr 1993.
- [18] T. Petitclerc, "Festschrift for Professor Claude Jacobs. Recent developments in conductivity monitoring of haemodialysis session," *Nephrol. Dial. Transplant.*, Vol. 14, pp. 2607-13, Nov 1999.
- [19] S. Kron, R. Wenkel, T. Leimbach, S. Aign, and J. Kron, "Effects of sodium on measuring relative blood volume during hemodialysis differ by techniques," *ASAIO J.*, Vol. 59, pp. 612-6, Nov-Dec 2013.
- [20] S. Kron, R. Wenkel, T. Leimbach, S. Aign, and J. Kron, "Effects of Osmotic Changes on Measuring Relative Blood Volume: Comparison of Three Hemodialysis Devices," *ASAIO J.*, Vol. 62, pp. 214-5, Mar-Apr 2016.
- [21] M. Friebel, J. Helfmann, and M. C. Meinke, "Influence of osmolarity on the optical properties of human erythrocytes," *J. Biomed. Opt.*, Vol. 15, p. 055005, Sep-Oct 2010.

- [22] R. H. Stokes and R. A. Robinson, *Electrolyte Solutions*, 2nd Ed., Dover Publ., 2002.
- [23] F. Locatelli, S. Di Filippo, and C. Manzoni, "Relevance of the conductivity kinetic model in the control of sodium pool," *Kidney Int. Suppl.*, Vol. 76, pp. S89-95, Aug 2000.
- [24] A. Tura, S. Sbrignadello, E. Mambelli, P. Ravazzani, A. Santoro, and G. Pacini, "Sodium concentration measurement during hemodialysis through ion-exchange resin and conductivity measure approach: in vitro experiments," *PLoS One*, Vol. 8, p. e69227, 2013.
- [25] K. Moret, D. C. Grootendorst, C. Beerenhout, and J. P. Kooman, "Conductivity pulses needed for Diascan(R) measurements: does it cause sodium burden?," *NDT Plus*, Vol. 2, pp. 334-5, Aug 2009.
- [26] T. Kailath, "Lectures Notes on Wiener and Kalman Filtering," Springer-Verlag, 1981.
- [27] Peter S. Maybeck, "The Kalman Filter: An Introduction to Concepts," in *Autonomous Robot Vehicles*, I.J. Cox, G. T. Wilfong (Eds), Springer-Verlag, 1990.
- [28] R. G. Brown and P. Y. C. Hwang, *Introduction to Random Signals and Applied Kalman Filtering*, 2nd Edition, John Wiley & Sons, 1992
- [29] J. B. Zhang, J. Lin, and X. D. Zhao, "Analysis of bias in measurements of potassium, sodium and hemoglobin by an emergency department-based blood gas analyzer relative to hospital laboratory autoanalyzer results," *PLoS One*, Vol. 10, p. e0122383, 2015.

# Chapter 4

## Modeling of sodium diffusion across the hollow fiber of the hemodialyzer

In the following chapter, a novel approach is proposed to couple two different models, a Finite-Element hollow fiber model and a simple one-pool kinetic model of the patient, in order to allow a time-sensitive and realistic simulation of the diffusion of sodium during the dialysis session. The resulting coupled-models simulation retains the level of detail of the hollow fiber model, but gains a dynamically-updated sodium concentration on the blood inlet side, which is also equivalent to the plasmatic concentration in the kinetic model. The proposed approach shows very good agreement with experimental data collected for validation, and may be useful for purposes of clinical investigation or dialyzer design.

Content of this chapter is based on the article “Finite-element modeling of time-dependent sodium exchange across the hollow fiber of a hemodialyzer by coupling with a blood pool model”, by Enrico Ravagli, Elena Grandi, Paolo Rovatti and Stefano Severi (*Int J Artif Organs*, 2016 Nov 11;39(9):471-478. doi: 10.5301/ijao.5000528).

Content of the paper was reproduced in conformity with the journal’s copyright policy.

## **Abbreviations**

1D: One-dimensional

2D: Two-dimensional

3D: Three-dimensional

BC: Boundary condition

FEM: Finite-element method

ODE: Ordinary differential equations

UF: Ultrafiltration

## **Keywords:**

Hemodialysis; Hollow fiber; Membrane; Numerical model; Sodium exchange.

## 4.1 Introduction

Hemodialysis for end-stage renal disease patients is a periodical procedure involving the removal of accumulated toxins and excess fluids, plus the rebalancing of the electrolyte concentrations [1]. The core of the process is the transfer of water and solutes across the membrane of the hemodialyzer, a bundle of hollow fibers for counter-current flow of blood and dialysis fluid (dialysate), potted inside a cylindrical vessel.

Many mathematical models of the dialysis process have been proposed, targeting different aspects of the process or employing different degrees of abstraction. One-dimensional (1D) models describe mass transfer along the flow direction in the single hollow fiber [2-3]. In two-dimensional (2D) models, flow and/or concentration fields are computed on a bi-dimensional surface representing the axial and radial directions of the blood-membrane-dialysate interface [4-8]. Three-dimensional (3D) models are also reported in literature [9-11]. Models with higher levels of abstraction describe the kinetics of body pools for substances like urea or sodium with ordinary differential equations (ODEs) [3, 12-16].

Performances for 1D and 2D hollow fiber models, and their response to changes in geometrical or operating parameters, are usually evaluated with fixed inlet blood solute concentration. This approach has the limitation of not taking into account the time-dependent solute concentration changes of the patient's blood entering the dialyzer, caused by the mass transfer across the membrane.

We propose a new approach to simulate the exchange of solutes in a hollow fiber model in a more dynamic and realistic way. A 2D hollow fiber model based on the Finite-Element Method (FEM) is coupled to an ODE model of the patient's blood pool, to dynamically update the solute concentration entering the dialyzer. The resulting ODE-FEM coupled model maintains the geometrical detail of the 2D representation and gains dynamic blood-side inlet solute concentration.

Sodium was chosen as solute of interest, due to its clinical importance as an osmotic regulator [17-18]. A set of in-vitro hemodialysis sessions were carried out to validate our model.

## 4.2 Methods

The FEM hollow fiber model was developed on COMSOL Multiphysics 5.0. ODEs to describe the blood pool were implemented as a separate module of the FEM model. Twelve in-vitro hemodialysis sessions were carried out on bovine blood to gather data for model validation. Blood gas samples and dialysate conductivity data were recorded. Model performances were evaluated according to two markers: plasmatic sodium concentration and outlet dialysate sodium concentration.

### 4.2.1 Hollow fiber FEM model

The hollow fiber model was developed on the basis of available data on modern high-flux hemodialyzers. As such, it is not representative of a specific dialyzer, but functional to our aim of investigating dynamic coupling between fiber and patient models.

A 2D geometry revolving around the central axis of the hollow fiber was chosen. Fig. 4.1a shows a schematic of the model, which includes three domains: half of the hollow fiber space, the hemodialyzer membrane, and dialysate fluid surrounding the fiber. The geometrical parameters values reproduce the properties of an average modern hemodialyzer (PolyFlux family, Baxter, Italy [19]), and are:  $L_1=107.5\mu\text{m}$ ,  $L_2=50\mu\text{m}$ ,  $L_3=70\mu\text{m}$ ,  $L_{\text{Fiber}}=23.5\text{cm}$ . The number of fibers inside an average hemodialyzer is in the range of 10000-14000. An average value  $n_{\text{Fiber}}=12000$  was employed where the effects of the average fiber had to be scaled up to the entire hemodialyzer.

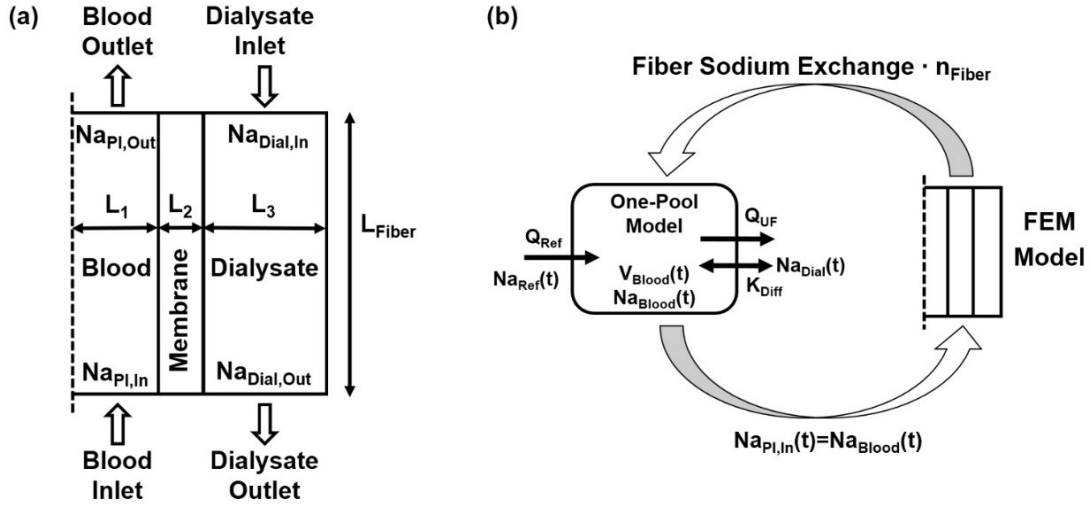


**Fig. 4.1 - Depiction of the finite-element hollow fiber model and its coupling with the blood pool model**

(a) Schematic depiction (not to scale) of the axially-revolving bi-dimensional FEM model of the hollow fiber of the hemodialyzer. Axis of revolution is represented in figure by the black dashed line. Thin black arrows represent the geometrical properties of the model. Wide black arrows represent inlet and outlet direction for the fluxes on blood and dialysate. (b) Schematization of the dynamical interplay between the FEM fiber model and the ODE blood pool model. Thin black arrows in the blood pool model represent exchange of liquid and solute mass. Wide black arrows represent the coupling between models.

Laminar flow was assumed inside the blood and dialysate domains. Velocity field  $u$  was computed according to theoretical equations (4.1-4.2). Eq. (4.1) is the Navier-Stokes momentum equation for laminar incompressible flow. The left-hand side of the equation account for the inertial forces, the first right-hand term accounts for pressure forces, and the last term accounts for viscous forces. In eq. (4.1)  $p$  is pressure and  $I$  is the identity matrix. Eq. (4.2) is the continuity equation for the conservation of mass.

$$\rho \frac{\partial \vec{u}}{\partial t} + \rho(\vec{u} \cdot \nabla)\vec{u} = \nabla \cdot [-pI + \mu(\nabla\vec{u} + (\nabla\vec{u})^T)] \quad (4.1)$$

$$\rho \nabla \cdot (\vec{u}) = 0 \quad (4.2)$$

Blood density and dynamic viscosity were set to  $\rho_{Blood}=1060\text{kg/m}^3$  and  $\mu_{Blood}=3.5\text{e-}3\text{Pa}\cdot\text{s}$ . Dialysate density and dynamic viscosity were assumed to be equal to water:  $\rho_{dial}=1000\text{kg/m}^3$ ,  $\mu_{dial}=8.9\text{e-}4\text{Pa}\cdot\text{s}$ .

Flow rates typical for hemodialysis sessions ( $Q_{Dial}=500\text{ml/min}$ ,  $Q_{Blood}=300\text{ml/min}$ ) were chosen both for simulations and experiments. The boundary condition (BC) described in eq. (4.3), where  $n$  is the normal versor, was applied to the blood and dialysate inlet ports of the filter, setting average inlet velocities to values reported in eqs. (4.4-4.5).

By setting the average inlet velocities according to eqs. (4.3-4.5) in a rigid model geometry without ultrafiltration, the desired  $Q_{Dial}$  and  $Q_{Blood}$  flow rates are achieved. No additional pull is required from the outlet ports, for this reason a zero-pressure BC was applied.

$$\vec{u} = -U_0\vec{n} \quad (4.3)$$

$$U_{0,Blood} = \frac{Q_{Blood}}{n_{Fiber} \cdot \pi \cdot L_1^2} \quad (4.4)$$

$$U_{0,Dial} = \frac{Q_{Dial}}{n_{Fiber} \cdot \pi \cdot ((L_1+L_2+L_3)^2 - (L_1+L_2)^2)} \quad (4.5)$$

Convective sodium transport due to ultrafiltration (UF) does not impact significantly on outlet dialysate sodium concentration, since UF rate (typically,  $15\text{ml/min}$ ) is much smaller than  $Q_{Dial}$ . Thus, UF was not implemented in the FEM model. It was, however, implemented in the kinetic model. Fluid velocity was set to zero inside the membrane domain.

A tangentially-moving wall BC was set at the external edge of the dialysate domain to develop a half-parabolic flow profile, by employing equations (4.6-4.7). In eq. (4.6),  $t$  is the tangent versor.

$$\vec{u} = U_{w,Dial}\vec{t} \quad (4.6)$$

$$U_{w,Dial} = 1.5 \cdot U_{0,Dial} \quad (4.7)$$

Diffusion and convection phenomena were modelled in the blood and dialysate domains according to theoretical equation (4.8), which is the convection-diffusion equation, where  $c_{Na}$  is local sodium concentration. In eq. (4.8), the first left-hand side term is the time derivative of sodium concentration, the second term represents diffusion, and the third term represent convection. Sodium diffusion coefficient  $D_{Na}$  was set to  $1.334e-9m^2/s$  [20].

$$\frac{\partial c_{Na}}{\partial t} + \nabla \cdot (-D_{Na} \nabla c_{Na}) + \vec{u} \cdot \nabla c_{Na} = 0 \quad (4.8)$$

Hemodialyzers membranes have a porous nature, with pores of different sizes allowing for low-flux or high-flux dialysis [21]. Porosity is defined as the ratio of total volume of the media which is available for flow and diffusion [22]. Various studies characterized different types of dialysis membranes with different techniques [8, 23-27]. In line with these considerations, sodium diffusion across the membrane was modelled as porous media transport, according to theoretical equations (4.9-4.10). Equation (4.9) is similar to equation (4.8), as it is a convection-diffusion equation. However, the nature of the material makes diffusion slower compared to diffusion in pure fluid, since the cross section available for movement is lower. The effective diffusion coefficient  $D_e$  can be determined as a function of the free diffusion coefficient  $D_{Na}$  by taking into account the porosity of the material and its tortuosity, as described in eq. (4.10), where  $\epsilon_p$  is the equivalent porosity coefficient and  $\tau_F$  is the tortuosity. Tortuosity is defined as the ratio between two distances that a particle of solute must travel across the porous material: the first is the actual distance between two points, travelled by following the fluid channel, and the second is the straight-line distance between those points. The relationship between porosity and tortuosity can be described by a model. In our case, the Millington and Quirk model [28] was chosen, as reported in eq. (4.11). Islam et al. [8] estimated porosity for each of the three layers composing the membrane of a Polyflux 210H hemodialyzer. Such hemodialyzer has geometrical properties very similar to those of the ones employed in the experimental part of this work. Based on the porosity values

reported in [8], an equivalent porosity coefficient  $\varepsilon_p=0.24$  was assumed for our membrane domain. Also, since convection across the membrane was not implemented in this model, the third term of equation (4.9) is null, since velocity  $u$  is equal to zero.

$$\varepsilon_p \frac{\partial c_{Na}}{\partial t} + \nabla \cdot (-D_e \nabla c_{Na}) + \vec{u} \cdot \nabla c_{Na} = 0 \quad (4.9)$$

$$D_e = \frac{\varepsilon_p}{\tau_F} D_{Na} \quad (4.10)$$

$$\tau_F = \varepsilon_p^{-\frac{1}{3}} \quad (4.11)$$

Inlet dialysate sodium concentration  $Na_{Dial,In}(t)$  was set either as constant or time-dependent in relation to the type of experimental session to be simulated. The time-dependent protocol is described in detail in the Experimental Data subsection.

A no-diffusion BC was applied on the external boundary of the dialysate domain. That is, at the distance  $L_3$  from the membrane, sodium is assumed to be in equilibrium with the surrounding dialysis fluid.

#### 4.2.2 ODE-FEM model coupling

Inlet plasmatic sodium concentration  $Na_{Pl,In}(t)$  is dynamically updated on the basis of the treatment simulation. The update is computed by coupling a one-pool ODE model of the patient's blood compartment to the FEM fiber model by taking into account the mass balance of sodium between the dialysate inlet and outlet ports. Fig. 4.1b schematizes the ODE model and its interplay with the FEM model.

Equations (4.12-4.13) are the theoretical equations for the single-pool ODE model, where  $V_{Blood}(t)$  is the volume of the blood pool and  $Na_{Blood}(t)$  its plasmatic sodium concentration.  $Na_{Dial}$  is the average sodium concentration in the hemodialyzer and  $K_{Diff}$  represents sodium diffusion across the membrane. Both

$Na_{Dial}$  and  $K_{Diff}$  are not directly used in our case, since equation (4.13) is modified according to equation (4.14) to make  $Na_{Blood}(t)$  dependent on the simulated sodium mass transfer across the FEM hemodialyzer, resulting in equation (4.15). Using total  $Q_{Dial}$  in equations (4.14-4.15) scales up the effect of the FEM model to account for  $n_{Fiber}$ -fibers working in parallel.

$$V_{Blood}(t) \dot{=} -Q_{UF}(t) + Q_{Ref}(t) \quad (4.12)$$

$$Na_{Blood}(t) \dot{=} \frac{K_{Diff} \cdot (Na_{Dial}(t) - Na_{Blood}(t)) + Q_{Ref}(t) \cdot (Na_{Ref}(t) - Na_{Blood}(t))}{V_{Blood}(t)} \quad (4.13)$$

$$K_{Diff} \cdot (Na_{Dial}(t) - Na_{Blood}(t)) = (Na_{Dial,In}(t) - Na_{Dial,Out}(t)) \cdot Q_{Dial} \quad (4.14)$$

$$Na_{Blood}(t) \dot{=} \frac{(Na_{Dial,In}(t) - Na_{Dial,Out}(t)) \cdot Q_{Dial} + Q_{Ref}(t) \cdot (Na_{Ref}(t) - Na_{Blood}(t))}{V_{Blood}(t)} \quad (4.15)$$

At each simulation step,  $Na_{Pl,In}(t)$  of the FEM model is set at the current value of  $Na_{Blood}(t)$ , then the new sodium exchange is computed and the value of  $Na_{Blood}(t)$  is updated. This way, the dynamics of the ODE and FEM models are effectively coupled.

### 4.2.3 Experimental data

A total number of twelve in-vitro dialysis sessions were carried out to gather data for model validation. Sessions were carried out on an Artis hemodialysis machine (Baxter, Medolla, Italy) using heparinized fresh bovine blood. Blood was diluted to 30% hematocrit using saline solution before session start. Each session was composed of a 1-hour stabilization phase and a 3-hours experimental phase. The start of the 3-hours experiment is considered as  $t=0$  in the following.

The stabilization phase was implemented to improve repeatability and start each 3-hours experiment at the desired  $Na_{Blood}(t=0)$  value. During stabilization phase, a peristaltic pump injects fresh dialysate inside the blood pool at  $Q_{Ref}=Q_{UF}=0.8$  L/h,

accelerating convergence to blood-dialysate equilibrium, while maintaining the original blood volume.

Different types of sessions have been carried out, implementing a combination of blood volume loss and/or sodium concentration steps. A complete summary of the experimental conditions for each session is reported in Table 4.1. Different filters of the Polyflux family were employed during the sessions (also reported in Table 4.1).

TABLE 4.1  
EXPERIMENTAL SESSIONS

#	Filter	$Q_{UF}$ [L/h]	$Q_{Ref}$ [L/h]	$Na_{Dial,In}$ [mM]	$Na_{Ref}$ [mM]	$Na_{Blood,Exp}(t=0)$ [mM]	$Na_{Blood}$ Error Mean $\pm$ SD [mM]	$Na_{Blood}$ Error Max [mM]
1	Polyflux 17L	0.8	0.63	Steps 133-147	140	138.95	1.07 $\pm$ 0.30	1.25
2	Polyflux 17L	0.8	0.63	Steps 147-133	140	138.25	0.60 $\pm$ 0.51	1.17
3	Polyflux 21L	0.8	0.63	Steps 133-147	140	141.9	2.02 $\pm$ 0.74	2.71
4	Polyflux 21L	0.8	0.63	Steps 147-133	140	139.55	1.11 $\pm$ 0.32	1.33
5	Polyflux 21L	0.8	0.63	Steps 133-147	140	141.15	0.27 $\pm$ 0.22	0.59
6	Polyflux 24S	0.8	0.63	Steps 147-133	140	140.3	0.58 $\pm$ 0.40	1.14
7	Polyflux 24S	0	0	Steps 147-133	140	138.35	2.32 $\pm$ 0.21	2.56
8	Polyflux 24S	0	0	Steps 133-147	140	138.45	2.28 $\pm$ 0.21	2.48
9	Polyflux 24S	0.8	0.63	Constant 140	140	137.8	2.45 $\pm$ 0.19	2.62
10	Polyflux 24S	0.8	0.63	Constant 140	145	141.65	3.40 $\pm$ 0.34	3.87
11	Polyflux 24S	0.8	0.63	Steps 147-133	140	137.4	2.89 $\pm$ 0.41	3.3
12	Polyflux 24S	0.8	0.63	Steps 133-147	140	137.7	2.19 $\pm$ 0.35	2.5
<b>Error on complete dataset:</b>							1.76 $\pm$ 1.03	3.87

For each experimental session,  $V_B(t=0)=5$  L. For the sessions with blood volume loss,  $Q_{UF}=0.8$  L/h. This rate has been paired with a refilling rate  $Q_{Ref}=0.63$  L/h to reach an end-session blood volume loss of  $\approx 500$  ml, corresponding to  $\approx 10\%$  relative blood volume variation. Both  $Q_{UF}=0.8$  L/h and the 10% volume loss are typical clinical values for average hemodialysis patients. Refilling has been

implemented by using the same peristaltic pump employed during the adjustment phase and previously prepared fresh dialysate.

In 10 sessions,  $\text{Na}_{\text{Dial,In}}(t)$  has been changed at 45-minute intervals during the session to implement concentration steps. In 5 of such sessions, the sodium concentration is set to 140-133-147-140 mM during these intervals. In the remaining sessions, the dual protocol with inverted steps is applied (140-147-133-140 mM). In 2 sessions,  $\text{Na}_{\text{Dial,In}}(t)$  has been kept constant at 140 mM throughout the whole session. In these sessions,  $\text{Na}_{\text{Blood}}(t=0)$  was set respectively to 140 and 145 mM during the stabilization phase.

Blood gas samples were taken at 45-minute intervals during the sessions (0, 45, 90, 135, 180 min). Samples have been analyzed with a Stat Profile pHox Ultra blood gas analyzer (Nova Biomedical, Waltham MA, USA) to measure  $\text{Na}_{\text{Blood,Exp}}(t)$ . At the end of each experiment, the session log has been downloaded from the internal memory of the machine to acquire electrical conductivity signals of inlet and outlet dialysate (respectively,  $\sigma_{\text{Dial,In}}(t)$  and  $\sigma_{\text{Dial,Out}}(t)$  measured by the machine's conductivity cells.

#### 4.2.4 Data processing

On each blood sample three consecutive measurements were performed. A systematic offset in the first of each group of measurements was observed. For this reason, reference data  $\text{Na}_{\text{Blood,Exp}}$  is based on the mean of the second and third measurements carried out on each sample.

Dialysate conductivity signals  $\sigma_{\text{Dial,In}}(t)$  and  $\sigma_{\text{Dial,Out}}(t)$  underwent median and low-pass filtering for artifact removal and smoothing. At specific times during the session, the hemodialysis machine went into a hydraulic bypass condition for safety or auto-calibration purposes. During this condition, dialysate conductivity signals were not available. A sample-and-hold procedure was applied to conductivity signals during bypass time intervals, setting conductivity at the last measured value before bypass.

Our coupled ODE-FEM model was used to simulate all of the experimental 3-hour sessions listed in Table 4.1 with the appropriate parameters, recording

computed values for  $\text{Na}_{\text{Blood}}(t)$ ,  $\text{Na}_{\text{Dial,In}}(t)$  and  $\text{Na}_{\text{Dial,Out}}(t)$  at intervals of 30 seconds.  $\text{Na}_{\text{Blood,Exp}}(t=0)$  was used as starting value for modelled  $\text{Na}_{\text{Blood}}(t)$ .

Performances of the coupled ODE-FEM models were evaluated using  $\text{Na}_{\text{Blood}}(t)$  and  $\text{Na}_{\text{Dial,Out}}(t)$  as our two markers of interest.

$\text{Na}_{\text{Blood,Exp}}$  was compared with  $\text{Na}_{\text{Blood}}(t)$  from the coupled ODE-FEM model (due to model coupling,  $\text{Na}_{\text{Blood}}(t)$  is also equal to  $\text{Na}_{\text{Pl,in}}(t)$ ). Comparison at  $t=0$  was excluded because  $\text{Na}_{\text{Blood,Exp}}(t=0)$  is also employed as the starting value for  $\text{Na}_{\text{Blood}}(t)$  in the simulations. Mean and maximum errors were calculated for each session and for the whole dataset.

Linear regression analysis has been used to study the correlation of modeled values of  $\text{Na}_{\text{Dial,Out}}(t)$  with experimentally measured  $\sigma_{\text{Dial,Out}}(t)$ . According to Kohlrausch's law of independent migration of ions, in diluted electrolytic solutions [29] the relationship between total ion content and electrical conductivity is described by the sum of the ionic concentrations, weighted by ion-specific molar conductivities. Given that sodium concentration in dialysate is 1-2 orders of magnitude higher than that of other ions, a linear concentration is expected with good approximation: for this reason, conductivity has been widely used in dialysis as a surrogate quantity in place of sodium concentration [30,31]. A rule of thumb is commonly used which predicts a 0.1 relationship between dialysate sodium concentration, expressed in [mM], and dialysate conductivity, expressed in [mS/cm]. For example, for 140 mM of sodium concentration, an electrical conductivity value of approximately 14.0 mS/cm is expected. On these bases, good correlation between modeled  $\text{Na}_{\text{Dial,In}}(t)$ - $\text{Na}_{\text{Dial,Out}}(t)$  and experimental  $\sigma_{\text{Dial,in}}(t)$ - $\sigma_{\text{Dial,Out}}(t)$  may be employed as an indicator of the model's performances. Due to the placement of the outlet conductivity cell far from the hemodialyzer inside the hemodialysis machine, a delay of  $\approx 140$  seconds is present in conductivity measurements. Modeled  $\text{Na}_{\text{Dial,Out}}(t)$ , which in the simulation is evaluated directly at the outlet port, has been shifted accordingly to align with conductivity measurements before estimation of correlation. One session was excluded from correlation estimation because the machine underwent

prolonged bypass right after application of a concentration step, and the sample-and-hold procedure could not account for this type of artifact.

Bland-Altman analysis was carried out for both evaluated markers. In the comparison between experimental  $\text{Na}_{\text{Blood,Exp}}(t)$  and simulated  $\text{Na}_{\text{Blood}}(t)$ , data from samples taken at  $t=0$  has been excluded because of its use as an initial condition for the simulations. To compare measured outlet dialysate conductivity  $\sigma_{\text{Dial,Out}}(t)$  with modelled  $\text{Na}_{\text{Dial,Out}}(t)$ , the estimated linear regression equation was employed to convert  $\text{Na}_{\text{Dial,Out}}(t)$  to an equivalent model-based conductivity. Confidence intervals were computed as  $\text{mean} \pm 1.96$  standard deviations.

### 4.3 Results

Figs. 4.2 and 4.3 show data from two experimental sessions and their associated model simulations. Fig. 4.2 refers to session #1, which implements the  $\text{Na}_{\text{Dial,in}}(t)$  steps protocol with low-high steps, whereas Fig. 4.3 refers to session #6 where the dual version of the protocol is used.

Panels 4.2a and 4.3a show an example of the response of simulated plasmatic sodium concentration to changes in  $\text{Na}_{\text{Dial,in}}(t)$ , with  $\text{Na}_{\text{Blood,Exp}}(t)$  as reference. Starting from  $\text{Na}_{\text{Blood,Exp}}(t=0)$ , simulated  $\text{Na}_{\text{Blood}}(t)$  moves in the direction of  $\text{Na}_{\text{Dial,in}}(t)$  due to diffusion in an effort to reach concentration equilibrium. As shown in panels 4.2a and 4.3a, the simulated  $\text{Na}_{\text{Blood}}(t)$  demonstrates good fitting of  $\text{Na}_{\text{Blood,Exp}}(t)$  data. Table 4.1 reports mean and maximum error between simulated  $\text{Na}_{\text{Blood}}(t)$  and experimental  $\text{Na}_{\text{Blood,Exp}}(t)$  calculated for each session and for the complete dataset. A mean error of  $1.76 \pm 1.03$  mM was found for the complete dataset, along with a 3.87 mM maximum error. The overall Bland-Altman analysis of the observed and estimated blood sodium concentrations in all the sessions is reported in Fig. 4.4a, together with its confidence intervals ( $-1.40 \pm 2.93$  mM).

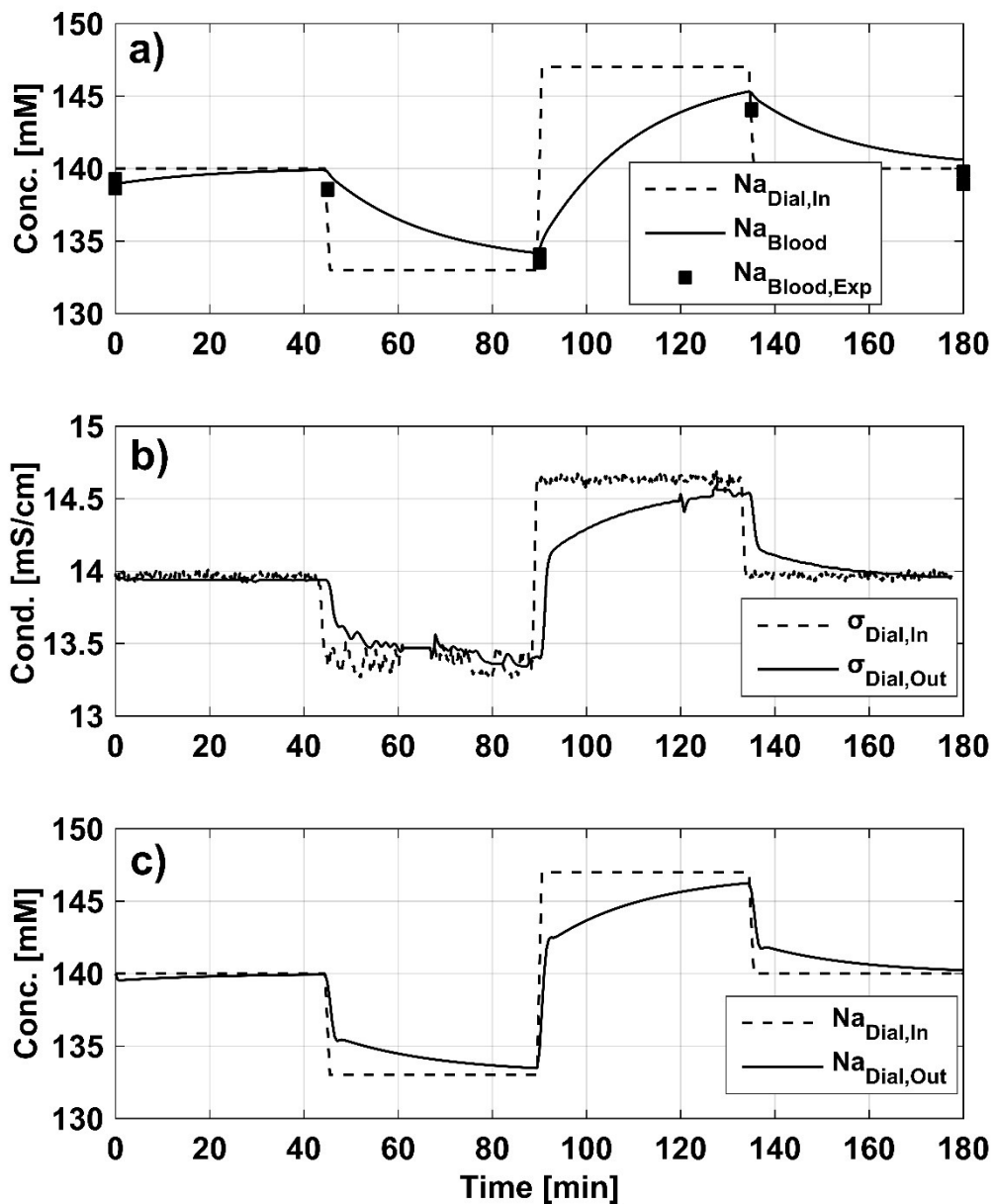
Panels 4.2b and 4.3b show  $\sigma_{\text{Dial,in}}(t)$  and  $\sigma_{\text{Dial,Out}}(t)$  recorded by the conductivity cells. The shape of the outlet conductivity response has a first almost-instantaneous response phase, then a second phase more similar to the

response of a first-order system. This is consistent with the nature of outlet dialysate, whose conductivity can be modelled as a mix of inlet and plasmatic conductivity [32-33].

Panels 4.2c and 4.3c show simulated inlet and outlet dialysate sodium concentration. The shape of modelled  $\text{Na}_{\text{Dial,Out}}(t)$  matches closely that of  $\sigma_{\text{Dial,Out}}(t)$ , including the mixed step response with an instantaneous and a delayed component. The only missing feature is the response delay, due to the fact that in the model  $\text{Na}_{\text{Dial,Out}}(t)$  is measured right at the edge of the outlet port, whereas  $\sigma_{\text{Dial,Out}}(t)$  is measured by the conductivity cell placed downstream at a longer distance.

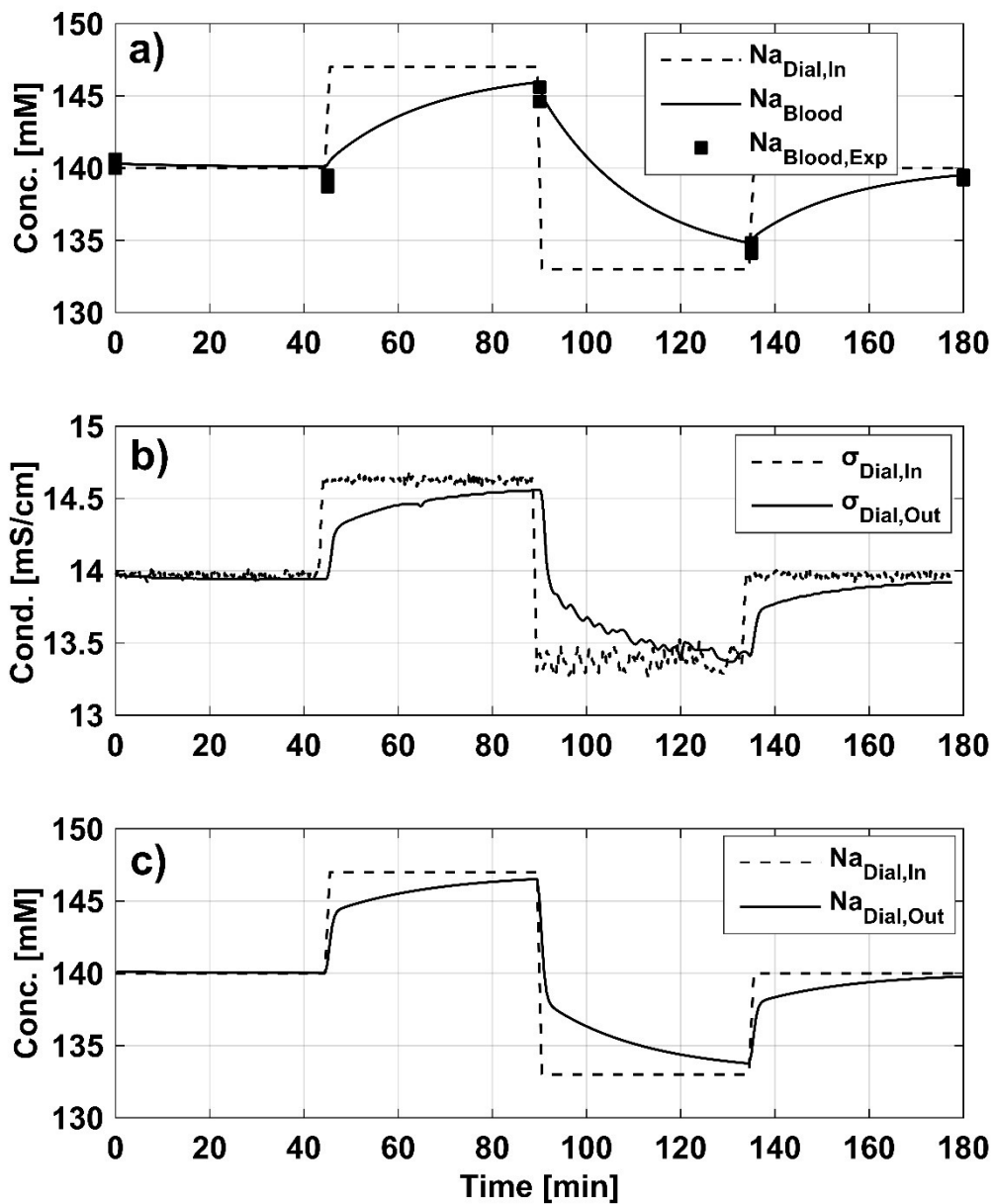
Correlation analysis between simulated  $\text{Na}_{\text{Dial,Out}}(t)$  and experimentally-measured  $\sigma_{\text{Dial,Out}}(t)$  on the whole dataset returns  $R^2=0.992$ . The estimated linear relationship is  $\sigma_{\text{Dial,Out}}=0.092 \cdot \text{Na}_{\text{Dial,Out}} + 1.068$ . The very high correlation between the two variables is reported graphically in Fig. 4.5, along with the estimated regression line. In Fig. 4.4b, Bland-Altman analysis is reported, showing small confidence intervals ( $0.000 \pm 0.056$  mS/cm).

Fig. 4.6 shows the evolution of sodium concentration along the 1-D blood-membrane interface, with clearly distinguishable dialysate-induced concentration variations.



**Fig. 4.2 – Experimental and model simulation results for session #1**

Comparison between experimental and simulated results for different markers. See Table 4.1 for details on experimental session #1. (a) Simulated plasmatic sodium concentration  $Na_{Blood}(t)$  (solid black line) in response to modeled changes in inlet dialysate sodium concentration  $Na_{Dial,In}(t)$  (dashed black line). Reference plasmatic sodium sampling  $Na_{Blood,Exp}(t)$  is reported as black squares. (b) Inlet dialysate conductivity  $\sigma_{Dial,In}(t)$  (dashed black line) and outlet dialysate conductivity  $\sigma_{Dial,Out}(t)$  (solid black line) recorded by the conductimetry cells. (c) Simulated inlet ( $Na_{Dial,In}(t)$ , dashed black line) and outlet ( $Na_{Dial,Out}(t)$ , dashed black line) dialysate sodium concentrations.



**Fig. 4.3 – Experimental and simulation results for session #6**

Comparison between experimental and simulated results for different markers. See Table 4.1 for details on experimental session #6. (a) Simulated plasmatic sodium concentration  $Na_{Blood}(t)$  (solid black line) in response to modeled changes in inlet dialysate sodium concentration  $Na_{Dial,In}(t)$  (dashed black line). Reference plasmatic sodium sampling  $Na_{Blood,Exp}(t)$  is reported as black squares. (b) Inlet dialysate conductivity  $\sigma_{Dial,In}(t)$  (dashed black line) and outlet dialysate conductivity  $\sigma_{Dial,Out}(t)$  (solid black line) recorded by the conductimetry cells. (c) Simulated inlet ( $Na_{Dial,In}(t)$ , dashed black line) and outlet ( $Na_{Dial,Out}(t)$ , dashed black line) dialysate sodium concentrations.

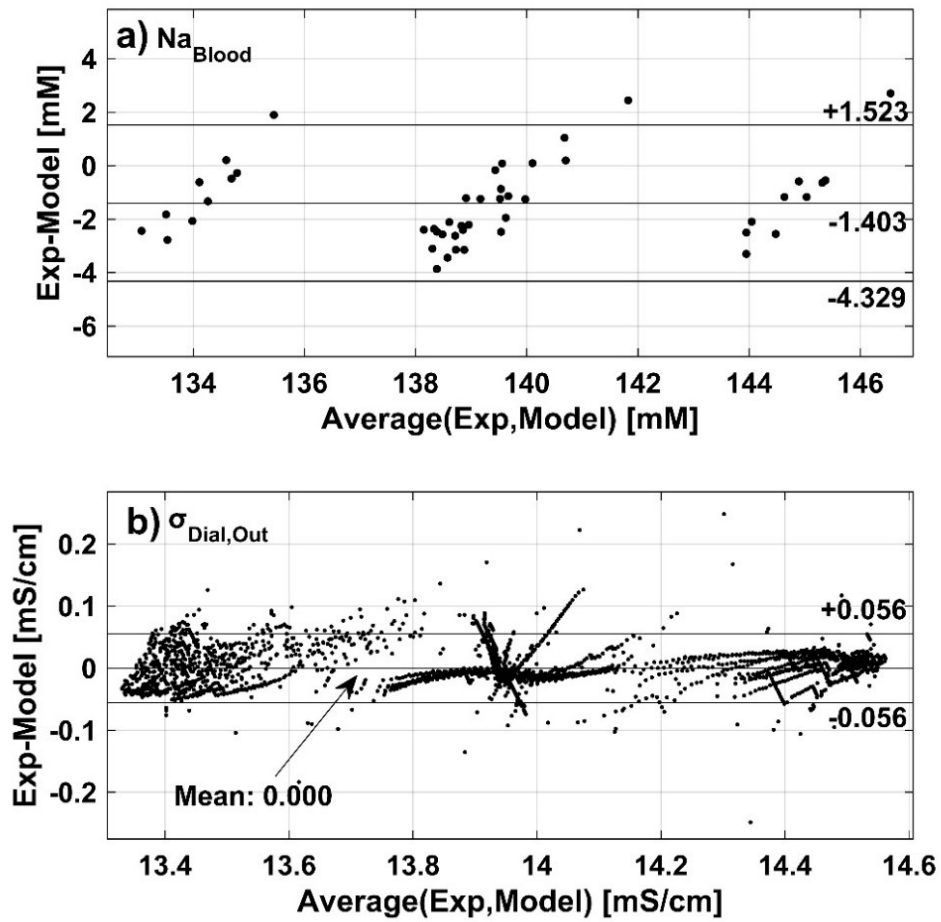


**Fig. 4.4 – Bland-Altman dispersion analysis for different markers**

Comparison of observed and estimated results by Bland-Altman dispersion analysis. (a) Comparison of experimental  $\text{Na}_{\text{Blood,Exp}}(t)$  and modelled  $\text{Na}_{\text{Blood}}(t)$ . (b) Comparison of experimental  $\sigma_{\text{Dial,Out}}(t)$  and regression-based equivalent conductivity based on modelled  $\text{Na}_{\text{Dial,Out}}(t)$ .

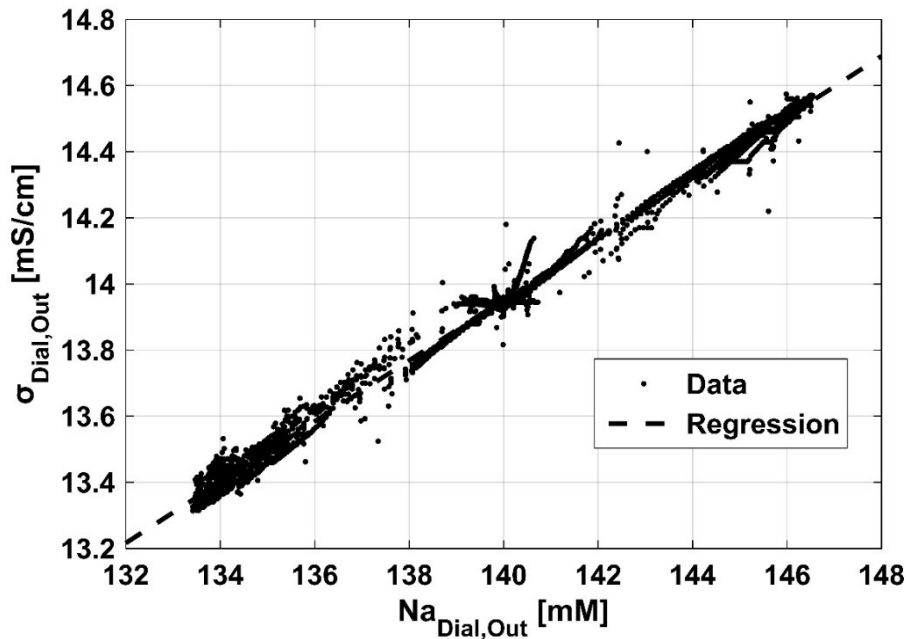


**Fig. 4.5 – Correlation between experimental outlet conductivity and simulated outlet sodium concentration**

Correlation between simulated  $Na_{Dial,Out}(t)$  and experimental  $\sigma_{Dial,Out}(t)$  is reported for the whole dataset (black dots). The estimated regression equation is also reported graphically in the form of the dashed black line.

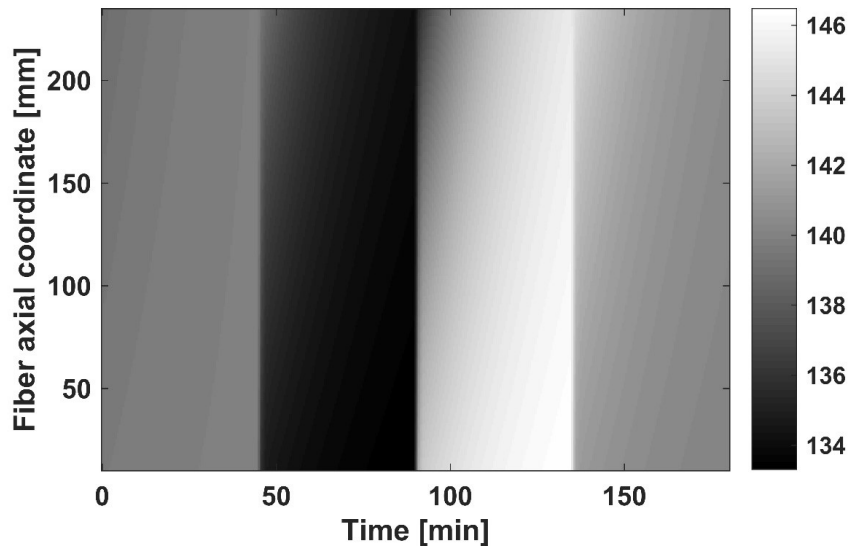


**Fig. 4.6 – Time evolution of sodium concentration along the blood-membrane interface**

Analysis of sodium concentration along the blood membrane interface, reported for a simulation based on the parameters of session #1. Color scale is proportional to sodium concentration in the 133-147 mM range. Blood flow direction is upward. Sodium concentration along the fiber is reported starting at 10 mm from the blood inlet point, up to the end of the fiber.

## 4.4 Discussion

In this work, a 2D FEM model of a hollow hemodialyzer fiber was developed and coupled to an ODE model of the patient's blood pool to show the viability of dynamic analysis of hollow fiber models. Our results in reproducing experimental data are a demonstration of the suitability of the developed model: although it reproduces an "average" hemodialyzer, the dynamics of a heterogeneous set of high-flux dialyzers (see Table 4.1) were correctly reproduced. To the best of our knowledge, it is the first time that a FEM hollow fiber model is validated by dynamical interplay with a virtual patient model, although a simplified one.

Results in fitting of plasmatic sodium concentration are, by themselves, already a good indication of the capability of our ODE-FEM model in reproducing the dynamic behaviour of the average hemodialyzer fiber. Although plasmatic sodium concentration is determined by the ODE blood pool model, such model is a good representation of a very simple experimental condition (animal blood in a glass beaker). Therefore, given its dynamic interaction with the FEM model, there would not be a good fit of blood gas data unless exchange with the hemodialyzer was simulated correctly.

It should also be observed that the average measurement error of a blood gas analyzer is in the order of 3 mM [34]: therefore, the mean error of our model falls within the range of measurement uncertainty for plasmatic sodium reference data. For this reason, a large fraction of maximum error could be ascribed to the blood gas analyzer and not to bad model performances.

The very high correlation obtained between outlet dialysate conductivity and sodium concentration is an additional indicator of the ODE-FEM model's good performances. Correlation accounts for the presence of offset and gain between the two compared variables, but the high estimated  $R^2$  value could only be obtained in the case of very similar time dynamics. Values of the regression coefficients are similar to values reported in literature for the relationship between sodium concentration and conductivity in dialysate: for example, Tura et al. [35] reported  $\sigma_{\text{Dial}}=0.08 \cdot \text{Na}_{\text{Dial}}+ 2.87$ . The value of the obtained regression slope, 0.092

(mS/cm)/mM, and the presence of a 1.068 mS/cm offset can be explained by the influence of ions other than sodium on total conductivity, as already mentioned in the Methods section.

Regarding the results of Bland-Altman analyses: evaluation of the first marker, plasmatic sodium concentration, shows that data points are concentrated into three main groups (Fig. 4.4a). This is expected because of the timing of blood sampling, always carried out at the end of a time step, corresponding to 45-minutes of application of low/medium/high sodium concentration to inlet dialysate in our stepwise protocol. However, the three groups show comparable error ranges: this positive finding demonstrates that error is not related to the value of plasmatic sodium concentration. Fig. 4.4a also shows a systematic negative error (-1.40 mM), indicating that the model slightly overestimates plasmatic sodium concentration. Modeling results are closer than experimental data to what is logically expected from our experimental procedure, that is, complete or nearly complete alignment to inlet dialysate sodium concentration. Our interpretation is that this can be actually not a modeling problem but the indication of the presence of negative, variable, bias in the sodium electrodes for blood gas analysis. Regardless of the interpretation, error dispersion is well within the limits of accuracy of the experimental measurements ( $\approx 3$  mM, as already mentioned [34]). Bland-Altman analysis of outlet dialysate conductivity (Fig. 4.4b) does not show any particular feature: data points are regularly distributed in a small error range ( $\pm 0.056$  mS/cm).

Both markers have been evaluated on a dataset of 12 experimental sessions. The size of the experimental dataset and the combination of sessions with different types of dialysate sodium time profile is an indication of the robustness of our validation.

#### **4.4.1 Limitations**

In the present work, reference data was gathered by means of blood gas analysis with an emergency-room grade analyzer and by recording inlet/outlet dialysate conductivity. This is currently the best available way for fast repeated sampling of

blood plasmatic sodium concentration. The possible inaccuracy of the instrument was partially compensated by repeating analysis three times for each sample.

Conductivity was measured in place of sodium concentration for inlet and outlet dialysate. This may constitute a limitation, but with our aim to gather reference data in dynamic conditions, having a continuous recording is a much greater benefit.

A simple one-pool ODE model was used to describe the blood compartment. Although more complex (e.g. double-pool), models exist, our representation was sufficiently detailed to correctly describe the experimental setup.

## 4.5 Conclusions

The results we obtained demonstrates the possibility of dynamical simulation of patient/dialyzer sodium exchange and of fiber model validation by dynamical analysis, which were the main targets of this work. Coupling our FEM hollow fiber model to a simple blood pool model proved to be an effective approach for implementing such dynamical analysis.

This innovative approach of merging together two different models, each with its own appropriate level of abstraction, presents some advantages compared to more traditional models employed on their own:

- From the perspective of kinetic modeling, it allows to take into account the exchange of solutes with the dialyzer in a more detailed way, compared to the use of a simple diffusion coefficient.
- From the designer's perspective, it allows the inclusion of feedback from the patient's physiology when investigating the behaviour of a hollow fiber with specific properties, which is usually done in steady-state conditions.
- From the clinical perspective, a more direct application of our coupled-models approach could be the fitting of experimental dialysate conductivity tracks and blood gas data by optimization of the kinetic model parameters, in order to develop customized patient models.

In future stages of the work, the simple one-pool patient-side model could be replaced with more detailed two-pools or three-pools models for the aim of clinical modeling. Additional electrolytes could also be added.

Modeling and sensing in dialysis are two approaches which show much potential for integration. The availability of sensors able to provide accurate and continuous measurements of physiological parameters during dialysis is critical for the development and validation of new mathematical models, as shown in this chapter. On the other hand, models may be useful to predict quantities which cannot be directly measured. One example of this type of approach is shown in Chapter 3.

## 4.6 References

- [1] Sargent JA, Gotch FA. Principles and biophysics of dialysis. In: *Replacement of Renal Function by Dialysis*, 2nd ed. Drukker W, Parsons FM, Maher JF. eds. Dordrecht, Martinus Nijhoff Publishers, 1983.
- [2] Galach M, Ciechanowska A, Sabalinska S, Waniewski J, Wojcicki J, Werynskis A. Impact of convective transport on dialyzer clearance. *J Artif Organs*. 2003;6(1):42-48.
- [3] Waniewski J. Mathematical modeling of fluid and solute transport in hemodialysis and peritoneal dialysis. *J Membrane Sci*. 2006;274(1-2):24-37.
- [4] Liao Z, Poh CK, Huang Z, Hardy PA, Clark WR, Gao D. A numerical and experimental study of mass transfer in the artificial kidney. *J Biomech Eng*. 2003;125(4):472-480.
- [5] Ding W, He L, Zhao G, Zhang H, Shu Z, Gao D. Double porous media model for mass transfer of hemodialyzers. *Int J Heat Mass Tran*. 2004;47(22):4849-4855.
- [6] Lu J, Lu W-Q. A numerical simulation for mass transfer through the porous membrane of parallel straight channels. *Int J Heat Mass Tran*. 2010;53(11-12):2404-2413.
- [7] Annan K. Mathematical modeling of the dynamic exchange of solutes during bicarbonate dialysis. *Math Comput Model*. 2012;55(5-6):1691-1704.
- [8] Islam MS, Szpunar J. Study of Dialyzer Membrane (Polyflux 210H) and Effects of Different Parameters on Dialysis Performance. *Open Journal of Nephrology*, 2013, 3, 161-167
- [9] Yamamoto K, Matsuda M, Hirano A, et al. Computational evaluation of dialysis fluid flow in dialyzers with variously designed jackets. *Artif Organs*. 2009;33(6):481-486.
- [10] Eloot S, De Wachter D, Van Tricht I, Verdonck P. Computational flow modeling in hollow-fiber dialyzers. *Artif Organs*. 2002;26(7):590-599.
- [11] Ding W, Li W, Sun S, et al. Three-dimensional simulation of mass transfer in artificial kidneys. *Artif Organs*. 2015;39(6): E79-89.
- [12] Mann H, Stiller S. Sodium modeling. *Kidney Int Supplement*. 2000;76:S79-88.
- [13] Gotch FA. Evolution of the single-pool urea kinetic model. *Semin dialysis*. 2001;14(4):252-256.
- [14] Ursino M, Coli L, Magosso E, et al. A mathematical model for the prediction of solute kinetics, osmolarity and fluid volume changes during hemodiafiltration with on-line regeneration of ultrafiltrate (HFR). *Int J Artif Organs*. 2006;29(11):1031-1041.
- [15] Sternby J, Daugirdas JT. Theoretical basis for and improvement of Daugirdas' second generation formula for single-pool Kt/V. *Int J Artif Organs*. 2015;38(12):632-637.
- [16] Casagrande G, Bianchi C, Vito D, et al. Patient-specific modeling of multicompartamental fluid and mass exchange during dialysis. *Int J Artif Organs*. 2016; 39(5): 220 - 227
- [17] Heineken FG, Evans MC, Keen ML, Gotch FA. Intercompartmental Fluid Shifts in Hemodialysis Patients. *Biotechnol Progr*. 1987;3(2):69-73.
- [18] Flanigan MJ. Role of sodium in hemodialysis. *Kidney Int Supplement*. 2000;76:S72-78.
- [19] <http://www.gambro.com/en/global/Products/Hemodialysis/Dialyzers/>. Accessed June 12, 2016.
- [20] EL Cussler. Diffusion: Mass transfer in Fluid Systems. 3rd ed. Cambridge University Press, 2009.
- [21] Boure T, Vanholder R. Which dialyser membrane to choose? *Nephrol Dial Transpl*. 2004;19(2):293-296.
- [22] Dullien FAL. Porous Media: Fluid Transport and Pore Structure. 2nd ed. Academic Press, 1991.
- [23] Broek AP, Teums HA, Bargeman D, Sprengers ED and Smolders CA. "Characterization of hollow fiber hemodialysis membranes: pore size distribution and performance," *J Membrane Sci*, 1992, 73 (2-3)143-152.
- [24] Yan F, De Jardin P, Schmitt A, Pusineri C. "Electrochemical characterization of a hemodialysis membrane," *J Phys Chem*. 1993;97(15):3824-3828.
- [25] Hayama M, Kohori F, Sakai K. "AFM observation of small surface pores of hollow-fiber dialysis membrane using highly sharpened probe," *J Membrane Sci*. 2002;197(1-2):243-249.

- [26] Barzin J, Feng C, Khulbe KC, Matsuura T, Madaeni SS, Mirzadeh H. "Characterization of polyethersulfone hemodialysis membrane by ultrafiltration and atomic force microscopy;" *J Membrane Sci.* 2004;237(1–2):77-85.
- [27] Hedayat A, Szpunar J, Kumar NAPK, Peace R, Elmoselhi H, Shoker A. "Morphological Characterization of the Polyflux 210H Hemodialysis Filter Pores," *Int J Nephrol.* 2012:6.
- [28] Millington RJ, Quirk JP. "Permeability of porous solids," *T Faraday Soc.* 1961;57(0):1200-1207.
- [29] Robinson RA, Stokes RH. - *Electrolyte Solutions.* 2nd revised ed. Dover Publications, 2002.
- [30] Polaschegg H D. "Automatic, noninvasive intradialytic clearance measurement," *Int J Artif Organs,* 1993;16:185-9.
- [31] Ficheux A, Argiles A, Mion H, and Mion C M. "Influence of convection on small molecule clearances in online hemodiafiltration," *Kidney Int,* 2000;57:1755-63.
- [32] Petitsclerc T. "Recent developments in conductivity monitoring of haemodialysis session," *Nephrol Dial Transpl.* 1999;14(11):2607-2613.
- [33] Moret K, Grootendorst DC, Beerenhout C, Kooman JP. "Conductivity pulses needed for Diascan® measurements: does it cause sodium burden?," *Nephrol Dial Transpl Plus.* 2009;2(4):334-335.
- [34] Zhang JB, Lin J, Zhao XD. "Analysis of bias in measurements of potassium, sodium and hemoglobin by an emergency department-based blood gas analyzer relative to hospital laboratory autoanalyzer results." *PloS One.* 2015;10(4):e0122383.
- [35] Tura A, Sbrignadello S, Mambelli E, Ravazzani P, Santoro A, Pacini G. "Sodium concentration measurement during hemodialysis through ion-exchange resin and conductivity measure approach: in vitro experiments." *PloS one.* 2013;8(7):e69227.

# Concluding Remarks

In this doctoral thesis two different methods for non-invasive sensing and estimation are presented, which aim at improving the quantity and quality of information available during the hemodialysis session. A new model for the diffusion of sodium during the session is also proposed.

In Chapter 2 an estimation method for plasmatic conductivity was presented. The method satisfies the requirements of compactness and non-invasiveness necessary for hemodialysis sensors. Quantitative results showed that the accuracy of the measurement and model-fitting process is comparable to that of the traditional method and even slightly better. However, the developed method is also much faster than the currently used systems and is viable for continuous estimation throughout the session, whereas current systems are based on a long step-like protocol that can only be applied a few times during the whole treatment. The next challenge for the further development of this technology will be the transition from measurements on a blood-mimicking fluid in a simple setup to measurements on whole blood flowing in a hemodialysis machine. Further experiments will clarify whether the complex nature of blood will require, for the estimation of plasmatic conductivity, a deeper analysis of the collected impedance measurement and/or the use of additional sensors.

The system described in Chapter 3 is an excellent example of how the limitations to viable sensing technologies in hemodialysis can be overcome by integrating data from different sources, whereas each single source may not provide much information by itself. In our specific case, the Kalman filter methodology proved to be a valid choice for the task, returning accurate and robust estimates for relative blood volume loss and plasmatic sodium concentration. Good results were also obtained when, during short time intervals,

the available information was reduced. The technology presented in this chapter is already at a more developed stage if compared to the conductivity estimation system, having been already validated with flowing blood on a real hemodialysis machine. However, more tests are needed in order to study the response of the system to parameters, which were in our case fixed: two among them, blood and dialysate flow rates.

The two measurement technologies presented in this thesis have been developed in parallel and their targets may seem to be partially overlapped, as plasmatic conductivity and plasmatic sodium concentration strongly correlates. That is, because sodium concentration is much higher compared to other plasmatic electrolytes and its influence on conductivity is the strongest one. The hybrid optical/conductivity estimator may seem the most logical choice between the two, as it offers the estimation of relative blood volume loss in addition to that of plasmatic sodium concentration. However, another more interesting option is viable: as reported in Chapter 3, the Kalman estimator architecture includes a mathematical relationship between inlet/outlet conductivity and sodium concentration, which by means of linear regression is employed as plasmatic conductivity. On the other hand, the conductivity estimation system in Chapter 2 will require, when working on whole blood, some kind of hematocrit compensation, which may be obtained by collecting optical data. This means that the developed Kalman-based architecture may include and integrate the information on plasmatic conductivity quite elegantly, resulting in a single piece of technology with the ability to extract different (kind of) data during the dialysis treatment non-invasively and return robust estimations. Also, the fact that the two sensors are based on different physical principles (one is optical and the other electrical) means that mechanical integration into one compact bloodline measurement cell is possible without interference between the two systems.

In Chapter 4, we presented a new integrated model simulating patient-dialyzer interaction for the purpose of describing sodium diffusion during the hemodialysis

session. This part of the doctoral work is not strictly related to the main topic of the thesis, that of non-invasive sensing technologies, however the data collected during the development of the work reported in Chapter 3, and the experience matured in the same context about modeling different aspects of the hemodialysis process, made this work possible. The model we created was able to reproduce data collected from the internal sensors of the hemodialysis machines and from blood sampling during in-vitro sessions with animal blood. Although data was not collected in the most realistic conditions (in-vivo sessions), our aim was to show that integration between modeling descriptions of different portions of the hemodialysis process is possible, even at different abstraction levels. The results obtained in model validation show that our aim was achieved. Many steps are possible for future development of this model. Among these, inclusion of solutes other than sodium and replacement of the one-pool patient model with the most recent bi-compartmental and tri-compartmental models presented in literature.

In conclusion, the work reported in this thesis demonstrates how, in spite of the severe restrictions placed on access to blood, it is still possible to find new ways to extract information on hematic properties during hemodialysis. The two best tools for this task are non-invasive sensing technologies, for example optical and electromagnetic methods, and the integration of data from multiple sources by means of mathematical models of the dialysis process.



# Acknowledgements

First of all, I would like to thank my supervisor, Prof. Stefano Severi, for guiding me during the PhD with patience and good advice. It is thanks to him if during the last three years I have grown not just professionally, but as a human being.

I give my most sincere thanks to Paolo Rovatti and his group at Gambro Dasco (now part of Baxter) for funding my PhD studentship and for supporting me during the experimental phase of my research.

I would like to thank Marco Crescentini and Prof. Marco Tartagni for their advice on sensors and measurement systems.

I am also grateful to Maurizio Lannocca for his technical help.

My special thanks go to Prof. Leif Sornmo and to Mattias Holmer, for welcoming me at Lund University and helping me with my research.

I would like to thank the reviewers of my thesis, Prof. Elisa Magosso, Giustina Casagrande, and the abovementioned Paolo Rovatti, for their useful comments and indications.

My experience as a PhD student would not have been the same without the presence of some people who I met along the way at the University of Bologna. Here I would like to acknowledge them.

Thanks to Elisa and Chiara, who welcomed me into the research group with warmth and friendship.

Thanks to Claudia, who started out as a colleague and ended up as a wonderful friend and traveling companion.

Thanks to Lucia. Your effort and dedication to research really inspired me. Also, thank you for tirelessly listening to my worries and anxieties.

Thanks to Valeria, who I met later on during my PhD studies, but quickly became one of my best friends.

I also feel the need to thank some close personal friends. Although they were not involved in my professional work, I believe it is not so simple to separate the components of one's own life. So, thanks to Francesco, Marco, Michela, Lucrezia and Luca for your friendship and the fun you provided.

My last and most heartfelt acknowledgement goes to my family, in particular to my parents, who always supported me in my studies. I promise someday I will get a real job!